EFFECTS OF LOADING RATE AND PORE PRESSURE ON COMPRESSIVE STRENGTH OF ROCKS

Supattra Khamrat

A Thesis Submitted in Partial Fulfillment of the Requirements for the Degree of Master of Engineering in Geotechnology

Suranaree University of Technology

Academic Year 2013

การศึกษาผลกระทบของอัตราการให้แรงและความดันน้ำต่อกำลังกดของหิน

นางสาวสุภัทรา คำราช

วิทยานิพนธ์นี้เป็นส่วนหนึ่งของการศึกษาตามหลักสูตรปริญญาวิศวกรรมศาสตรมหาบัณฑิต
สาขาวิชาเทคโนโลยีธรณี
มหาวิทยาลัยเทคโนโลยีสุรนารี
ปีการศึกษา 2556

EFFECTS OF LOADING RATE AND PORE PRESSURE ON COMPRESSIVE STRENGTH OF ROCKS

Suranaree University of Technology has approved this thesis submitted in partial fulfillment of the requirements for a Master's Degree.

Thesis Examining Committee

____

(Dr. Prachya Tepnarong)

Chairperson

____

(Prof. Dr. Kittitep Fuenkajorn)

Member (Thesis Advisor)

____

(Dr. Decho Phueakphum)

Member

สุภัทรา คำราช : การศึกษาผลกระทบของอัตราการให้แรงและความดันน้ำต่อกำลังกดของหิน (EFFECTS OF LOADING RATE AND PORE PRESSURE ON COMPRESSIVE STRENGTH OF ROCKS) อาจารย์ที่ปรึกษา : ศาสตราจารย์ ดร.กิตติเทพ เฟื่องขจร, 88 หน้า.

วัตถุประสงค์ของการศึกษาคือ เพื่อหาผลกระทบของแรงดันน้ำต่อกำลังกดและความยืดหยุ่นของหินแกรนิต หินมาร์ล และหินอ่อน ในการทดสอบได้เสนอวิธีการตรวจวัดค่าแรงดันน้ำของหินแบบทางอ้อมโดยใช้ตัวอย่างหินขนาดเท่ากับ 50×50×100 ลูกบาศก์มิลลิเมตร มีการทดสอบภายใต้สภาวะแห้งและสภาวะอิ่มตัวด้วยน้ำ อัตราการให้แรงกดต่อตัวอย่างหินผันแปรระหว่าง 0.001 ถึง 10 เมกะปาสคาลต่อวินาที และทำการผันแปรความเค้นล้อมรอบระหว่าง 0 ถึง 12 เมกะปาสคาล โดยใช้โครงกดทดสอบในสามแกนจริง ผลการทดสอบระบุว่า ค่ากำลังกดของหินในสภาวะอิ่มตัวด้วยน้ำมีค่าน้อยกว่าสภาวะแห้งโดยเฉพาะอย่างยิ่งที่ระดับความเค้นล้อมรอบและอัตราการให้แรงกดสูง ค่าสัมประสิทธิ์ความยืดหยุ่นในสภาวะแห้งมีค่าสูงกว่าสภาวะอิ่มตัวด้วยน้ำ และค่าอัตราส่วนปัวซ์ซองในสภาวะอิ่มตัวด้วยน้ำมีค่าเพิ่มขึ้นเพียงเล็กน้อยจากสภาวะแห้ง หลังจากนั้นได้นำค่ากำลังกดสูงสุดของหินในสภาวะแห้งมาคำนวณโดยใช้สมการทางคณิตศาสตร์เพื่อแยกผลกระทบของอัตราการให้แรงกดออกจากค่ากำลังกดสูงสุดของหินในสภาวะอิ่มตัวด้วยน้ำ และด้วยเหตุนี้จึงสามารถหาผลกระทบของแรงดันน้ำที่แท้จริงได้ ผลการคำนวณระบุว่าค่ากำลังกดและค่าสัมประสิทธิ์ความยืดหยุ่นมีค่าลดลงและค่าอัตราส่วนปัวซ์ซองมีค่าเพิ่มขึ้นเมื่อแรงดันน้ำเพิ่มขึ้น จากการศึกษาในครั้งนี้สามารถนำข้อมูลดังกล่าวไปประยุกต์ใช้ในการประเมินเสถียรภาพของหินประดับในอาคารหรืออาคารที่ก่อสร้างด้วยหินภายใต้ความชื้นระดับต่างๆและสามารถประเมินค่าความแข็งและค่าการเปลี่ยนแปลงรูปร่างของเขื่อนหรือฐานรากต่างๆในสภาวะแห้งและสภาวะอิ่มตัวด้วยน้ำได้

สาขาวิชา เทคโนโลยีธรณี ลายมือชื่อนักศึกษา ____________________

ปีการศึกษา 2556 ลายมือชื่ออาจารย์ที่ปรึกษา_______________

SUPATTRA KHAMRAT : EFFECTS OF LOADING RATE AND PORE PRESSURE ON COMPRESSIVE STRENGTH OF ROCKS. THESIS ADVISOR : PROF. KITTITEP FUENKAJORN, Ph.D., P.E., 88 PP.

ROADING RATE/WATER CONTENT/STRENGTH/ELASTIC PROPERTIES

The objective of this study is to experimentally determine the effects of pore pressure on the compressive strengths and elasticity of granite, marl and marble. An indirect approach for determining the pore pressure in low porosity rocks is presented. Rectangular rock specimens (50×50×100 mm^3) under dry and saturated conditions are axially loaded under different rates from 0.001 to 10 MPa/s. The constant confining pressures are maintained between 0 and 12 MPa using polyaxial load frame. The results indicate that the strengths of the saturated specimens are lower than those of the dry ones particularly under the high confining pressures and loading rates. The elastic modulus of dry specimens is higher than that of the saturated specimens and the Poisson's ratios of saturated specimens are slightly higher than the dry specimens. The strengths obtained from the dry testing are used to quantitatively correct the loading rate effect from the saturated strengths, and hence the true effect of pore pressure can be revealed. The pore pressures notably reduce the compressive strength and elastic modulus, and increase the Poisson's ratio. The results can be used to assess the mechanical stability of these decorating and building stones as applied under various moisture contents and predict the strength and deformation of rock embankments and foundations under dry and saturated conditions.

School of Geotechnology　　　　Student's Signature__________________

Academic Year 2013　　　　Advisor's Signature__________________

ACKNOWLEDGMENTS

I wish to acknowledge the funding supported by Suranaree University of Technology (SUT).

I would like to express my sincere thanks to Prof. Dr. Kittitep Fuenkajorn for his valuable guidance and efficient supervision. I appreciate his strong support, encouragement, suggestions and comments during the research period. My heartiness thanks to Dr. Prachya Tepnarong and Dr. Decho Phueakphum for their constructive advice, valuable suggestions and comments on my research works as thesis committee members. Grateful thanks are given to all staffs of Geomechanics Research Unit, Institute of Engineering who supported my work.

Finally, I would like to thank beloved parents for their love, support and encouragement.

Supattra Khamrat

TABLE OF CONTENTS

Page

TABLE OF CONTENTS (Continued)

Page

TABLE OF CONTENTS (Continued)

Page

LIST OF TABLES

Table **Page**

LIST OF FIGURES

Figure **Page**

LIST OF FIGURES (Continued)

Figure **Page**

LIST OF FIGURES (Continued)

Figure **Page**

LIST OF FIGURES (Continued)

Figure **Page**

LIST OF FIGURES (Continued)

Figure **Page**

SYMBOLS AND ABBREVIATIONS

$w_{ave.}$	=	Average water content
$\partial\sigma_1/\partial t$	=	Loading rate
$\sigma_{1,f}$	=	Compressive strength at failure
σ_2	=	Intermediate stress
σ_3	=	Minor principal stress
$\sigma_{1,f,dry}$	=	Strength of dry specimen tested at various loading rates
$\sigma^{*}_{1,f,dry}$	=	New (adjusted) maximum principal stress of dry condition corresponding to $\partial\sigma_1/\partial t$ = 0.1 MPa/s
$\sigma_{1,f,sat}$	=	Strength of saturated specimen tested at various loading rates
$\sigma^{*}_{1,f,sat}$	=	New (adjusted) maximum principal stress of saturated condition corresponding to $\partial\sigma_1/\partial t$ = 0.1 MPa/s
σ_u	=	Uniaxial compressive strength
σ^{*}_{u}	=	New (adjusted) uniaxial compressive strength
σ'_1	=	Major principal effective stress
σ'_3	=	Minor principal effective stress
σ_m	=	Mean stress
ε_1	=	Major principal strains
ε_2	=	Intermediate principal strains
ε_3	=	Minor principal strains
E	=	Young's modulus

SYMBOLS AND ABBREVIATIONS (Continued)

ν	=	Poisson’s ratio
G	=	Shear modulus
K	=	Bulk modulus
E_{dry}	=	Elastic modulus of dry condition
E^{*}_{dry}	=	New (adjusted) elastic modulus of dry condition corresponding to $\partial\sigma_1/\partial t = 0.1$ MPa/s
ν_{dry}	=	Poisson’s ratio of dry condition
ν^{*}_{dry}	=	New (adjusted) Poisson’s ratio of dry condition corresponding to $\partial\sigma_1/\partial t = 0.1$ MPa/s
E_1	=	Elastic modulus along the major directions.
E_2	=	Elastic modulus along the intermediate directions.
E_3	=	Elastic modulus along the miner directions.
τ	=	Shear strength
σ_n	=	Normal stress
c	=	Cohesion
ϕ	=	Friction angle
τ_{oct}	=	Octahedral shear stresses
$\tau_{oct,f}$	=	Octahedral shear stresses at failure
γ_{oct}	=	Octahedral shear strains
$\gamma_{oct,f}$	=	Octahedral shear strains at failure
W_d	=	Distortional strain energy
W_m	=	Mean strain energy

SYMBOLS AND ABBREVIATIONS (Continued)

P_w	=	Pore pressure
χ	=	Empirical constant for equation (5.2)
γ	=	Empirical constant for equation (5.2)
ω	=	Empirical constant for equation (5.3)
ι	=	Empirical constant for equation (5.3)
κ	=	Empirical constant for equation (5.7)
ξ	=	Empirical constant for equation (5.7)
α	=	Empirical constant for equation (5.8)
β	=	Empirical constant for equation (5.8)
υ	=	Empirical constant for equation (5.9)
η	=	Empirical constant for equation (5.9)
λ	=	Empirical constant for equation (5.10)
φ	=	Empirical constant for equation (5.10)
a	=	Empirical constant for equation (5.14)
b	=	Empirical constant for equation (5.14)
d	=	Empirical constant for equation (5.15)
e	=	Empirical constant for equation (5.15)
f	=	Empirical constant for equation (5.25)
g	=	Empirical constant for equation (5.25)
h	=	Empirical constant for equation (5.25)

CHAPTER I

INTRODUCTION

1.1 Background and rationale

The compressive strength and deformability of decorating stones are important parameters for the design parameters in construction and building projects (Cobanoglu and Celik, 2012; Torok and Vasarhelyi, 2010; Vasarhelyi, 2005; Ludovico-Marques et al., 2012). These parameters can be applied in the design and stability analysis of geologic structures (e.g., slope embankments, dam foundation and tunnels). Water content is one of the most important factors influencing rock strength. It makes rock strength decrease remarkably after only 1% water saturation (Vasarhelyi and Van, 2006; Dyke and Dobereiner, 1991). Most of the researches have focused on the influence of water on the high porosity rocks. The effects of pore pressures on the compressive strengths and deformability of low porosity rocks have rarely been studied. Accurate measurement of the magnitudes and effects of pore pressure in low porosity rocks is however difficult.

1.2 Research objectives

The objective of this study is to experimentally determine the effects of pore pressure on the compressive strengths and elasticity of Tak granite, Lopburi marl and Lopburi marble. These rocks have been widely used as decorating and building stones. The rock strengths are determined for various stress rates and confining pressures both under dry and saturated conditions. The applied axial stresses are controlled at constant rate of 0.001, 0.01, 0.1, 1.0 and 10 MPa/s. The confining pressures are varied from 0, 3, 7, to 12 MPa. Polyaxial load frame (Fuenkajorn and Kenkhunthod, 2010) is used in this study.

The other goal of this study has been to establish a relation between the compressive strength and elastic parameters of the rock with the pore pressure. An indirect approach for determining the pore pressures in low porosity rocks is presented here. The strengths obtained from the dry testing are used to quantitatively correct the loading rate effect from the saturated strengths, and hence the true effect of pore pressure can be revealed. The results can be used to assess the mechanical stability of these decorating and building stones as applied under various moisture contents and predict the strength and deformation of rock embankments and foundations under dry and saturated conditions.

1.3 Scope and limitations

1. Laboratory experiments are conducted on Tak granite, Lopburi marl and Lopburi marble specimens.
2. The nominal dimensions of rectangular block are $50\times50\times100$ mm^3.
3. The applied loading rate varies from 0.001, 0.01, 0.1, 1 to 10 MPa/s with the confining pressures varying from 0, 3, 7 to 12 MPa.
4. The testing is performed under fully drained for the saturated specimens.
5. The testing is performed under dry and saturated conditions.
6. All tests are conducted under ambient temperature.
7. Up to 40 samples are tested for each rock type.

1.4 Research methodology

The research methodology shown in Figure 1.1 comprises 6 steps; including 1) literature review, 2) sample collection and preparation, 3) laboratory testing (uniaxial and triaxial compression test), 4) data analysis, 5) discussions and conclusions and 6) thesis writing and presentation.

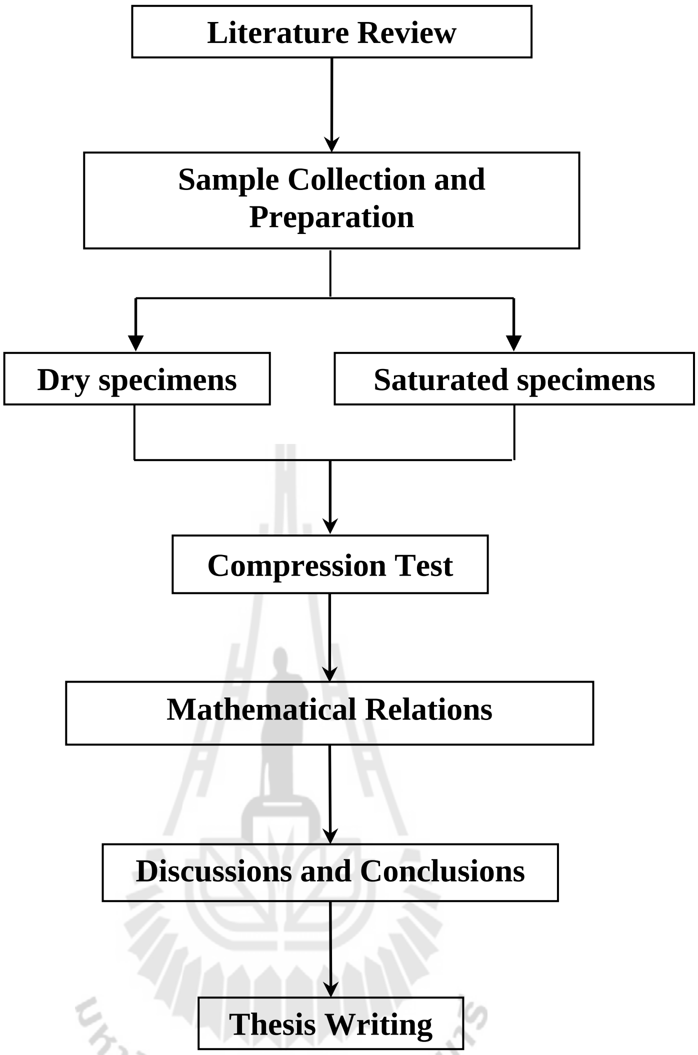

Figure 1.1 Research methodology.

1.4.1 Literature review

Literature review is carried out on experimental researches relevant to the effects of pore pressure on strengths and elasticity of rocks. The sources of information are from text books, journals, technical reports and conference papers. A summary of the literature review is given in chapter two.

1.4.2 Sample preparation

The rock samples used in this research are Tak granite, Lopburi marl and Lopburi marble. Sample preparations are carried out in the laboratory at the Suranaree University of

Technology. The specimens have been prepared to obtain rectangular blocks with nominal dimensions of $50\times50\times100$ mm^3 for the uniaxial and triaxial compression tests.

1.4.3 Laboratory test

The laboratory testing includes uniaxial and triaxial compression tests. Loading rates vary from 0.001, 0.01, 0.1, 1 to 10 MPa/s. A polyaxial load frame is used to apply confining pressures from 0, 3, 7 to 12 MPa. The test methods and calculation follow relevant ASTM standard practices. The elastic modulus and compressive strength are measured. Perforated neoprene sheets have been placed at the interface between loading platens and rock surfaces to minimize the friction for saturated condition. The tests are performed by increasing the axial stress to the rock specimen. The axial and lateral strains are measured as a function of time until failure occurs. The dial gages are installed to measure the axial and lateral strains. During the test, the axial strain, lateral strain, and time are monitored. The maximum load at the failure and failure modes are recorded.

1.4.4 Mathematical relations

Terzaghi's effect stress law equation can calculate the pore pressure in saturated rock of a rock required to initiate failure from an initial state of stress defined by the maximum principal (σ_1) isolated from the effect of loading rate and the minimum principal stress (σ_3). The result is used to determine the mathematical relation between the compressive strength and elastic parameters with the pore pressure.

1.4.5 Discussions, conclusion and thesis writing.

All study activities, methods, and results are documented and complied in the thesis.

1.5 Thesis contents

This research thesis is divided into six chapters. The first chapter includes background and rationale, research objectives, scope and limitations and research methodology. **Chapter II** presents results of the literature review to improve an understanding of the effect of pore pressure on compressive strengths and deformability of rock. **Chapter III** describes sample preparation. **Chapter IV** describes the laboratory testing. **Chapter V** presents analysis method. **Chapter VI** presents discussions, conclusions and recommendation for future studies.

CHAPTER II

LITERATURE REVIEW

2.1 Introduction

Relevant topics and previous research results are reviewed to improve an understanding the effects of pore pressure on mechanical properties of rock. These include the effects of pore pressure or water content on the compressive strengths, elastic parameters, cohesion and friction angle of rocks. The effects of loading rate on rock strength and elasticity are also investigated. Initial review results are summarized below.

2.2 Effects of pore pressure on rock

Torok and Vasarhelyi (2010) study the influence of fabric and water content on the mechanical properties of two types of Hungarian travertine, a massive less porous and a laminated porous type from north Hungary. Analyses included the determination of density, ultrasonic wave velocity, effective porosity and the uniaxial compressive strength of both air-dry and water saturated specimens. The apparent density of both dry and water saturated samples was calculated by mass volume ratio according to ISRM (1981). The determination of the effective porosity of the samples was accomplished by using water immersion method. The procedure for measuring uniaxial compressive strength (UCS) was performed according to the suggested methods of ISRM (1981), with a continuous load on the specimen of 0.5-1 MPa/s. Direct pulse transmission technique was employed to measure the ultrasonic pulse velocity. The mechanical and physical properties have been compared and the relationships between the different petrophysical constituents have been analyzed by using statistical methods. Linear correlation was found between density and ultrasonic pulse velocity of both dry and saturated samples. The massive travertine has higher density, lower porosity, higher ultrasonic pulse velocity and UCS than the laminated ones. Despite the differences in fabric of the Hungarian travertines linear regressions have been established between the air-dry and water saturated densities and air-dry and water saturated ultrasonic pulse velocities. The slopes of the lines are close to each other; therefore it can be assumed that the influence of the degree of saturation is the same for the different petrophysical parameter.

Vasarhelyi (2003) determines the unconfined compressive strength (UCS), the tangent and secant Young's modulus of 35 British sandstones tested in the dry and saturated states. Although the 35 British sandstones have different mineral contents, porosity, grain size, etc. The data for UCS and tangent/secant Young's modulus given by Hawkins and McConnell (1992) have been analysed and a linear regression established between the petrophysical constants of the dry and saturated materials. The high R^2 values show that there is a distinct relationship between the dry and saturated properties. Statistically the saturated UCS is 75.6% of the dry (Figure 2.1), while the saturated tangent and secant moduli are 76.1 and 79.0% of the dry samples respectively (Figure 2.2). The slopes of the lines are close to each other; thus it can be assumed that the influence of the degree of saturation is the same for the different petrophysical constants.

The relationship between these constants was also examined. In every case, the slopes of the lines were independent of the water content. These values were around 176 and 147 for the UCS/tangent and UCS/secant moduli respectively and about 0.82 for the E_{tan}/E_{sec} relationship (Figures 2.3 and 2.4).

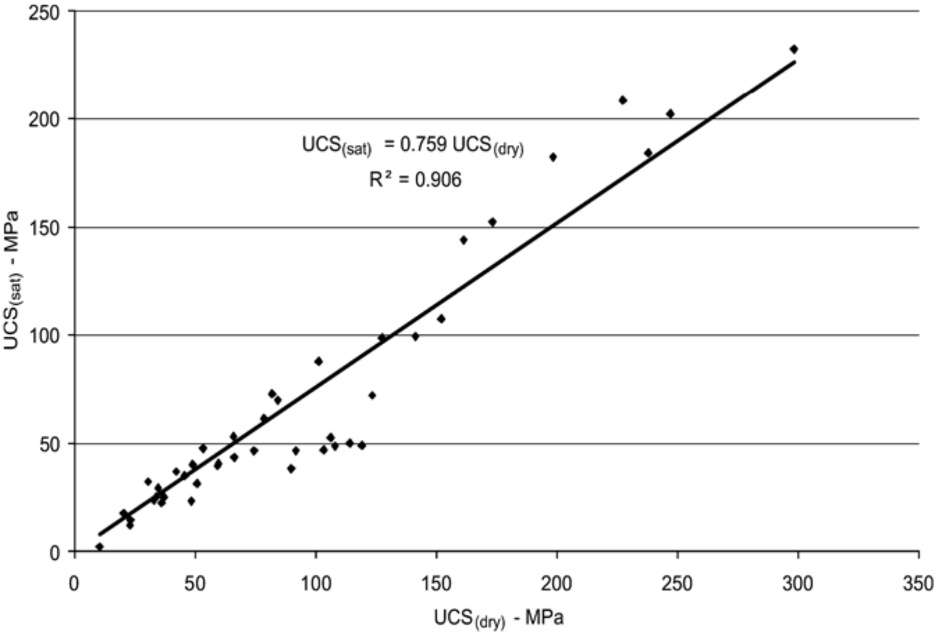

Figure 2.1 Relationships between dry and saturated UCS for 35 British sandstones (Vasarhelyi, 2003).

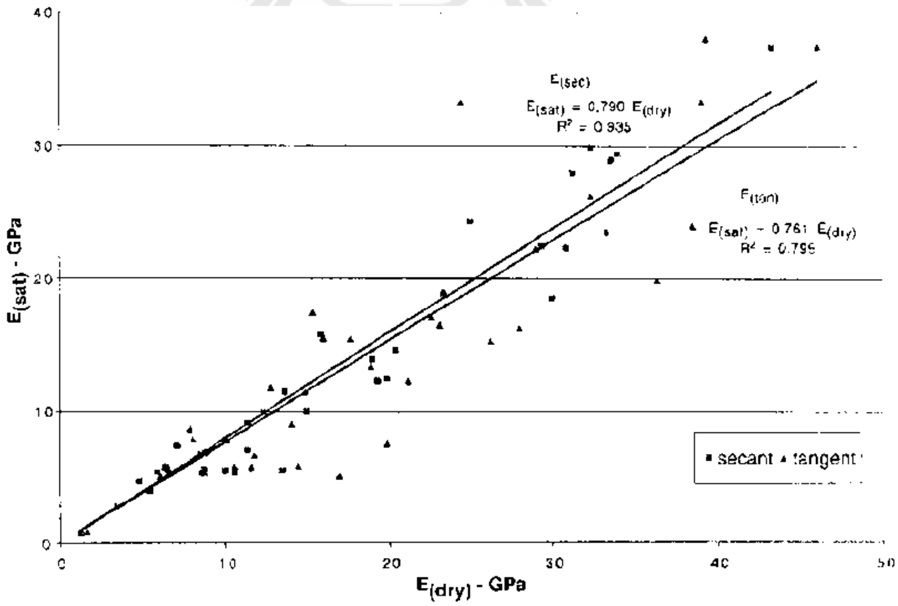

Figure 2.2 Relationships between dry and saturated Young’s modulus for 35 British sandstones (Vasarhelyi, 2003).

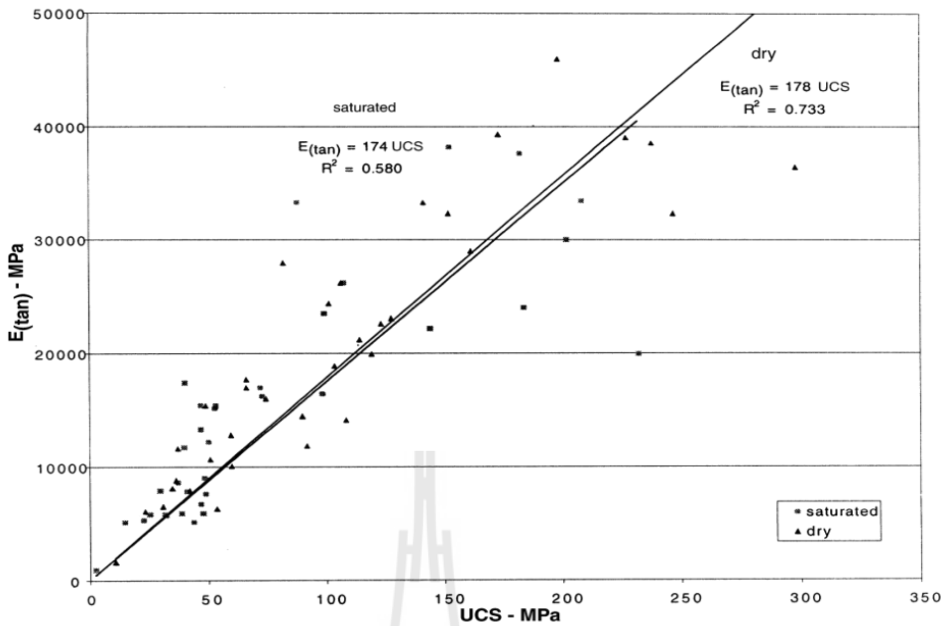

Figure 2.3 Relationships between the unconfined compressive strength (UCS) and the tangent Young's modulus (E_{tan}) in dry and saturated conditions (Vasarhelyi, 2003).

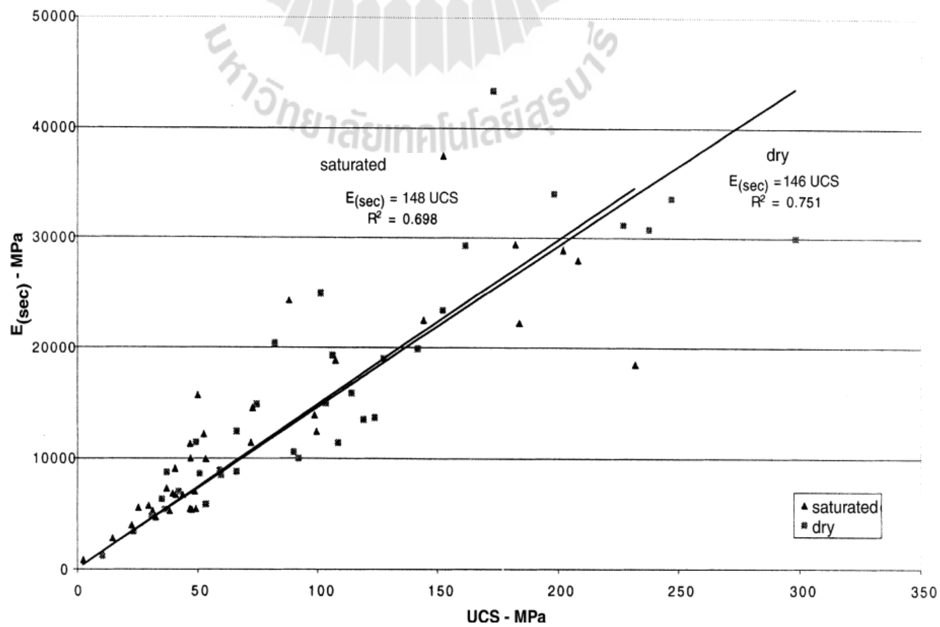

Figure 2.4 Relationships between the unconfined compressive strength (UCS) and the tangent Young's modulus (E_{sec}) in dry and saturated conditions (Vasarhelyi, 2003).

Vasarhelyi and Van (2006) study the rock strengths under dry and water saturated conditions to show a method for estimating the sensitivity of sandstone rocks to water content. From an analysis of the results of Hawkins and McConnell (1992), they found that the relationship between water content and uniaxial compressive strength could be described by an exponential equation of the form:

$$\sigma_c(w) = a \cdot \exp(-bw + c) \tag{2.1}$$

where σ_c (w) is the uniaxial compressive strength (MPa), w is the water content (%) and a, b and c are constants. Figure 2.5 shows the best-fit lines plotted for the 15 different rock types for water content values up to 5%. It is apparent that the strength of the rock is very sensitive to the water content an increase in water content of as little as 1% from the dry state can have a marked effect on strength.

The disadvantage of the analysis method of Hawkins and McConnell (1992) is that the saturated condition differs for each of the investigated sandstone. Further, the suggested fitting curve of Equation (2.1) of Hawkins and McConnell changes if the relative water content goes to infinity.

For a better representation of the moisture dependence, they suggest a recalculation of the material constants a, c, b. with the water content expressed using an absolute measure such as the degree of saturated, S. This means that for all rock, S=0 in the case of dry conditions and S=1 in the case of fully conditions.

However, they suggest a different form for the exponential function of Equation (2.1), considering that the fully saturated condition is achieved at 100% water content. In the proposed expression, given by Equation (2.2), the exponential dependence is preserved.

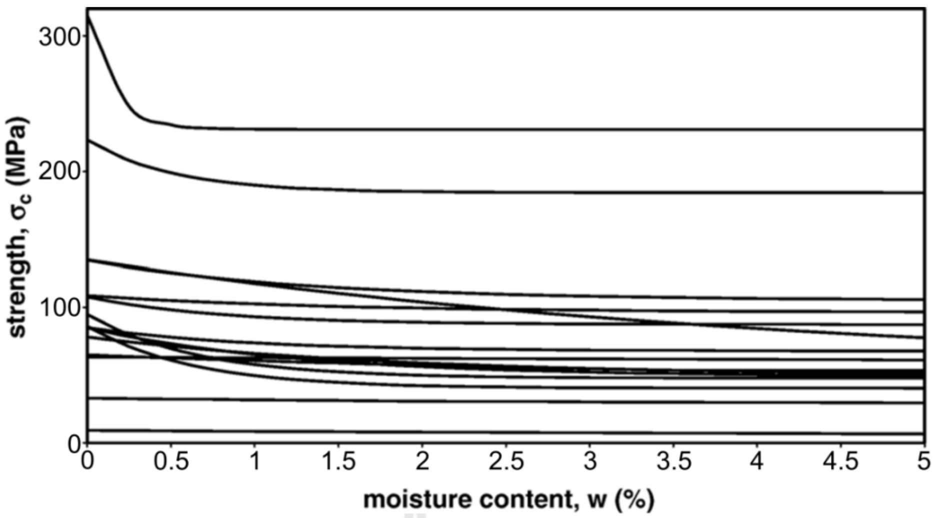

Figure 2.5 Relationships between strength (σ_c) as function of water content (w) of 15 different rock types for water content values up to 5% (Vasarhelyi and Van, 2006).

$$\sigma_c(w) = a^* + c^* e^{-b^* w} \tag{2.2}$$

$$a^* = \sigma_{co} - ((\sigma_{co} - \sigma_{csat})/1 - e^{-b^*}) \tag{2.3}$$

$$b^* = -\ln (0.1/(\sigma_{co} - \sigma_{csat})) \tag{2.4}$$

$$c^* = (\sigma_{co} - \sigma_{csat})/(1 - e^{-b^*}) \tag{2.5}$$

The strength-water content curve recalculated using the proposed expressions (Equation (2.2)) are presented at Figure 2.6. An advantage of the presented method is that less tests are necessary for calculating the influence of the water content on the rock properties. From measurements of the density and the uniaxial compressive strength in case of dry and saturated petrophysical states, the strength as a function of water content can be easily determined, both in terms of relative (i.e. water content as a percentage of the rock mass) and absolute (i.e. degree of saturation) scales.

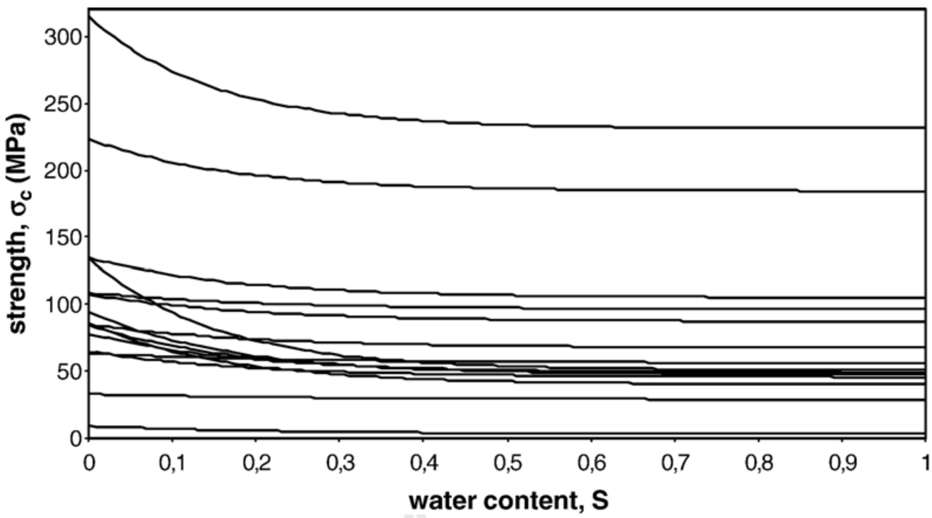

Figure 2.6 Relationships between strength (σ_c) as function of water content (s) (Vasarhelyi and Van, 2006).

Cobanoglu and Celik (2012) determine the compressive and flexural strength of Denizli travertine. In that study, 7×7×7 cm sized cube and 3×7×18 cm prism shaped samples were used for uniaxial compressive and flexural strength tests. The uniaxial compressive strength tested in the dry, saturated and freezing. The results show the saturated condition obtained UCS values are lower than dry conditions. The UCS tested travertine ranged from 9.58 MPa to 132.32 MPa for dry conditions and from 8.40 MPa to 131.11 MPa for saturated conditions. A comparison between the UCS (dry) and UCS (saturated) mean values for all 154 samples tested under uniaxial compression is plotted in Figure 2.7. Wet to dry strength ratios of travertines are ranging between 0.780 and 0.994 and the average value is 0.922. The ratio of dry UCS to UCS after freezing values ranges between 1.03 and 1.14. The relationship between dry UCS and UCS after freezing has been determined in Figure 2.8. An average values of the flexural strength under concentrated load (FLS_3) and constant moment (FLS_4) tests for the Denizli travertines were obtained as 13.78 MPa and 14.79 MPa, respectively. A schematic diagram of FLS3 and FLS4 tests is presented in Figure 2.9.

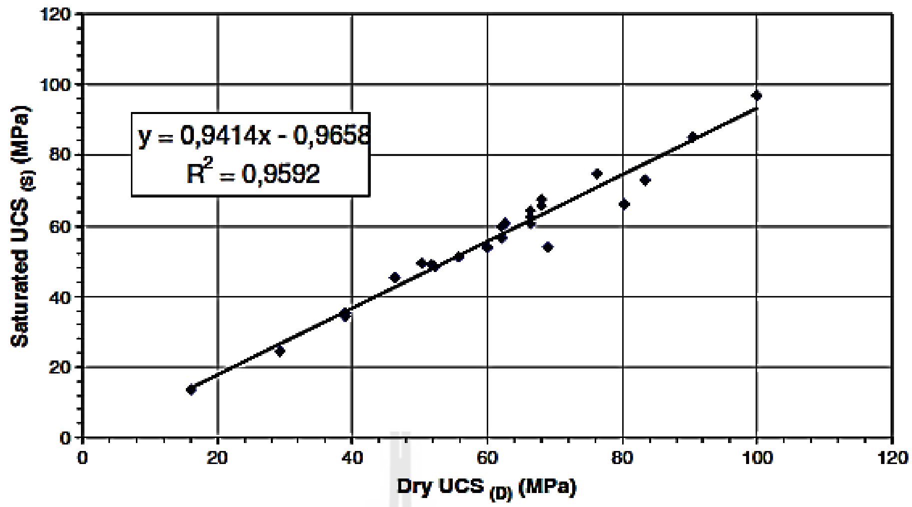

Figure 2.7 Relationships between dry and saturated UCS values of travertine (Cobanoglu and Celik , 2012).

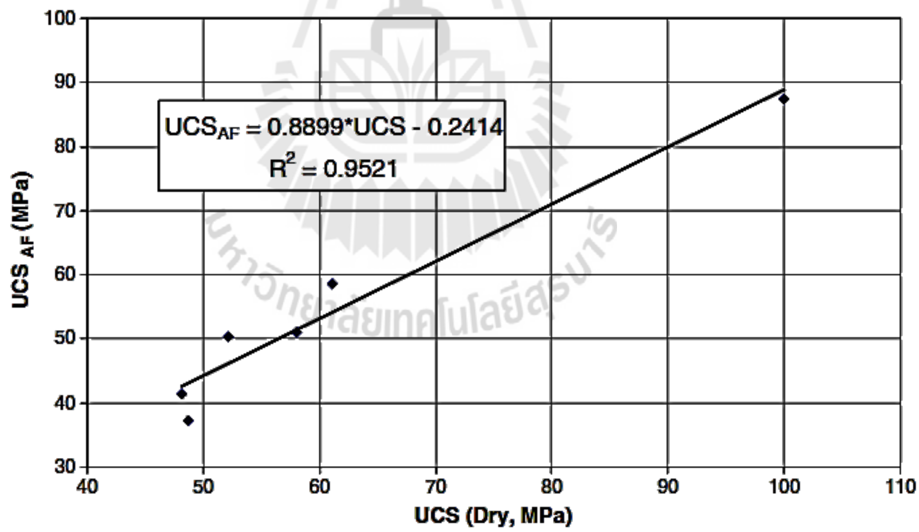

Figure 2.8 Relationships between dry UCS and UCS_{AF} (Cobanoglu and Celik, 2012).

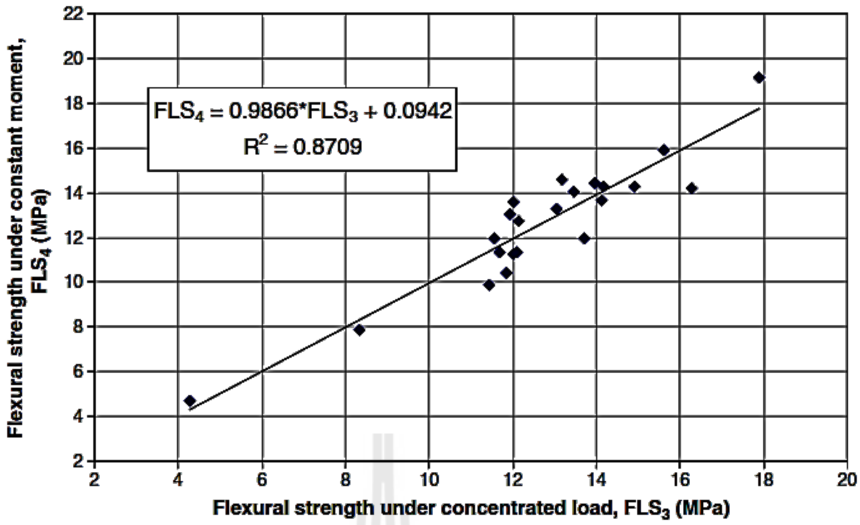

Figure 2.9 Relationships between 3 and 4 point flexural strength values of travertines (Cobanoglu and Celik , 2012).

Yilmaz (2010) study the influence of water content on the unconfined strength and elastic modulus of gypsum rock samples tested under dry and saturated conditions. UCS and E_t versus water content graphs (Figure 2.10) indicated that even a very small increase in water content (1-2) % causes a considerable loss in the strength of gypsum. The results show that the UCS and E_t of gypsum have been reduced by water immersion and that the strength of gypsum is very sensitive to water content.

The relationships between dry and saturated parameters were analyzed using correlations between $UCS_{dry} - UCS_{sat}$, $E_{t,dry} - E_{t,sat}$ (Figure 2.11) and relationships derived as expressed by empirical equations of $UCS_{sat} = 0.3492UCS_{dry}$ and $E_{t,sat} = 0.5363E_{t,dry}$. Test results revealed that as the water content increased from dried to saturated condition, the values of UCS and E_t decreased as much as, 64.07 and 53.05%, respectively. Saturated gypsum reached failure at relatively low stress compared to dry gypsum

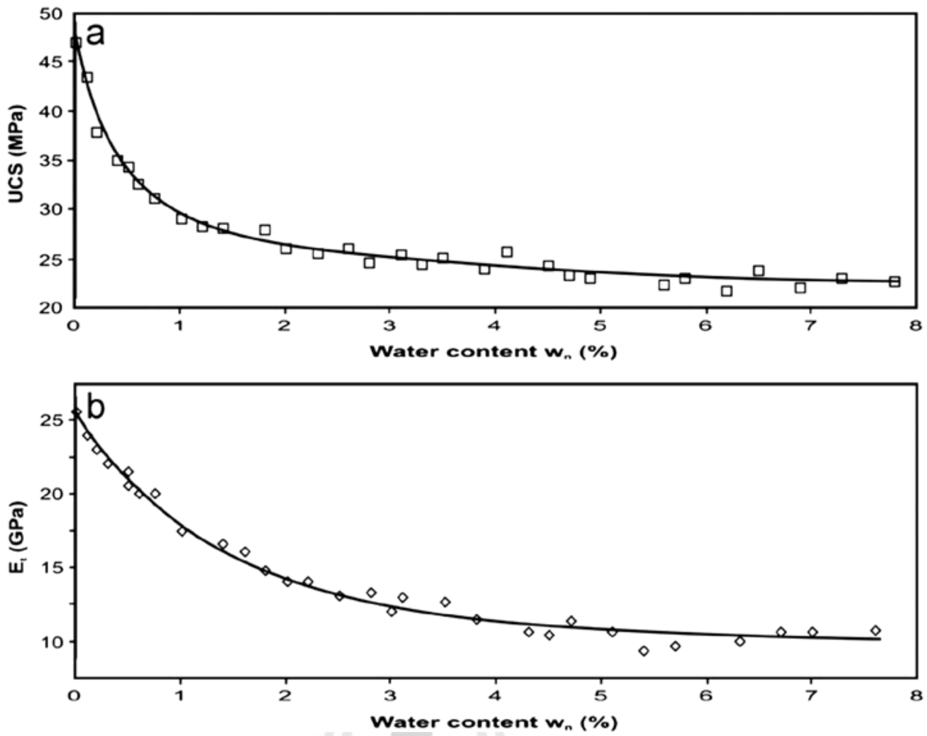

Figure 2.10 Curves of water content versus unconfined compressive strength (a) and elasticity modulus (b) (Yilmaz, 2010).

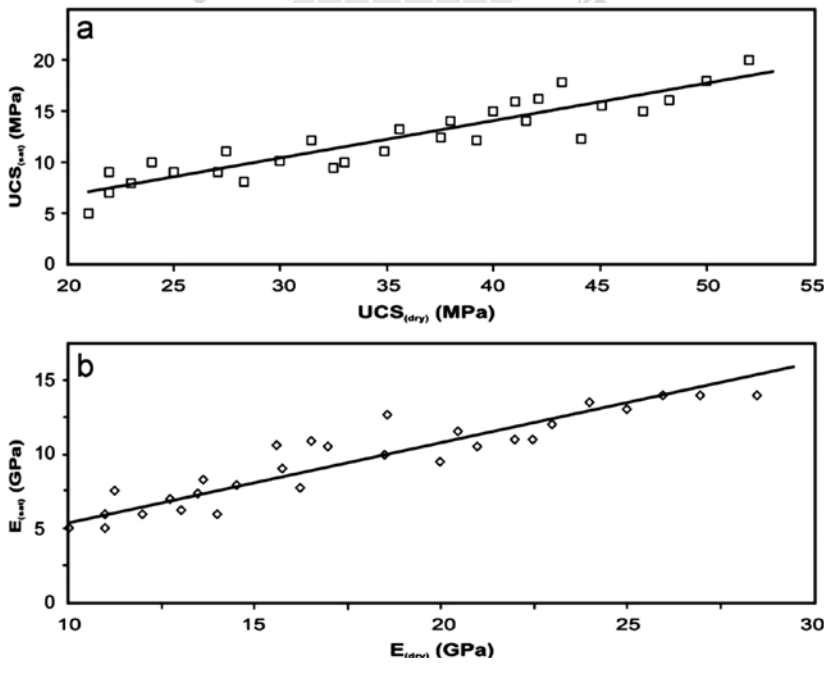

Figure 2.11 Relationships between dry and saturated unconfined compressive strength (a) and elasticity modulus (b) of gypsum samples (Yilmaz, 2010).

Masuda (2001) performs uniaxial and triaxial compressive tests using granite and andesite samples under various constant axial strain rates in dry and wet states. For constant strain-rate tests the strain rates varied from 10^{-4} to 10^{-8} s^{-1} and confining pressure varied from 0.1 to 200 MPa. Constant-stress creep tests for granite samples have been also conducted. A series of constant stress tests of the dry granite rocks were carried out under confining pressure of 50 MPa. Results of the studies show that the failure strength of granite rocks decreased linearly as the logarithm of the strain rate decreased (Figure 2.12). The strain rate dependence of the failure strength is increased at higher confining pressures. The strain rate effect is more apparent on the failure strengths of wet than dry samples in a lower confining pressure range.

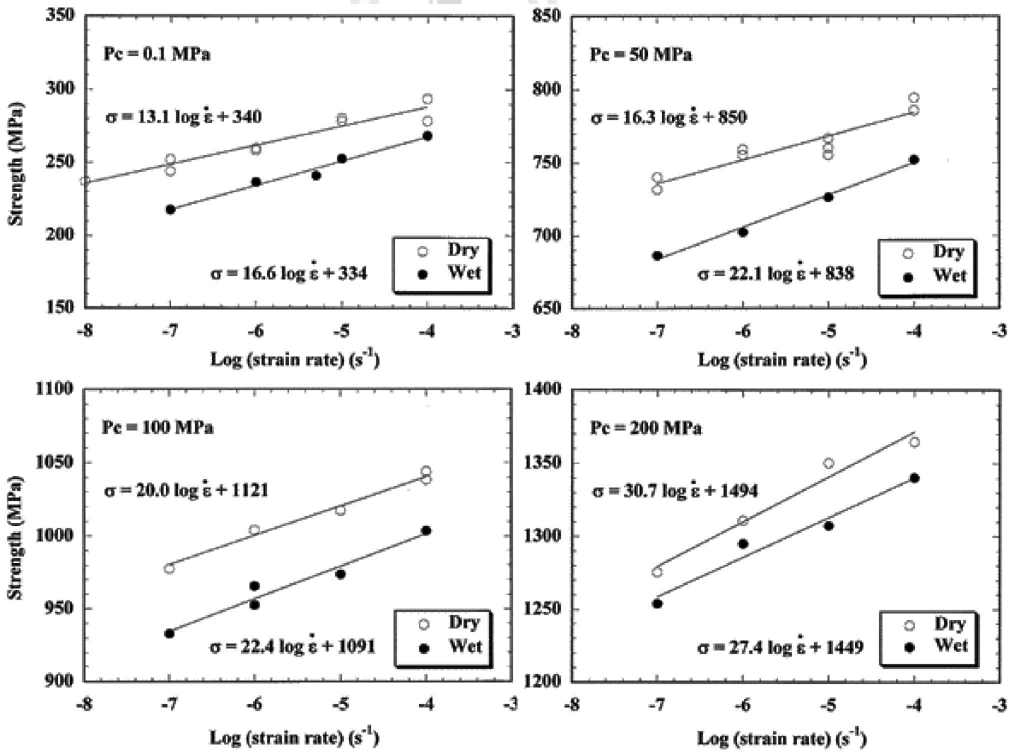

Figure 2.12 Compressive strength of granitic rocks as a function of strain rates under the varied confining pressures (Masuda, 2001).

Similar effects of water and confining pressure on the strain rate dependence of fracture strength were observed in another series of experiments on andesite rocks. In the constant-stress creep experiments, the creep failure strength decreased as the logarithm of the time to failure increased. Figure 2.13 shows the relation between the applied stress and time to failure observed in this study. The least squares fit of the equation below in applied:

$$\sigma_c = -E \log t_f + F \tag{2.6}$$

where E and F are constant values.

Vasarhelyi (2005) determine the effect of water content on rock strength. The samples tested in both dry and saturated conditions: apparent density, uniaxial compressive strength, tensile strength and elastic modulus. Right circular cylinders were prepared, according to the ISRM suggested methods (ISRM, 1978a), with a diameter of 54 mm and with height to diameter ratio 2:1. Standard values of the uniaxial compressive strength (σ_c) and of the tangent modulus of elasticity (E) were obtained in conjunction with the complete stress-strain curve.

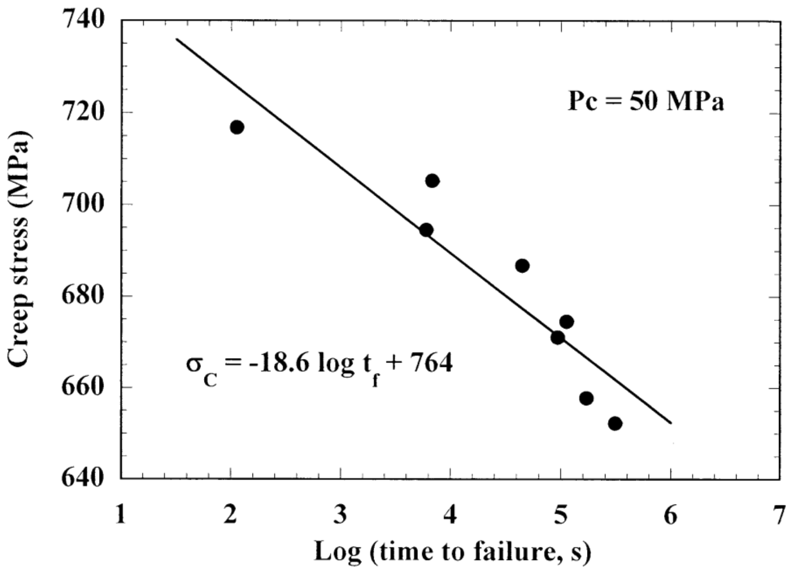

Figure 2.13 Creep stresses of granite rocks and time to failure (Masuda, 2001).

Also, Brazilian tests were performed to determine the indirect tensile strength (σ_t) according to the ISRM (1978b) suggested method. The diameter of the samples was 54mm, with a height to diameter ratio 1:1. The Miocene limestone is a soft rock with a high, variable porosity (14–52%). The measured strength under saturated conditions is plotted as a function of the strength under dry conditions in. It appears that the saturated strength is linearly related to the dry strength. The slope of the trend line is nearly the same for uniaxial compressive and tensile strength –0.659 (R^2 = 0.884) and 0.667 (R^2 = 0.826); thus it can be concluded that:

$$\sigma_{sat} = 0.659\sigma_{dry} \quad (R^2 = 0.933) \tag{2.7}$$

The relationship between the values at the elastic modulus measured under saturated and dry conditions expressed by empirical equations of. relationships $E_{(sat)} = 0.657\ E_{(dry)}$ The ratio of the uniaxial compressive strength to the Brazilian tensile strength under dry and saturated conditions are similar: 0.129 (R^2 = 0.741) and 0.136 (R^2 = 0.886) in case of dry and saturated conditions, respectively. The other goal of this work has been to establish a connection between the density of the limestone and the measured petrophysical parameters. The uniaxial compressive strength was represented as a function of density as shown in Figure 2.14. Using the least squares fitting method a relation of the following form was found:

$$\sigma = ae^{b\rho} \tag{2.8}$$

where a and b are material constants, ρ is the density (in dry or saturated petrophysical states) and σ is the measured strength. The same equation can be used for both the tensile strength and the elastic modulus. Table 2.1 summarizes these material constants and gives the calculated R^2 values for the considered petrophysical parameters.

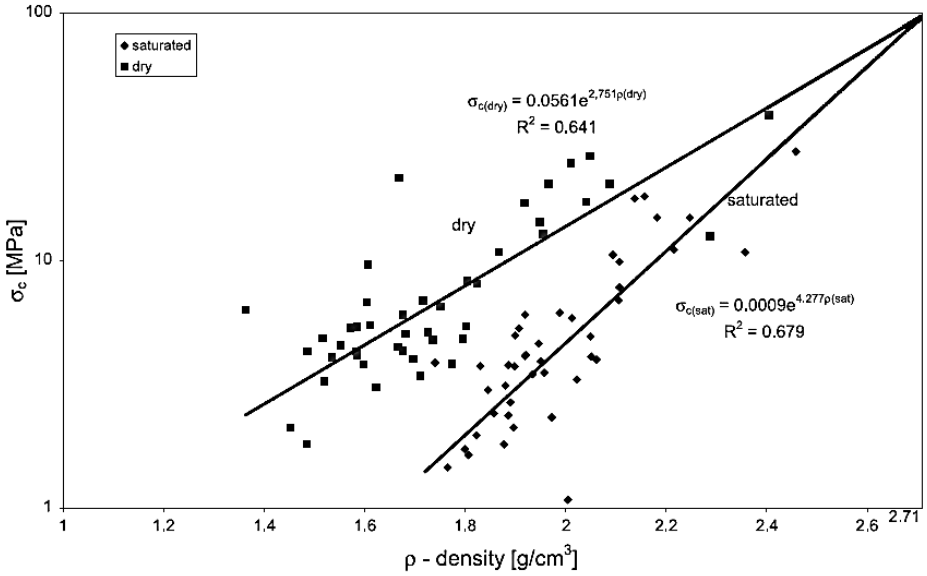

Figure 2.14 The uniaxial compressive strength (σ_c) as function of density (ρ) in case of dry and saturated petrophysical states (Vasarhelyi, 2005).

Table 2.1 The measured material constants for Equation (2.8) in case of dry and saturated conditions (Vasarhelyi, 2005).

	a		*b*		R^2	
	Dry	Saturated	Dry	Saturated	Dry	Saturated
σ_c	0.0561	0.0009	2.751	4.277	0.641	0.679
σ_t	0.0039	0.00009	3.135	4.379	0.573	0.567
E	0.0088	0.0005	3.126	4.063	0.660	0.578

Li et al. (2012) study the influence of water content and anisotropy on the strength and deformability of two meta-sedimentary rocks by triaxial compressive tests. These specimens were separated into four main groups, which were meta-siltstone in dry condition, meta-siltstone in wet condition, meta-sandstone in dry condition and meta-sandstone in wet condition. The specimens in each group were then tested in multiple subgroups under four different confining pressures. The water contents of both tested rocks are very low, for instance, 0.17% for meta-siltstone and 0.10% for meta-sandstone. The triaxial compressive strength generally increased with increasing confining pressures. Meanwhile, the water content affected the triaxial compressive strength and deformability of rocks. Based on the Mohr–Coulomb failure criterion, it was found that the cohesion increased and friction angle decreased from dry to wet conditions for both tested rock types. Based on the Hoek–Brown failure criterion, the Hoek–Brown constant of m_i was found to decrease 45% for wet meta-siltstone and decrease 25% for wet meta-sandstone. The influence of water on deformability of tested rocks is reflected as a reduction of Young's modulus and increase of Poisson's ratio, which indicates that the wet meta-sedimentary rocks will deform more than that of the dry ones under the same stress condition.

Hawkins and McConnell (1992) determine the influence of the water content on the strength of 35 sandstones (Figure 2.15). They found that the relationship between water content and uniaxial compressive strength could be described by an exponential equation of the form

$$\sigma_c(w) = ae^{-bw + c} \tag{2.9}$$

where σ_c (w) is the uniaxial compressive strength (MPa), w is the water content (%) and a, b and c are constants. It is obvious that the strength at zero water σ_{c0} = a +c, the strength at full saturation σ_{csat} = c. The parameter b is a dimension less constant defining the rate of strength loss with increasing water content.

Li and Reddish (2004) present the preliminary results from laboratory based tests carried out on UK coal strata, aimed at quantifying the effects of water on rock properties, particularly on broken rocks, which are common in the subsidence overburden post mining. This approach specifically refers to the UCS, UTS and the relationship between time and water content of intact and broken rocks. Comparisons are made between these two rock conditions. The experimental results and analytic solutions show that more water can

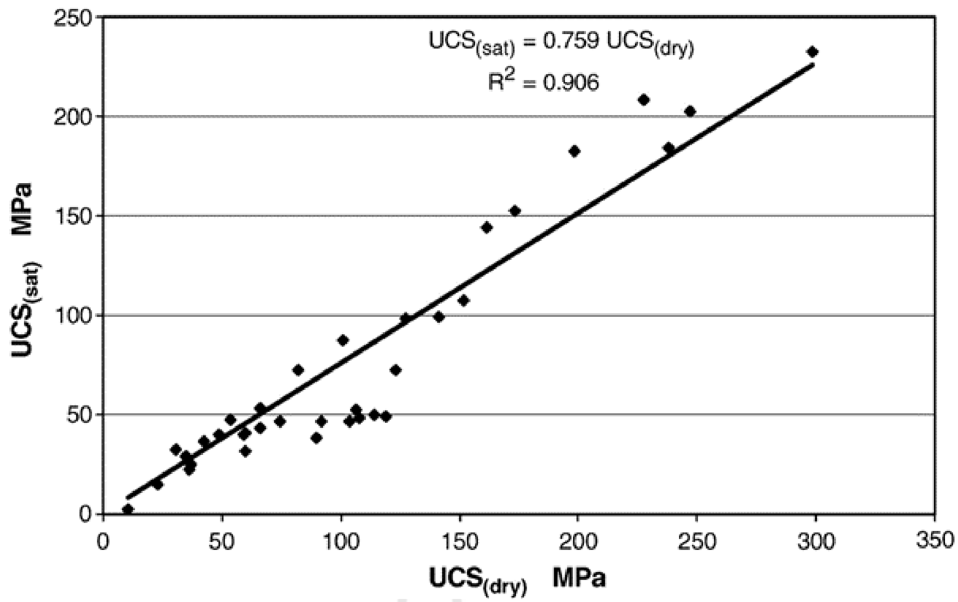

Figure 2.15 Relationships between dry and saturated uniaxial compressive strength (UCS) for 35 British sandstones (Hawkins and McConnell, 1992).

penetrate into broken rocks within shorter time. The strength of rocks can be deteriorated due to water or breaking. The water can make already broken rocks fail more easily. Also, proportionately more strength will be lost due to breaking when rocks are saturated. The state, intact or broken, appears to predominantly control the friction angle. The degree of saturation controls the cohesion. Further work is being undertaken on testing the strength of rocks at various moisture contents.

Palchik and Hatzor (2004) determine the uniaxial compressive strength, poin load strength, and indirect tensile (Brazilian) strength of a very porous chalk formation. The validity of the porosity calculation was confirmed by measuring grain volume using a Helium porosimeter. It was established that the point load strength and uniaxial compressive strength in porous Adulam chalks decrease with increasing porosity, while the same effect of porosity on Brazilian tensile strength was present but not significant. Two exponential models relating porosity to uniaxial and point load strengths are proposed (Figures 2.16 and 2.17).

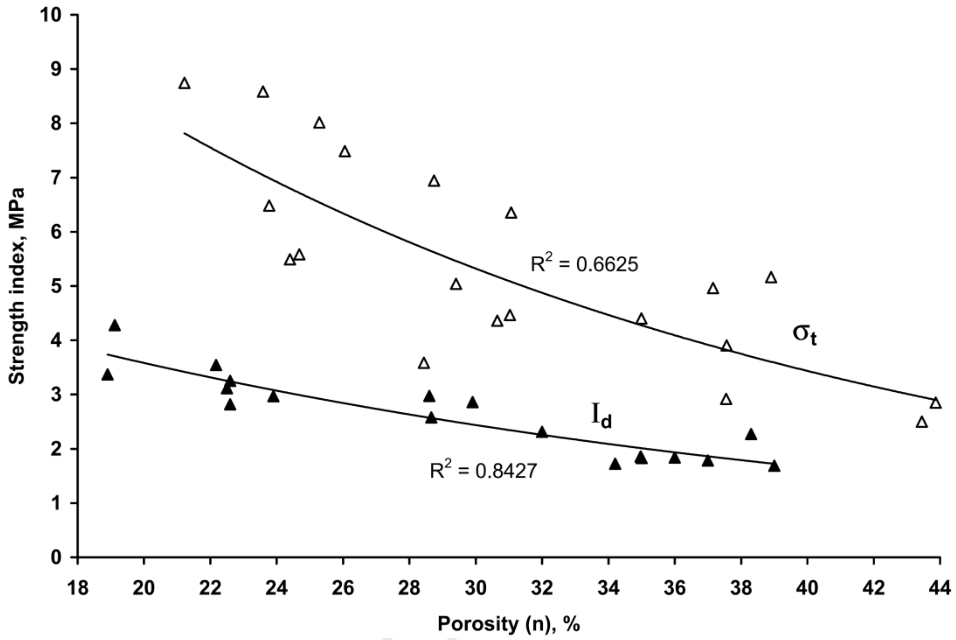

Figure 2.16 Influence of porosity on point load strength and Brazilian strength (Palchik and Hatzor, 1999).

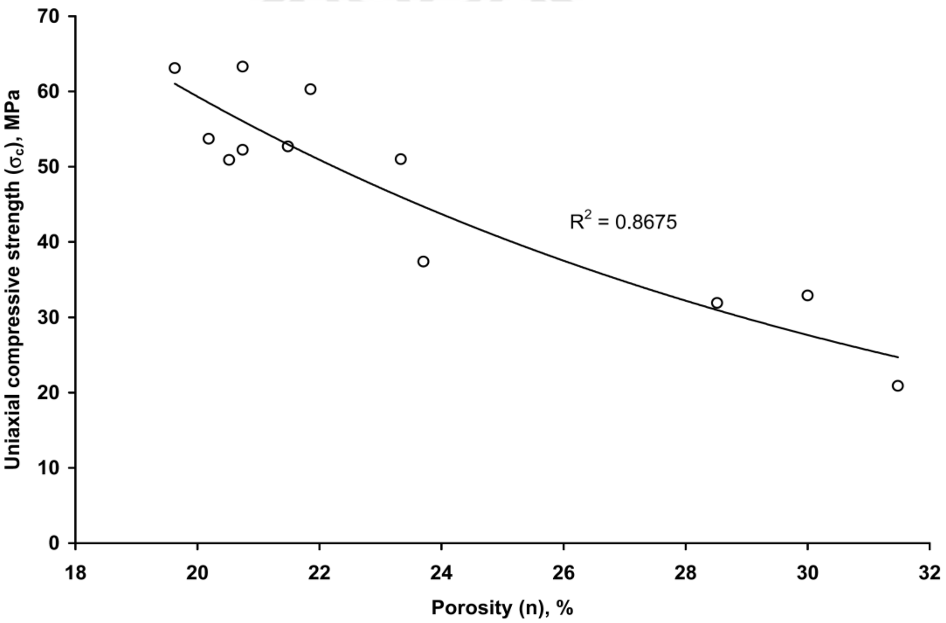

Figure 2.17 Influence of porosity on uniaxial compressive strength (Palchik and Hatzor, 1999).

2.3 Effects of loading rate on compressive strength and elastic parameters

Li et al. (1999) study the effects of strain rate on rock material properties under triaxial compression on the Bukit Timah granite of Singapore. A samples were tested at four strain rates (10^{-4} to 10^{-1}) and six confining pressures (20, 50, 80, 110, 140 and 170 MPa). The test results show that the compressive strength generally increases with increasing strain rate and confining pressure, as shown in Figures 2.18 and 2.19. The rate of increment of compressive strength with strain rate is lower at higher confining pressure. The results for the Young’s modulus and the Poisson’s ratio at different strain rates and confining pressure are scattered. The Young’s modulus seems to increase slightly with increasing confining pressure, but appears to be unaffected by strain rate. The Poisson’s ratio seems to increase slightly with increasing strain rate and confining pressure. Further tests are needed to overcome the scattering of the results and to obtain conclusive indications on the possible changes of the Young’s modulus and the Poisson’s ratio.

Kenkhunthod and Fuenkajorn (2010) study the influence of loading rate on deformability and compressive strength of three Thai sandstones. Uniaxial and triaxial compressive strength tests have been performed using a polyaxial load frame to assess the influence of loading rate on the strength and deformability of three Thai sandstones. The applied axial stresses are controlled at constant rates of 0.001, 0.01, 0.1, 1.0 and 10 MPa/s. The confining pressures are maintained constant at 0, 3, 7 and 12 MPa. The sandstone strengths and elastic moduli tend to increase exponentially with the loading rates. The average Poisson’s ratios are 0.36, 0.38 and 0.15 for the PP, PW and PK sandstones, respectively. They tend to be independent of the loading rates. Post-test observations indicate that under confining pressures of 7 MPa or less, the specimens fail by a combination of compressive shear and splitting tension modes. Under the confining pressure of 12 MPa extension fractures dominate. An empirical loading rate dependent

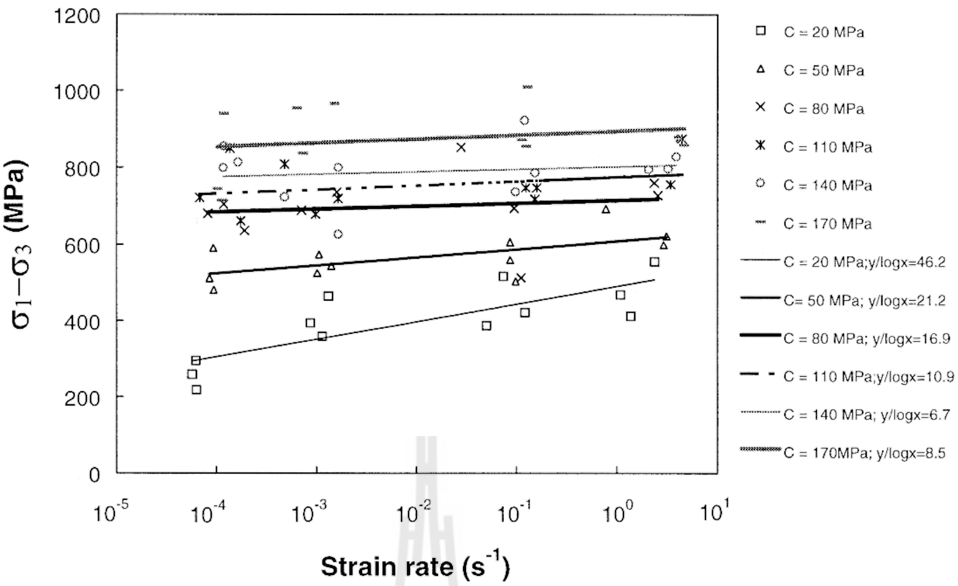

Figure 2.18 Variation of the compressive strength with the strain rate at different confining pressure (Li et al., 1999).

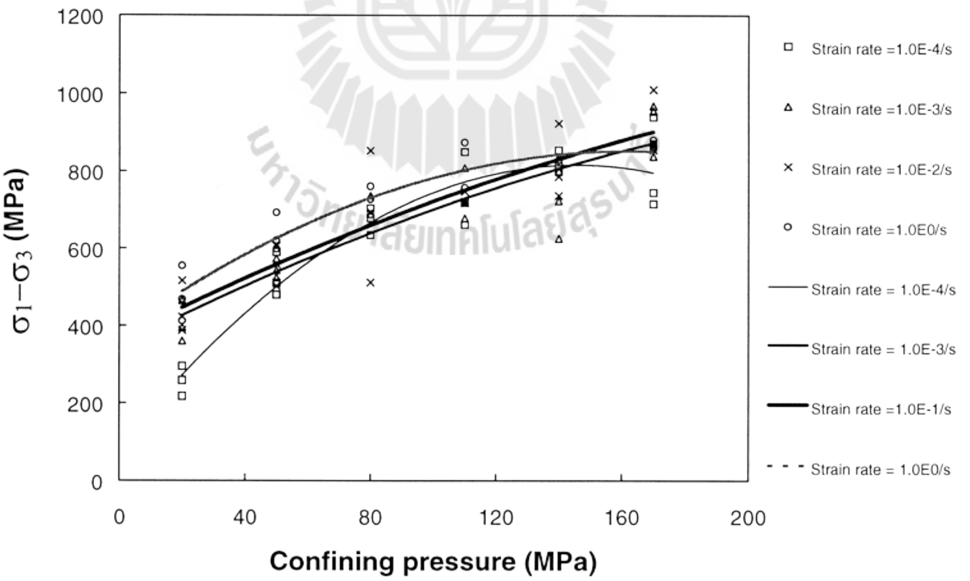

Figure 2.19 Variation of the compressive strength with the confining pressure at different strain rates (Li et al., 1999).

formulation of both deformability and shear strength is developed for the elastic and isotropic rocks. It is based on the assumption of constant distortional strain energy of the rock at failure under a given mean normal stress. The proposed multiaxial criterion well describes the sandstone strengths within the range of the loading rates used here. It seems reasonable that the derived loading rate dependent equations for deformability and shear strength are transferable to similar brittle isotropic intact rocks.

Fuenkajorn et al. (2012) study the effects of loading rate on strength and deformability of the Maha Sarakham salt. The uniaxial and triaxial compression tests have been performed to assess the influence of loading rate on the compressive strength and deformability of the Maha Sarakham salt. The lateral confining pressures are maintained constant at 0, 3, 7, 12, 20 and 28 MPa while the axial stresses are increased at constant rates of 0.001, 0.01, 0.1, 1.0 and 10 MPa/s until failure occurs. It was also found that the salt elasticity and strength increase with the loading rates, as shown in Figure 2.20. The elastic (tangent) modulus determined at about 40% of the failure stress varies from 15 to 25 GPa, and the Poisson's ratio from 0.23 to 0.43. The elastic parameters tend to be independent of the confining pressures. The strains induced at failure decrease as the loading rate increases.

Ray et al. (1999) describe the effect of cyclic loading and strain rate on the mechanical behavior of sandstone. The results indicate that the percentage decrease in uniaxial compressive strength was found to increase with the increase in applied stress level and direct proportionality between the two parameters was found. The uniaxial compressive strength of Chunar sandstone was determined at strain rates of 2.5×10^{1}/s, 2.5×10^{0} and 2.5×10^{-1}/s and found to be 99.5 MPa, 75.1 MPa and 64.0 MPa, respectively (Figure 2.21). A clear increase in uniaxial compressive strength was, therefore, observed with increase in strain rate. The failure strength was found to increase with the increase of strain rate and an abrupt increase in strength was noticed at the strain rate of 2.5×10^{1}/s. Fatigue stress was found to increase with the increase in strain rate and Young's modulus was found to increase with the increase in strain rate (Figure 2.22).

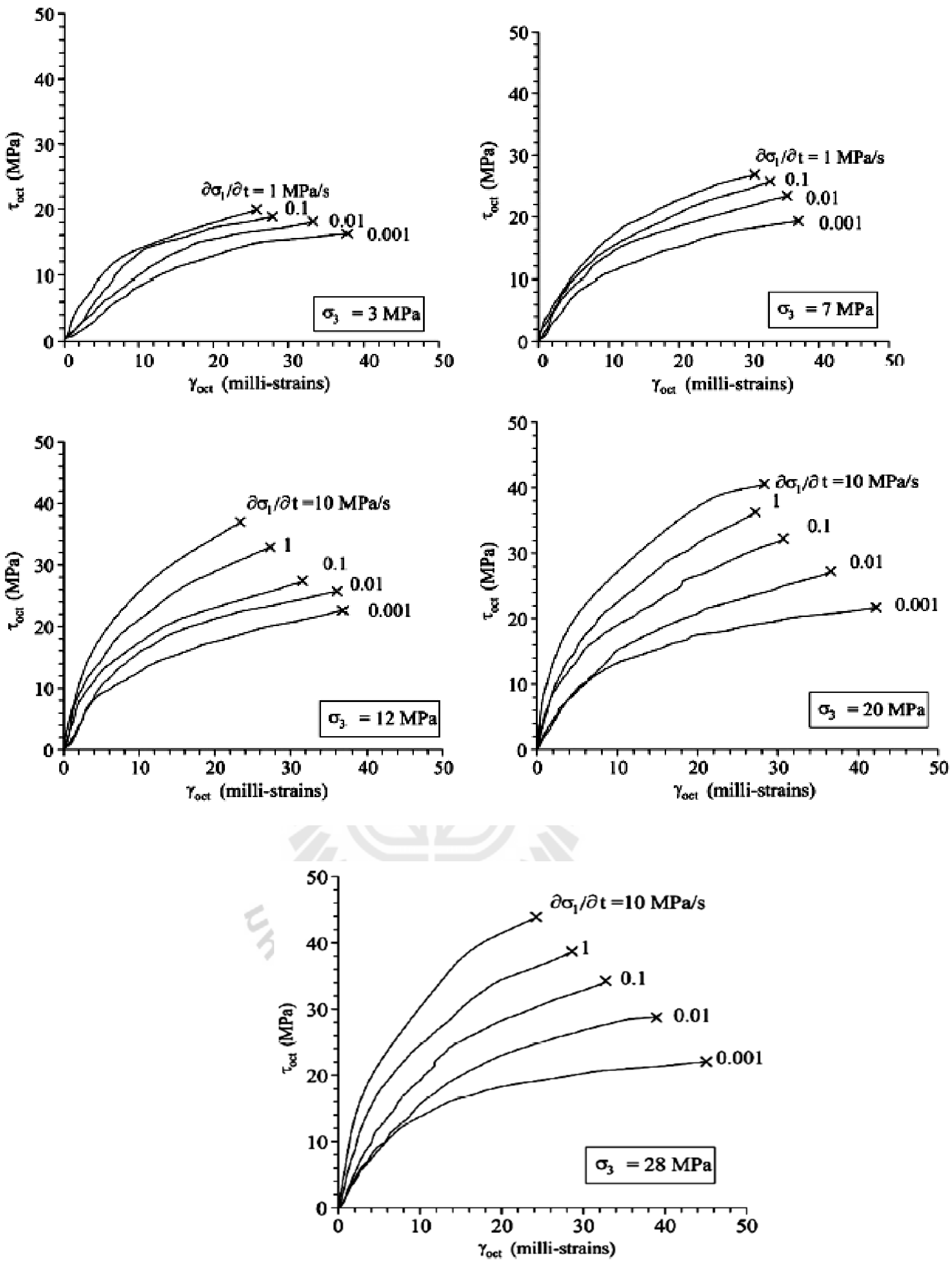

Figure 2.20 Octahedral shear stress (τ_{oct}) as a function of octahedral shear strain (γ_{oct}) for various confining pressures (σ_3) and loading rates ($\partial\sigma_1/\partial t$) (Fuenkajorn et al., 2012).

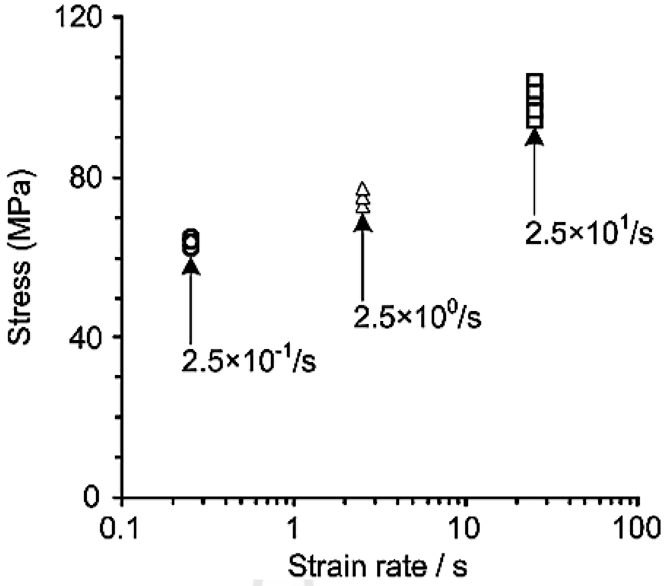

Figure 2.21 Stress as function of strain rate (Ray et al., 1998).

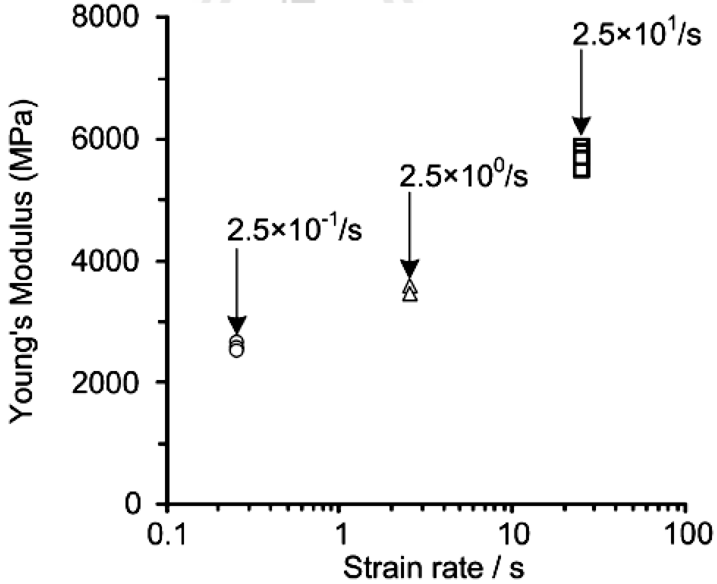

Figure 2.22 Young's modulus as function of strain rate (Ray et al., 1998).

2.4 Conclusion of review

The pore pressure can reduce the strength of rock. The rock compressive strengths decrease significantly as the water content increases. In term of deformability, the pore pressure is also reflected as a reduction of Young's modulus and increase of Poisson's ratio, which indicates that the saturated rocks will deform more than that of the dry ones under the same stress condition. Based on the Mohr–Coulomb failure criterion, it was found that the cohesion increased and friction angle decreased from dry to wet conditions. The rock compressive strength decreased with the loading rate and increased with the confining pressure under the same loading rate. A general trend of Young’s modulus increases with increasing loading rate and tend to be independent of the confining pressure. The Poisson’s ratios tend to be independent of the loading rate and confining pressure.

CHAPTER III

SAMPLE PREPARATION

3.1 Introduction

This chapter describes the rock sample preparation. The types of rock used in this study are also popular for use as a decorating stone in towers, monuments, temples, footpath and houses. The rock samples used in this study are Tak granite (Atherton et al., 1992), Lopburi marl and Lopburi marble (Bunopas, 1992) which were from different parts of Thailand (Figure 3.1). Their mechanical properties play a significant role in the stability of building and foundation construction.

3.2 Sample preparation

The specimens have been prepared to obtain rectangular blocks with nominal dimensions of $50\times50\times100$ mm^3 for the compression tests (Figure 3.2). A minimum of 40 specimens are prepared for each rock types. The specimens are cut and ground to obtain the perpendicularity and parallelism to comply with the (ASTM D4543-85). They are prepared to test under dry and fully saturated conditions. Under dry condition the specimen are over dried for 24 hours before testing. Under saturated condition, each rock specimens are submerged under water in pressure vacuum chamber until its weight becomes unchanged. These specimens are referred to as saturated specimens (Figure 3.3). The granite, marl and marble have average water contents ($w_{ave.}$) of 0.14%, 2.71% and 0.09% respectively (Figure 3.4). Tables 3.1 through 3.6 shows the dimensions and weigh of the specimen under dry and saturated conditions.

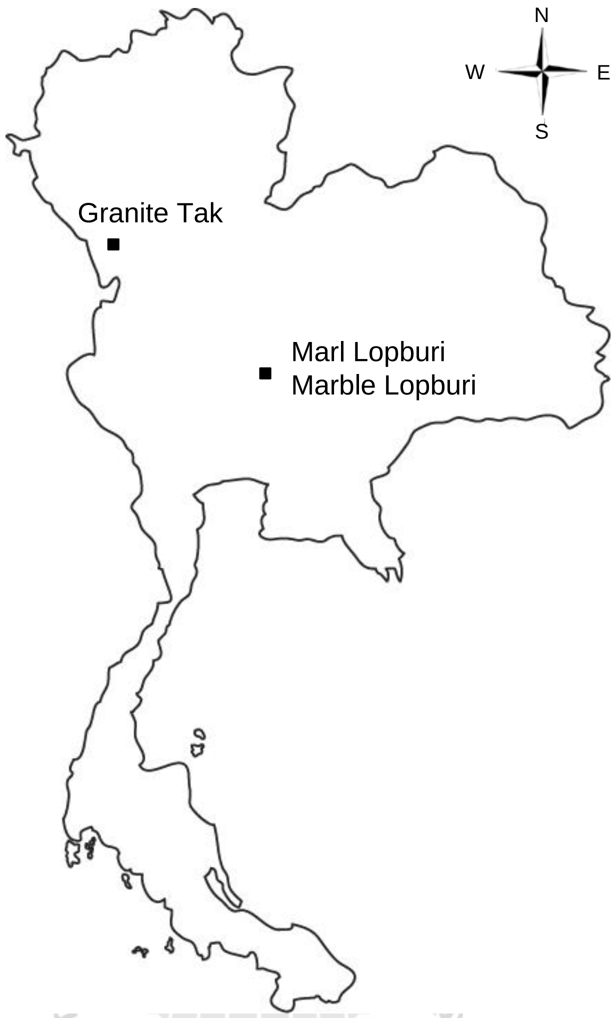

Figure 3.1 Area of rock tested in this study.

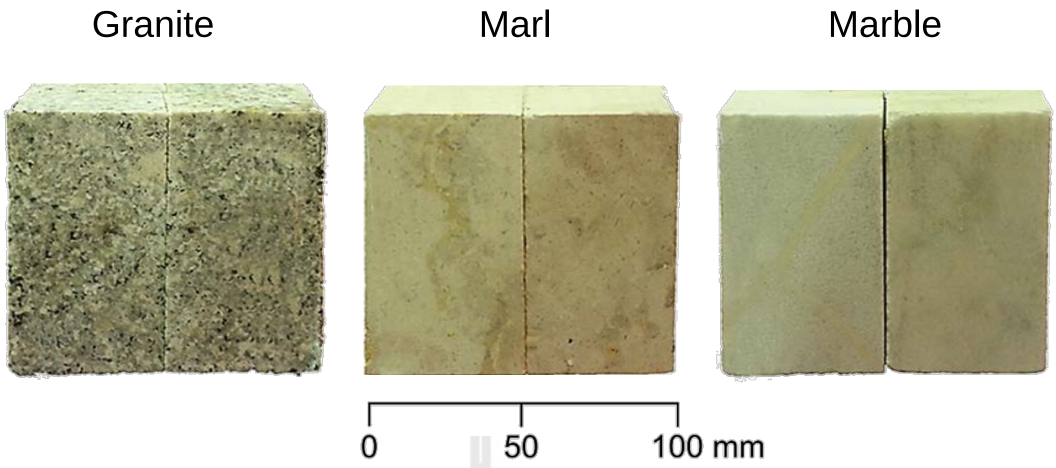

Figure 3.2 Some rectangular block specimens of granite, marl and marble used in the triaxial testing.

Figure 3.3 Saturated rock specimens submersed under water in vacuum chamber.

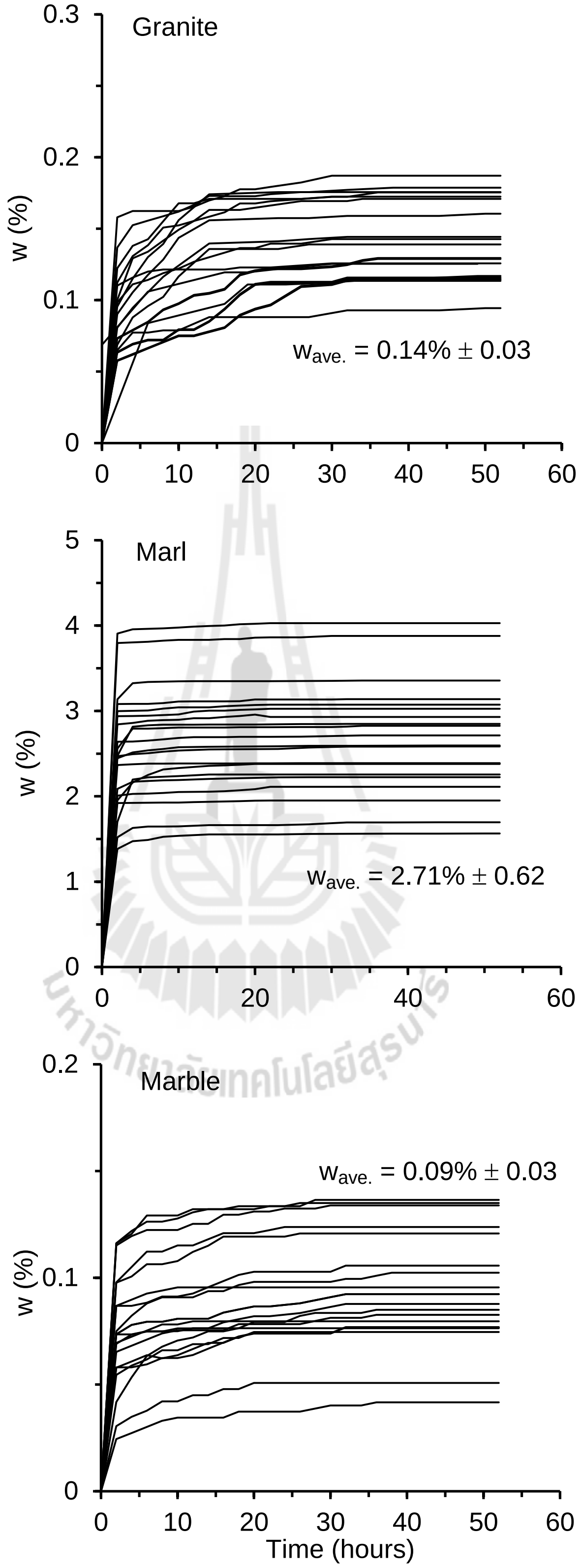

Figure 3.4 Water contents as function of time.

Table 3.1 Dry granite specimens prepared for triaxial compression test.

Specimen No.	Weigh (g)	Dimension (cm^3)	Dry density (g/cc)
GR-01-Dry	670.35	50.80×49.40×99.90	2.67
GR-02-Dry	667.70	51.90×49.28×99.44	2.63
GR-03-Dry	669.43	50.08×50.36×100.00	2.65
GR-04-Dry	668.30	50.90×50.00×100.00	2.63
GR-05-Dry	667.05	50.50×49.64×99.92	2.66
GR-06-Dry	670.92	49.44×49.86×99.76	2.73
GR-07-Dry	678.65	50.10×50.74×100.00	2.67
GR-08-Dry	679.15	49.90×51.00×100.72	2.65
GR-09-Dry	673.31	50.24×50.34×99.70	2.67
GR-10-Dry	675.29	50.00×50.40×99.62	2.69
GR-11-Dry	671.43	50.40×49.50×100.00	2.69
GR-12-Dry	652.96	50.00×49.34×99.62	2.66
GR-13-Dry	663.77	50.00×50.44×100.00	2.63
GR-14-Dry	669.51	49.72×50.90×100.10	2.64
GR-15-Dry	655.52	49.56×50.04×99.90	2.65
GR-16-Dry	671.69	49.80×50.80×100.00	2.66
GR-17-Dry	667.49	50.00×50.56×99.74	2.65
GR-18-Dry	681.91	50.16×51.50×99.84	2.64
GR-19-Dry	662.77	50.16×50.24×100.08	2.63
GR-20-Dry	654.94	49.82×49.72×100.56	2.63

Table 3.2 Saturated granite specimens prepared for triaxial compression test.

Specimen No.	Weigh (g)	Dimension (cm^3)	Wet density (g/cc)	Water content (%)
GR-21-Sat	676.00	50.66×51.18×100.20	2.60	0.125
GR-22-Sat	667.18	50.00×50.46×100.64	2.63	0.117
GR-23-Sat	678.82	50.18×51.30×100.28	2.63	0.090
GR-24-Sat	646.42	48.84×49.40×101.86	2.63	0.178
GR-25-Sat	660.37	49.40×50.00×102.00	2.62	0.139
GR-26-Sat	625.80	49.34×48.24×99.00	2.66	0.144
GR-27-Sat	644.30	49.40×49.90×99.74	2.62	0.161
GR-28-Sat	654.19	49.30×49.50×102.00	2.63	0.170
GR-29-Sat	646.12	48.80×49.70×99.50	2.68	0.171
GR-30-Sat	660.84	49.00×49.70×101.80	2.67	0.175
GR-31-Sat	647.76	49.00×49.70×100.70	2.64	0.142
GR-32-Sat	637.69	48.20×50.00×99.40	2.66	0.187
GR-33-Sat	649.59	50.00×49.60×100.50	2.61	0.110
GR-34-Sat	649.92	50.00×49.80×100.40	2.60	0.113
GR-35-Sat	630.40	50.20×48.55×99.50	2.60	0.129
GR-36-Sat	635.99	49.10×50.00×99.85	2.59	0.175
GR-37-Sat	695.90	51.24×50.86×100.22	2.66	0.125
GR-38-Sat	695.73	50.40×51.20×102.26	2.64	0.120
GR-39-Sat	694.68	51.06×51.00×110.10	2.42	0.114
GR-40-Sat	675.62	51.70×49.70×100.70	2.61	0.128

Table 3.3 Dry marl specimens prepared for triaxial compression test.

Specimen No.	Weigh (g)	Dimension (cm^3)	Dry density (g/cc)
MR-01-Dry	620.51	50.20×49.60×99.62	2.50
MR-02-Dry	637.54	49.56×50.10×100.20	2.56
MR-03-Dry	628.23	50.60×49.62×100.20	2.50
MR-04-Dry	639.82	49.90×50.00×99.60	2.57
MR-05-Dry	629.17	50.00×50.00×99.70	2.52
MR-06-Dry	614.96	49.80×50.20×99.50	2.47
MR-07-Dry	601.41	49.72×50.10×99.40	2.43
MR-08-Dry	604.68	50.00×49.80×100.00	2.43
MR-09-Dry	633.06	50.50×50.00×99.80	2.51
MR-10-Dry	616.39	49.64×50.00×99.60	2.49
MR-11-Dry	606.48	49.74×49.28×99.90	2.48
MR-12-Dry	642.62	51.00×50.50×100.20	2.49
MR-13-Dry	643.82	51.00×49.80×99.60	2.55
MR-14-Dry	612.56	49.70×50.00×99.50	2.48
MR-15-Dry	637.43	50.00×50.40×99.62	2.54
MR-16-Dry	633.97	50.00×50.20×100.00	2.53
MR-17-Dry	595.40	50.30×49.80×99.70	2.38
MR-18-Dry	649.13	50.40×51.20×100.00	2.52
MR-19-Dry	616.57	50.20×50.00×100.50	2.44
MR-20-Dry	622.56	50.00×50.20×99.80	2.49

Table 3.4 Saturated marl specimens prepared for triaxial compression test.

Specimen No.	Weigh (g)	Dimension (cm^3)	Wet density (g/cc)	Water content (%)
MR-21-Sat	642.62	51.40×50.00×100.70	2.48	2.580
MR-22-Sat	637.90	51.00×50.60×100.00	2.47	1.696
MR-23-Sat	625.41	50.90×50.50×100.20	2.43	2.595
MR-24-Sat	635.12	50.75×50.60×100.50	2.46	1.564
MR-25-Sat	622.80	50.30×50.80×100.00	2.44	2.224
MR-26-Sat	651.75	49.60×50.00×100.00	2.63	2.260
MR-27-Sat	637.64	50.50×50.50×99.92	2.50	2.379
MR-28-Sat	618.12	50.30×50.08×100.86	2.43	3.356
MR-29-Sat	623.48	50.24×50.26×100.08	2.47	2.848
MR-30-Sat	618.34	50.50×49.82×100.80	2.44	2.826
MR-31-Sat	610.16	50.25×50.60×100.30	2.39	2.110
MR-32-Sat	630.81	49.04×51.78×100.08	2.48	3.073
MR-33-Sat	619.04	49.00×50.96×100.90	2.46	3.025
MR-34-Sat	618.45	49.20×49.22×100.64	2.54	2.931
MR-35-Sat	598.65	49.52×50.28×100.28	2.40	4.028
MR-36-Sat	612.90	50.00×49.40×100.20	2.48	2.710
MR-37-Sat	622.77	49.60×50.00×100.00	2.51	3.878
MR-38-Sat	616.00	49.40×49.00×100.40	2.53	3.137
MR-39-Sat	632.26	49.00×49.34×100.40	2.60	2.750
MR-40-Sat	625.64	49.40×50.00×99.00	2.56	1.950

Table 3.5 Dry marble specimens prepared for triaxial compression test.

Specimen No.	Weigh (g)	Dimension (mm^3)	Dry density (g/cc)
MB-01-Dry	692.85	50.00×50.50×100.00	2.74
MB-02-Dry	690.42	49.62×50.50×99.80	2.76
MB-03-Dry	693.58	50.00×50.40×100.10	2.75
MB-04-Dry	692.16	50.40×49.50×100.10	2.77
MB-05-Dry	699.05	50.20×50.42×100.50	2.75
MB-06-Dry	687.43	49.60×50.00×100.30	2.76
MB-07-Dry	688.84	49.30×49.80×99.72	2.81
MB-08-Dry	690.12	50.00×50.00×100.00	2.76
MB-09-Dry	693.96	50.20×50.00×100.00	2.76
MB-10-Dry	688.05	50.50×50.00×100.50	2.71
MB-11-Dry	698.05	50.90×50.50×100.40	2.70
MB-12-Dry	701.78	50.30×51.00×100.30	2.73
MB-13-Dry	688.27	50.30×49.80×101.00	2.72
MB-14-Dry	691.29	49.82×50.70×100.00	2.74
MB-15-Dry	695.15	50.40×49.64×100.34	2.77
MB-16-Dry	683.08	49.22×50.10×100.40	2.76
MB-17-Dry	683.25	50.20×49.22×100.76	2.74
MB-18-Dry	696.83	49.92×50.62×100.10	2.75
MB-19-Dry	694.30	49.90×50.20×99.90	2.77
MB-20-Dry	691.66	50.60×49.62×100.50	2.74

Table 3.6 Saturated marble specimens prepared for triaxial compression test.

Specimen No.	Weigh (g)	Dimension (cm^3)	Wet density (g/cc)	Water content (%)
MB-21-Sat	697.02	51.00×50.50×100.80	2.68	0.070
MB-22-Sat	689.66	50.75×50.50×100.80	2.67	0.083
MB-23-Sat	695.15	51.00×50.75×100.90	2.66	0.087
MB-24-Sat	693.92	51.10×50.00×100.65	2.70	0.076
MB-25-Sat	689.52	51.30×50.20×100.70	2.66	0.077
MB-26-Sat	694.36	50.50×49.64×100.00	2.77	0.080
MB-27-Sat	693.53	49.56×50.50×100.10	2.77	0.102
MB-28-Sat	694.92	50.00×50.50×99.90	2.75	0.124
MB-29-Sat	695.80	50.70×50.00×99.90	2.75	0.121
MB-30-Sat	694.65	50.00×50.10×100.00	2.77	0.134
MB-31-Sat	688.83	49.80×49.90×100.00	2.77	0.135
MB-32-Sat	688.85	50.40×50.50×99.80	2.71	0.136
MB-33-Sat	689.69	49.50×50.70×99.70	2.76	0.050
MB-34-Sat	696.92	50.00×50.60×100.30	2.75	0.042
MB-35-Sat	693.12	49.70×50.50×100.40	2.75	0.092
MB-36-Sat	691.20	49.50×50.60×99.60	2.77	0.095
MB-37-Sat	690.92	49.80×50.60×100.00	2.74	0.077
MB-38-Sat	681.82	50.84×50.50×100.58	2.67	0.090
MB-39-Sat	697.25	50.16×50.96×100.82	2.71	0.079
MB-40-Sat	685.16	50.76×49.66×100.30	2.71	0.106

CHAPTER IV

LABORATORY TESTING

4.1 Introduction

The objective of the laboratory testing is to assess the effects of pore pressure on the compressive strength and elasticity of the rock specimens. This chapter describes the method and results of the laboratory experiments. The tests are divided into two groups; uniaxial compression tests and triaxial compression tests. The initial results have been studied to determine the effects of confining pressure and loading rate effects on compressive strength and elastic properties of rock. The results obtained have are also compared with other researches.

4.2 Uniaxial compression tests

The objective of the uniaxial compression tests is to determine the ultimate strength and the deformability of the dry and saturated specimens under uniaxial load at various loading rates. The test procedures follow the American Society for Testing and Materials (ASTM D 7012-07) and the suggested methods by ISRM (Bieniawski and Bernede, 1978). The tests are performed by applying uniform axial stress under constant rate to the rectangular rock specimen and measuring the increase of axial strains as a function of time (Figure 4.1). The specimens are loaded failure under stress rates varying from 0.01, 0.1, 1 to 10 MPa/s. The post-failure characteristics are observed and recorded.

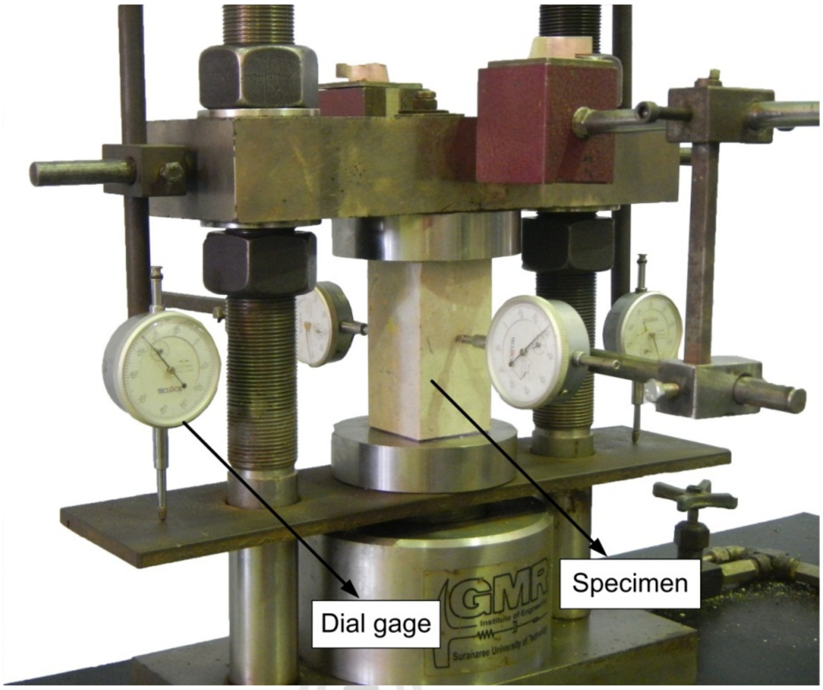

Figure 4.1 Marl specimen placed under uniaxial load frame.

4.3 Triaxial compression tests

All the tests are conducted using a polyaxial load frame (Figure 4.2) apply constant and uniform lateral stresses (confining pressures) to the rock specimens while the axial stress is increased at a constant rate until failure occurs. Exhaustive reviews of the polyaxial load frame have recently been given in Fuenkajorn et al. (2012). The testing system is always calibrated before testing. In this study, σ_2 and σ_3 are equal ranging from 0, 3, 7, 12 MPa, and the constant axial loading rates from 0.001, 0.01, 0.1, 1 to 10 MPa/s. Perforated neoprene sheets have been placed at the interface between loading platens and rock surfaces to minimize the friction for saturated condition. After installing the rectangular specimen into the load frame, dead weights are placed on the steel bar to obtain the pre-defined magnitude of the uniform lateral stress (σ_3) on the specimen. The test is started by increasing the vertical stress at the predefined rate using the hydraulic pump. Both the axial strain and lateral strain were properly recorded directly by a dial gage during the testing. The failure stresses are recorded and mode of failure examined.

4.4 Test results

Figures 4.3 through 4.5 shows some post-test marble specimens from the triaxial compression test under confining pressures (σ_3) from 0, 3, 7 to 12 MPa with loading rates ($\partial\sigma_1/\partial t$) of 1 and 0.001 MPa/s for both dry and saturated conditions. Compressive shear failure is observed for slow loading while extension failure is found in high loading specimens. The high confining pressures create heavy fractures.

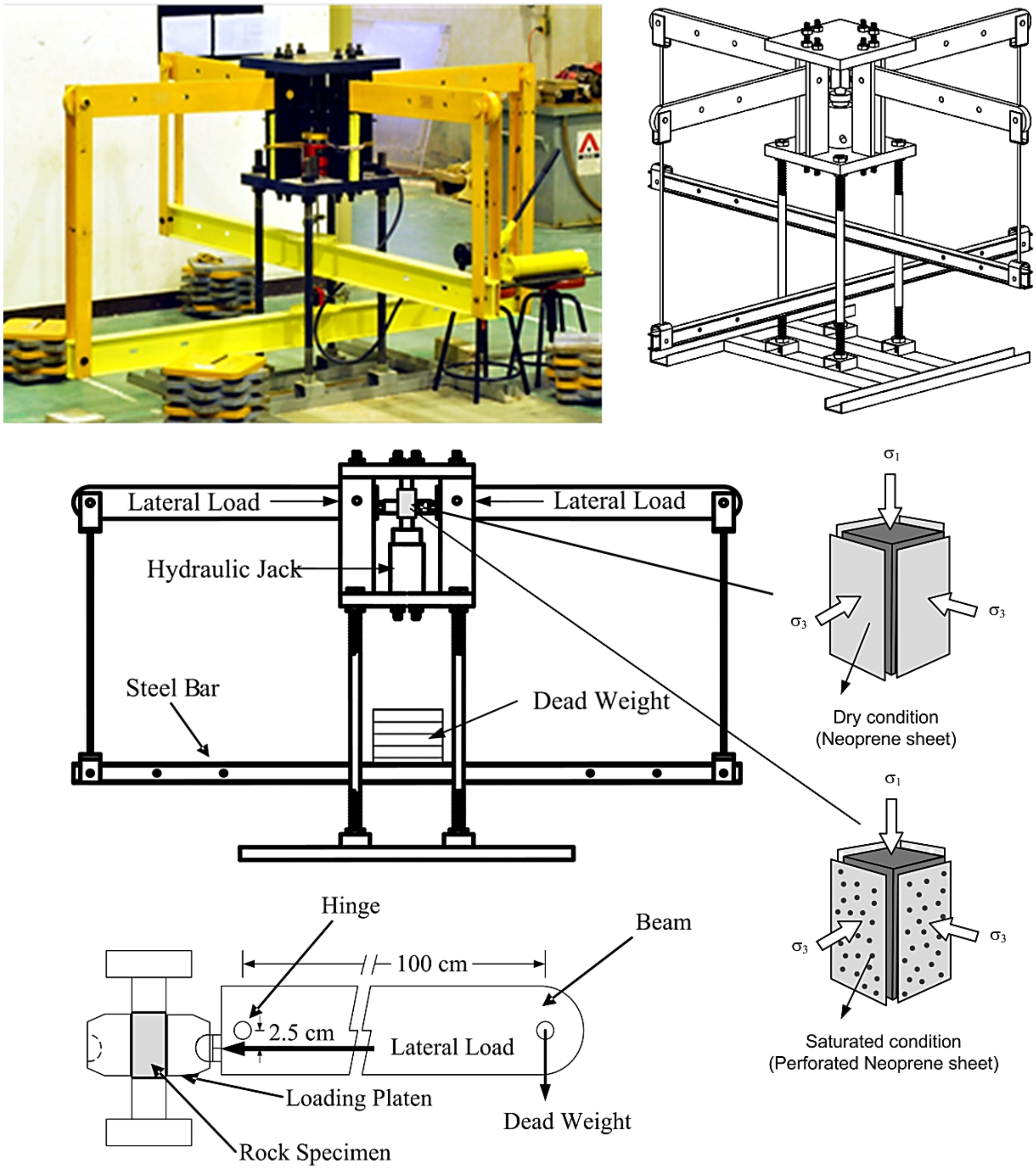

Figure 4.2 Polyaxial load frame used in this study.

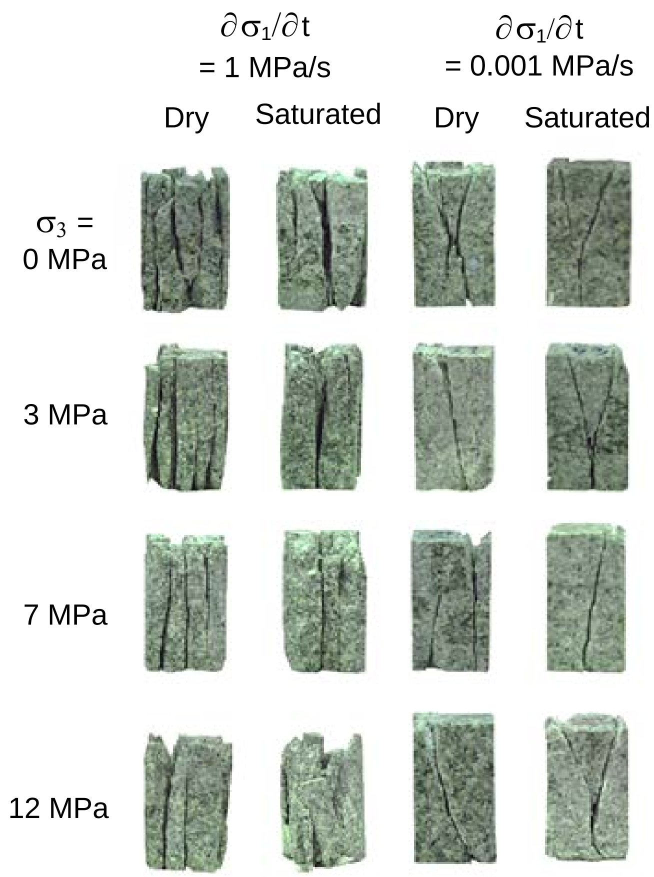

Figure 4.3 Some post-test granite specimens from the triaxial compression test.

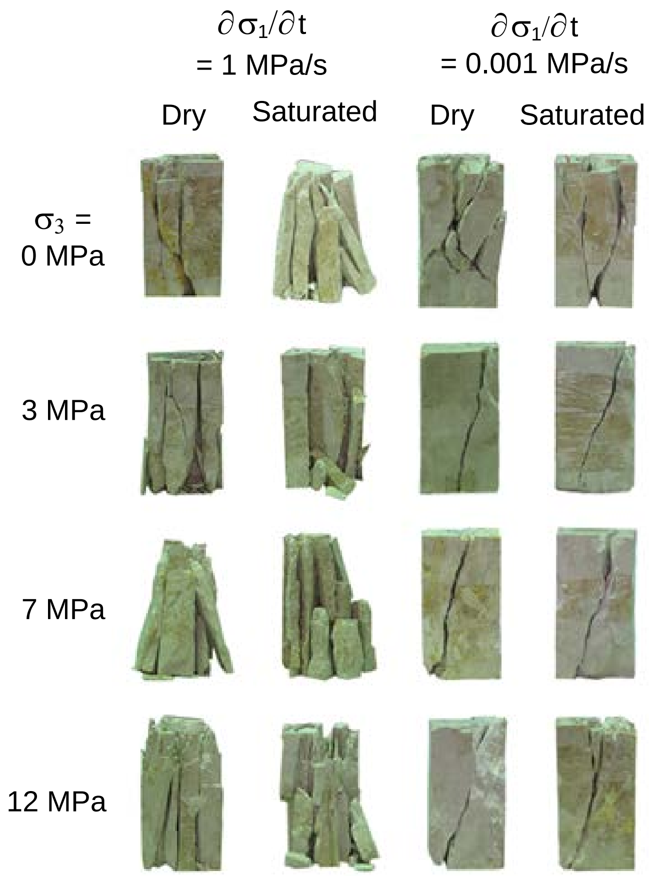

Figure 4.4 Some post-test marl specimens from the triaxial compression test.

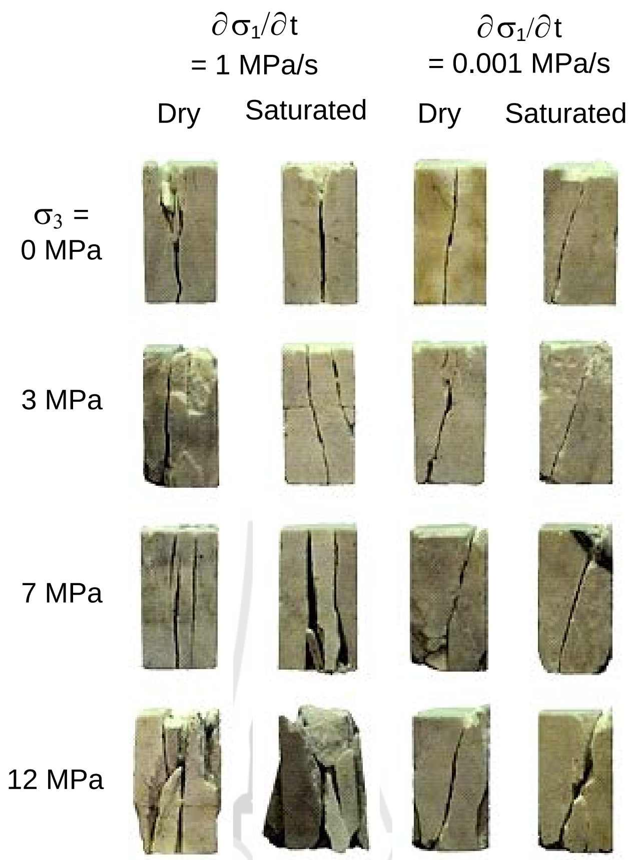

Figure 4.5 Some post-test marble specimens from the triaxial compression test.

Figures 4.6 through 4.8 shows the stress-strain curves at different loading rates and confining pressure tested under dry and saturated conditions. The stress-strain relations are nonlinear, particularly under the low loading rates. Higher loading rates applied result in higher stresses and lower strains at failure. Under the same strain rate, the stress and strain increase with confining pressure no matter under dry or saturated condition. The effect of the pore pressure on the rock is reflected as the reduction of stresses and increment of strains. Result for the compressive strength ($\sigma_{1,f}$), Young's modulus (E) and Poisson's ratio (ν) under dry and saturated conditions are interpreted from these curves and listed in Tables 4.1 and 4.2.

4.5 Strength properties

The compressive strength increases with confining pressures and loading rates. The effect of the loading rate on the rock strength becomes larger under higher confining pressures. Similar testing results have been observed by Li et al. (1999) and Masuda (2001). The strengths of the saturated specimens are lower than those of the dry specimens, particularly under high confining pressures and high loading rates. These results generally agree with the experimental observations by Cobanoglu and Celik (2012), Masuda (2001), Hawkins and McConnell (1992), Vasarhelyi (2003, 2005). This is because under low loading rates the rock specimens are subject to the consolidated drained condition as the pore water has sufficient time to seep out from the specimens. Under high loading rates however the specimens are subject to the consolidated undrained condition where the trapped pore water builds up the pore pressure and reduces the total failure stresses of the rocks. Figure 4.9 shows the maximum principal stress as a function of the applied loading rates. The maximum principal stresses at failure are plotted as a function of the minimum principal stresses in Figure 4.10

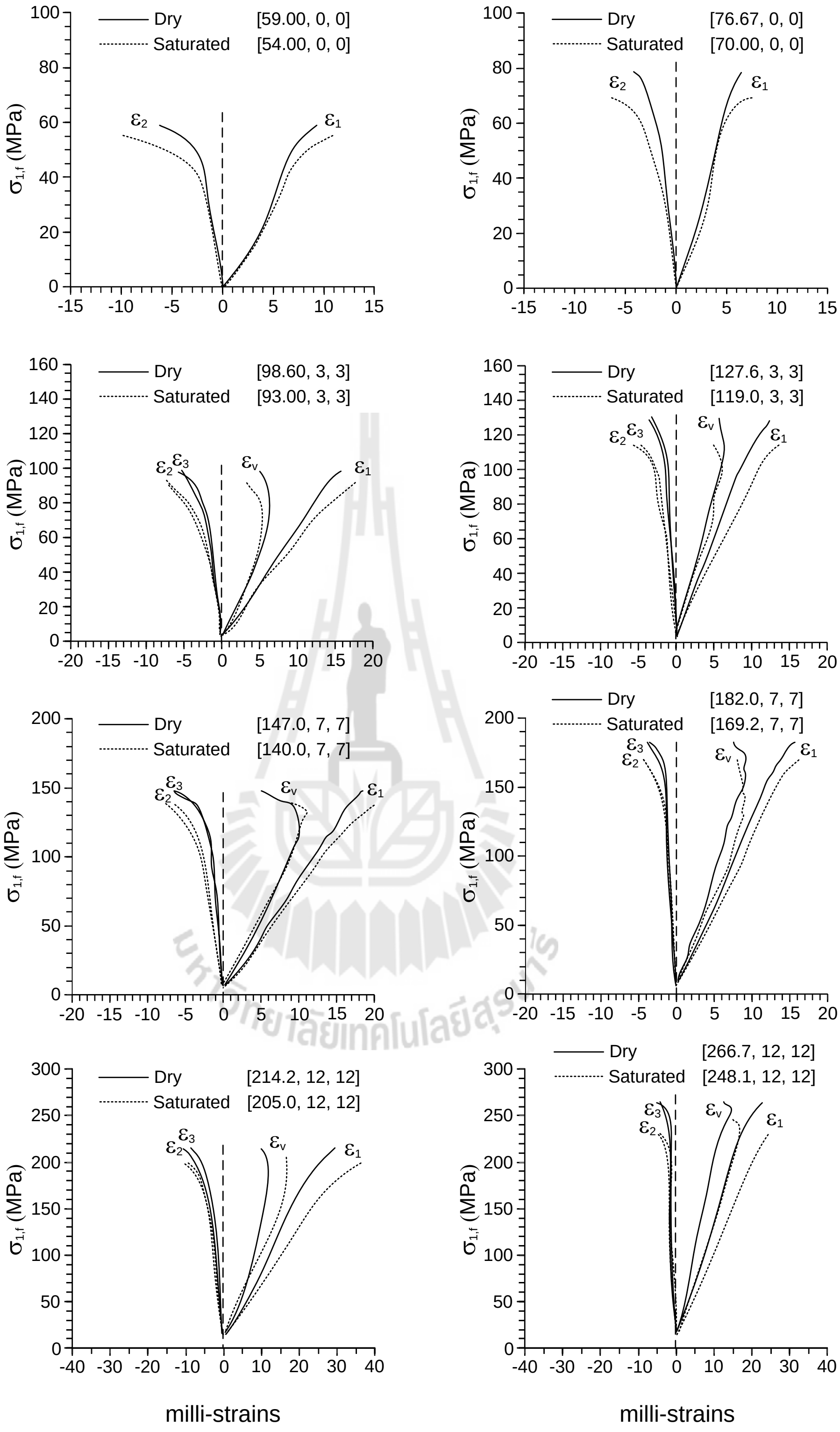

Figure 4.6 Stress-strain curves obtained from some granite specimens with loading rates of 0.001 MPa/s (left) and 1 MPa/s (right). Numbers in brackets indicate [σ_1, σ_2, σ_3 at failure].

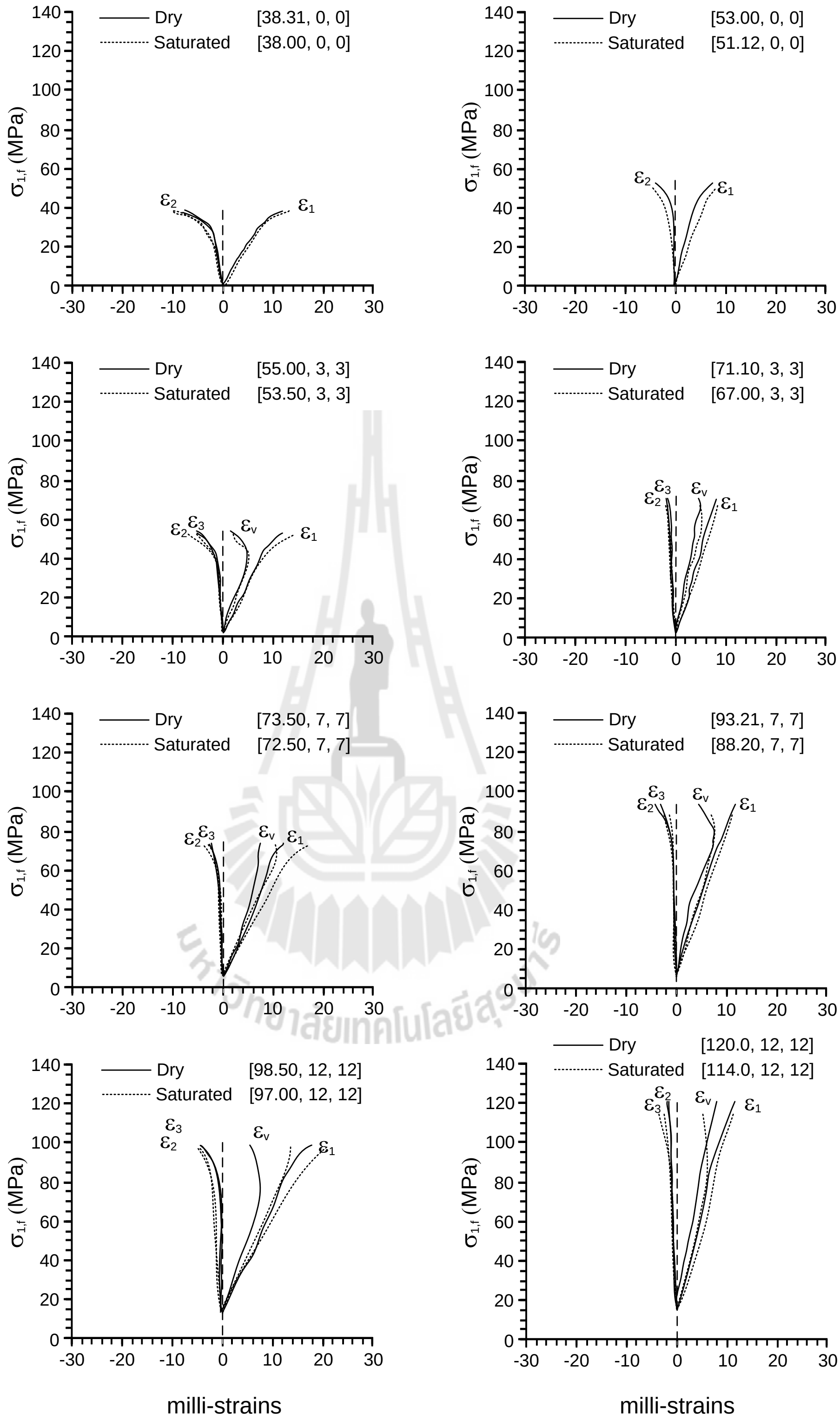

Figure 4.7 Stress-strain curves obtained from some marl specimens with loading rates of 0.001 MPa/s (left) and 1 MPa/s (right). Numbers in brackets indicate [σ_1, σ_2, σ_3 at failure].

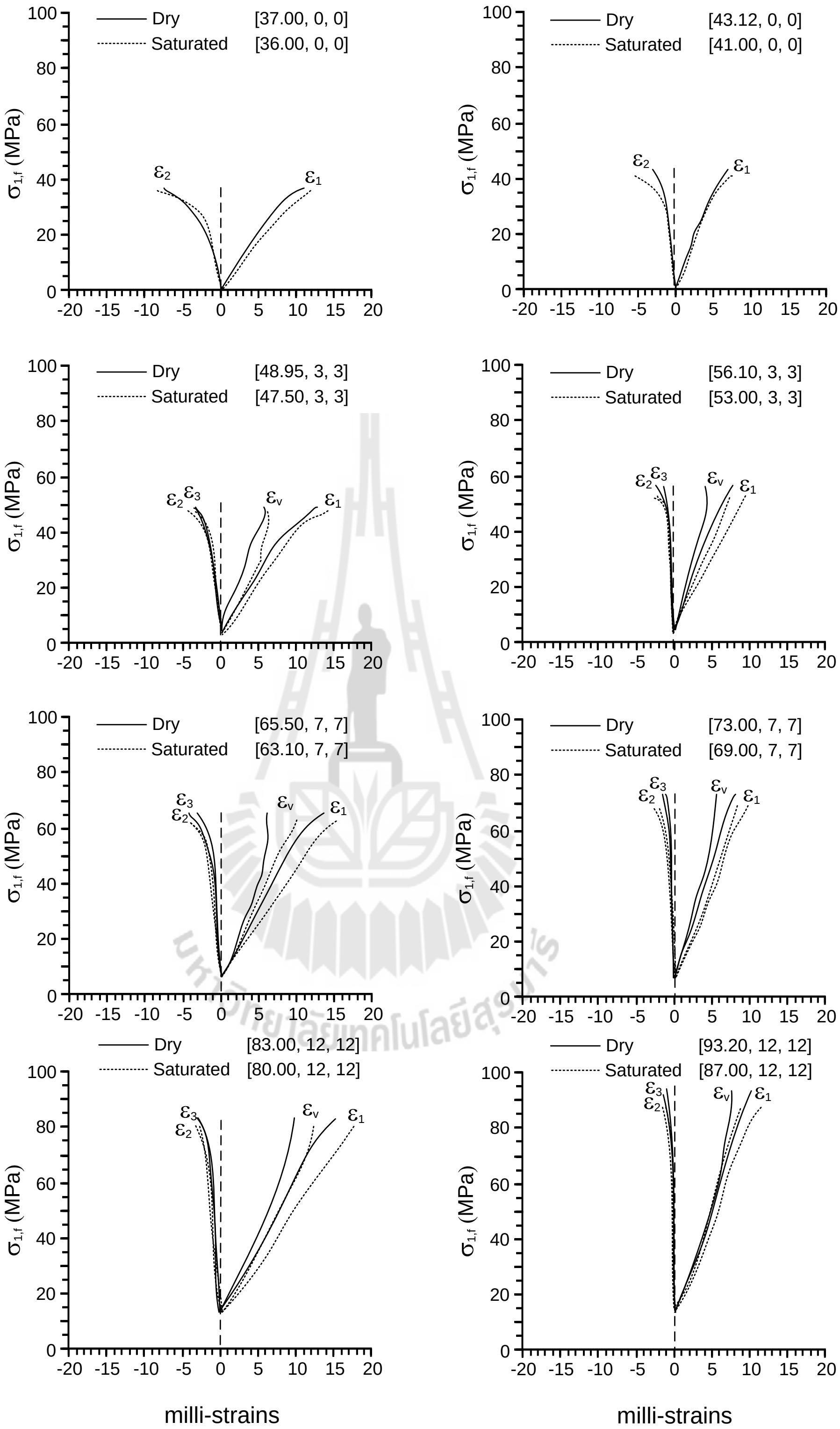

Figure 4.8 Stress-strain curves obtained from some marble specimens with loading rates of 0.001 MPa/s (left) and 1 MPa/s (right). Numbers in brackets indicate [σ_1, σ_2, σ_3 at failure].

Table 4.1 Compressive strengths of dry specimens under various loading rates.

Type of rock	Loading Rate (MPa/s)	σ_3 = 0 (MPa)			σ_3 = 3 (MPa)			σ_3 = 7 (MPa)			σ_3 = 12 (MPa)		
		σ_1 (MPa)	E (MPa)	ν	σ_1 (MPa)	E (MPa)	ν	σ_1 (MPa)	E (MPa)	ν	σ_1 (MPa)	E (MPa)	ν
Granite	10	86.0	N/A	N/A	142.1	N/A	N/A	203.0	N/A	N/A	N/A	N/A	N/A
	1	76.7	13.64	0.28	127.6	12.12	0.29	182.0	12.64	0.27	266.7	12.45	0.29
	0.1	69.7	10.75	0.29	114.0	9.08	0.29	169.2	10.08	0.28	243.0	9.83	0.28
	0.01	64.3	8.11	0.27	104.0	7.31	0.30	158.5	8.16	0.29	225.3	8.75	0.29
	0.001	59.0	6.25	0.28	98.6	5.83	0.27	147.2	7.06	0.29	214.2	7.31	0.30
Marl	10	62.0	N/A	N/A	81.0	N/A	N/A	103.0	N/A	N/A	130.0	N/A	N/A
	1	53.0	9.88	0.30	71.0	8.88	0.29	93.2	9.11	0.31	120.4	10.99	0.28
	0.1	47.0	8.08	0.31	63.2	7.46	0.27	85.4	8.18	0.30	111.5	9.67	0.29
	0.01	41.7	6.36	0.27	56.7	6.44	0.30	78.5	6.73	0.29	104.0	7.88	0.31
	0.001	38.3	4.63	0.29	53.3	5.15	0.27	73.5	5.32	0.29	98.5	6.38	0.30
Marble	10	46.3	N/A	N/A	62.1	N/A	N/A	82.0	N/A	N/A	103.0	N/A	N/A
	1	43.0	9.28	0.27	56.3	8.75	0.26	73.2	9.10	0.28	93.0	9.41	0.27
	0.1	39.7	7.22	0.26	53.4	7.11	0.30	69.3	7.79	0.28	88.3	7.94	0.27
	0.01	38.2	6.45	0.32	50.9	6.48	0.26	66.8	6.73	0.28	85.0	6.72	0.28
	0.001	36.8	5.08	0.31	49.0	5.10	0.29	64.8	5.49	0.27	83.2	5.57	0.27

Table 4.2 Compressive strengths of saturated specimens under various loading rates**.**

Type of rock	Loading Rate (MPa/s)	σ_3 = 0 (MPa)			σ_3 = 3 (MPa)			σ_3 = 7 (MPa)			σ_3 = 12 (MPa)		
		σ_1 (MPa)	E (MPa)	ν	σ_1 (MPa)	E (MPa)	ν	σ_1 (MPa)	E (MPa)	ν	σ_1 (MPa)	E (MPa)	ν
Granite	10	80.0	N/A	N/A	120.0	N/A	N/A	174.1	N/A	N/A	N/A	N/A	N/A
	1	72.2	9.77	0.31	112.2	10.21	0.28	165.0	10.56	0.27	232.3	9.80	0.27
	0.1	66.0	8.16	0.30	101.6	8.54	0.27	156.2	9.65	0.27	221.2	7.72	0.27
	0.01	61.8	6.87	0.29	97.3	6.23	0.29	143.8	7.79	0.28	204.0	6.90	0.26
	0.001	57.4	5.19	0.29	91.9	5.63	0.29	139.0	6.45	0.29	197.8	6.31	0.29
Marl	10	58.1	N/A	N/A	73.0	N/A	N/A	93.0	N/A	N/A	118.0	N/A	N/A
	1	51.4	7.98	0.32	67.0	8.13	0.29	88.0	8.21	0.29	113.8	9.41	0.29
	0.1	45.9	6.31	0.31	60.8	7.21	0.27	81.5	7.17	0.28	107.5	8.00	0.28
	0.01	41.2	4.85	0.31	56.0	6.18	0.29	77.3	6.25	0.27	101.7	6.36	0.28
	0.001	38.0	4.11	0.32	52.5	4.49	0.28	72.5	5.61	0.28	97.0	5.95	0.29
Marble	10	44.2	N/A	N/A	56.1	N/A	N/A	73.3	N/A	N/A	92.0	N/A	N/A
	1	42.5	7.11	0.29	53.9	7.13	0.29	69.0	6.98	0.27	87.7	7.21	0.30
	0.1	40.0	6.22	0.26	51.5	5.50	0.29	66.5	5.88	0.27	85.0	6.49	0.29
	0.01	38.2	5.26	0.26	48.9	4.68	0.28	64.0	4.81	0.30	81.7	5.57	0.28
	0.001	37.0	4.01	0.31	47.5	3.99	0.27	62.2	4.30	0.30	80.0	4.56	0.29

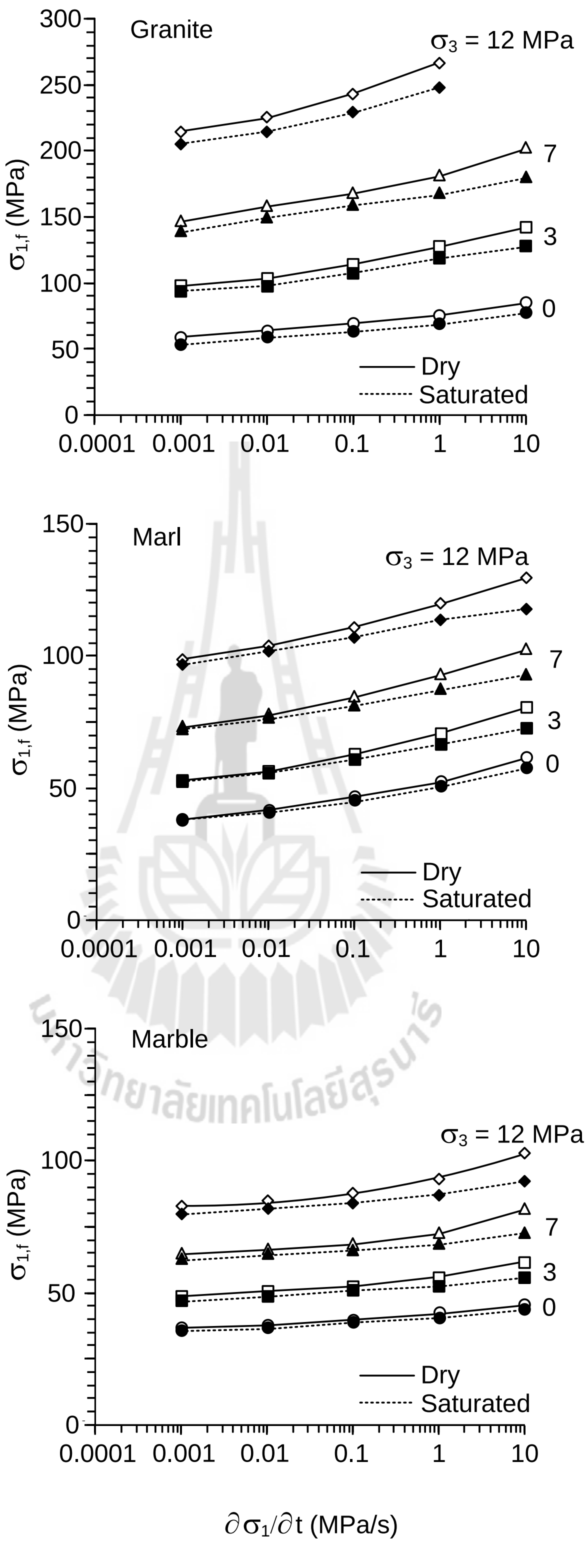

Figure 4.9 Maximum principal stresses as a function of applied loading rate for dry and saturated specimens.

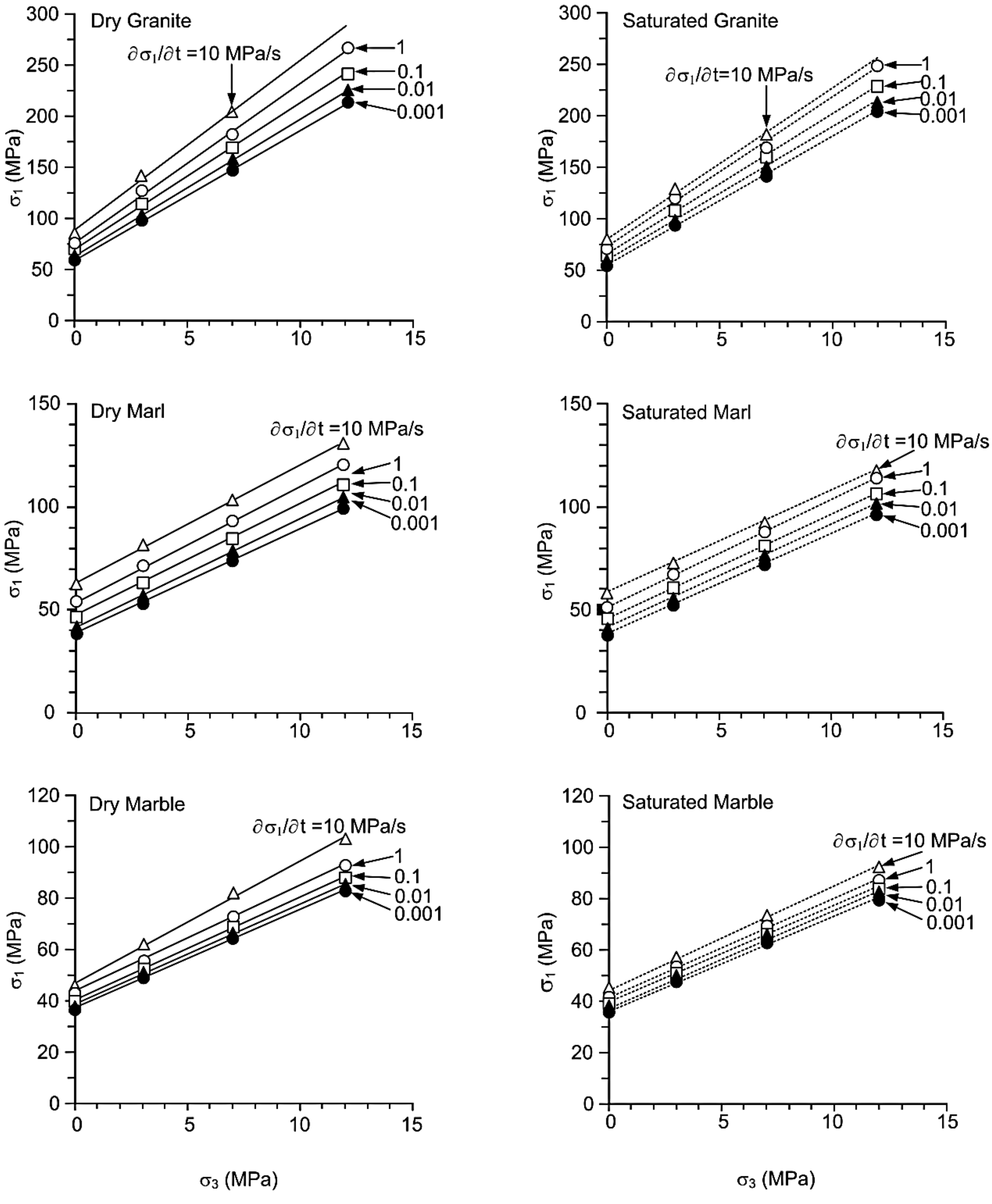

Figure 4.10 Maximum principal stresses at failure as a function of the minimum principal stresses for dry (left) and saturated (right) specimens.

The octahedral shear stresses and shear strains at failure are also determined using the following relations (Jaeger et al., 2007):

$$\tau_{oct} = (1/3)\ [2\ (\sigma_1 - \sigma_3)^2\ ]^{1/2} \tag{4.1}$$

$$\gamma_{oct} = (1/3)\ [(\varepsilon_1 - \varepsilon_2)^2 + (\varepsilon_1 - \varepsilon_3)^2 + (\varepsilon_2 - \varepsilon_3)^2]^{1/2} \tag{4.2}$$

where σ_1, σ_2 and σ_3 are the major, intermediate and minor principal stress, ε_1, ε_2 and ε_3 are the major, intermediate and minor principal strains.

To show the effects of loading rate on the rock strength and deformability the applied octahedral shear stresses are plotted as a function of octahedral shear strain in Figures 4.11 thought 4.13. The shear stress-strain relations are nonlinear, particularly under low loading rates. Higher loading rates applied result in higher octahedral shear stresses and lower octahedral shear strains at failure. The effect of the pore pressure on the rock is reflected as the reduction of octahedral shear stresses and increment of octahedral shear strains.

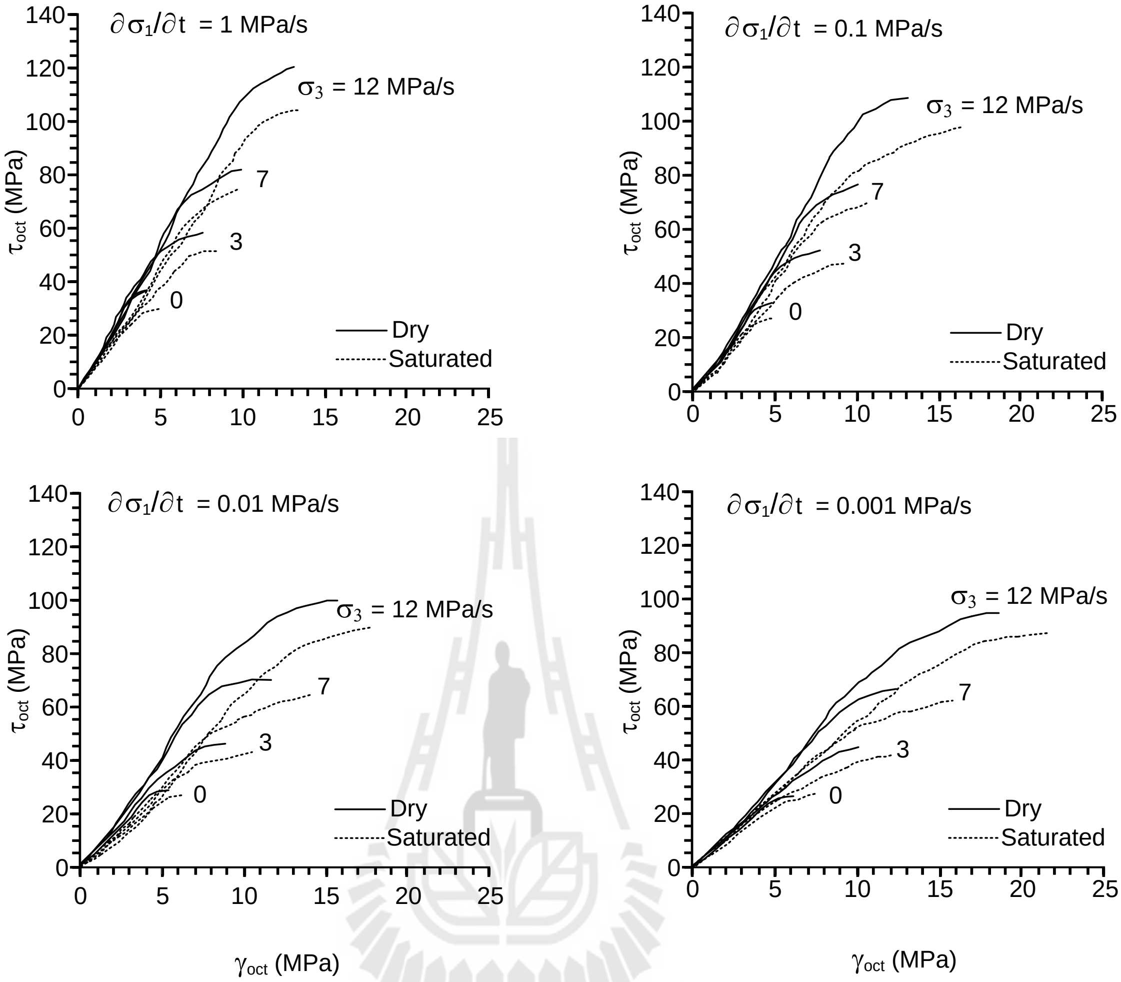

Figure 4.11 Octahedral shear stresses as a function of octahedral shear strain for dry and saturated specimens for granite.

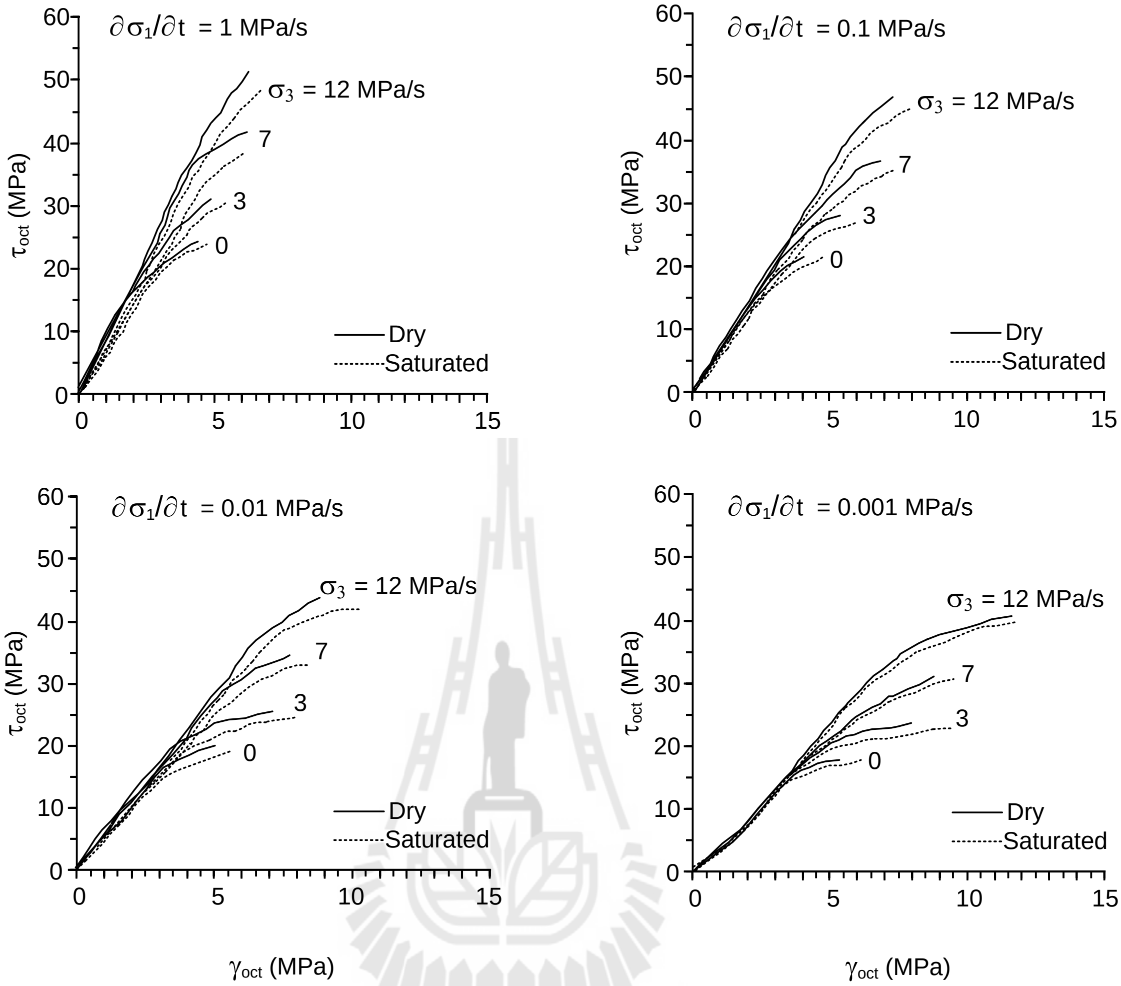

Figure 4.12 Octahedral shear stresses as a function of octahedral shear strain for dry and saturated specimens for marl.

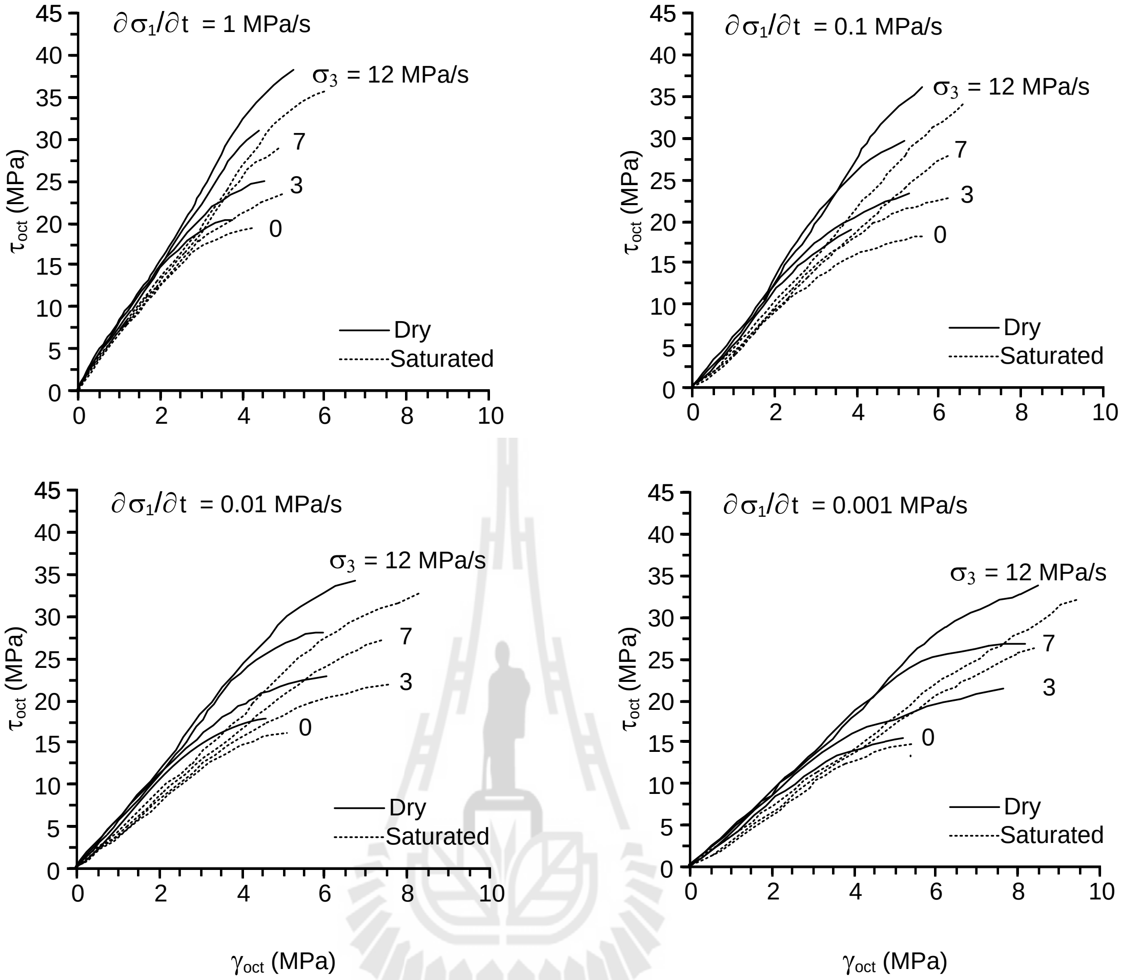

Figure 4.13 Octahedral shear stresses as a function of octahedral shear strain for dry and saturated specimens for marble.

CHAPTER V

ANALYSIS OF TEST RESULTS

5.1 Introduction

The objective of this chapter is to determine the effects of pore pressure on elastic and strength parameters. The coulomb and strain energy density criteria are used. The pore pressure in saturated rocks is isolated from the effect of loading rate and the minimum principal stress (σ_3). The result is used to determine the mathematical relation between the compressive strength and elastic parameters and the pore pressure.

5.2 Coulomb criterion

Based on the Coulomb strength criterion the cohesion and internal friction angle of the rocks have been calculated. The cohesions of the dry and saturated specimens are comparable (Figure 5.1). The dry specimens yield slightly higher friction angles than the saturated specimens, particularly low porosity rock (Figure 5.2). The shear strength (τ) can be represented by:

$$\tau = c + \sigma_n \tan \phi \qquad (5.1)$$

where σ_n is the normal stress, c is the cohesion and ϕ is the friction angle. They can be determined as a function of the stress rate as follows:

$$c = \chi \cdot \ln(\partial\sigma_1/\partial t) + \psi \qquad (5.2)$$

$$\phi = \omega \cdot \ln(\partial\sigma_1/\partial t) + \iota \qquad (5.3)$$

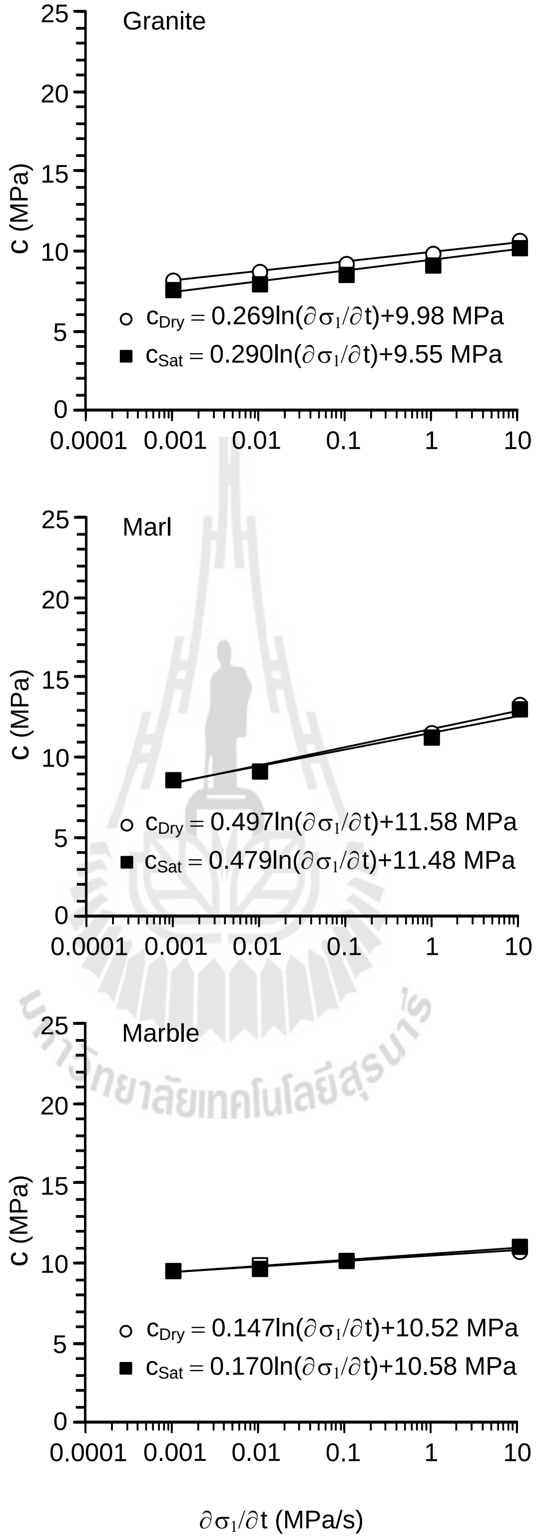

Figure 5.1 Cohesion as a function of applied loading rate for dry (c_{Dry}) and saturated (c_{Sat}) specimens.

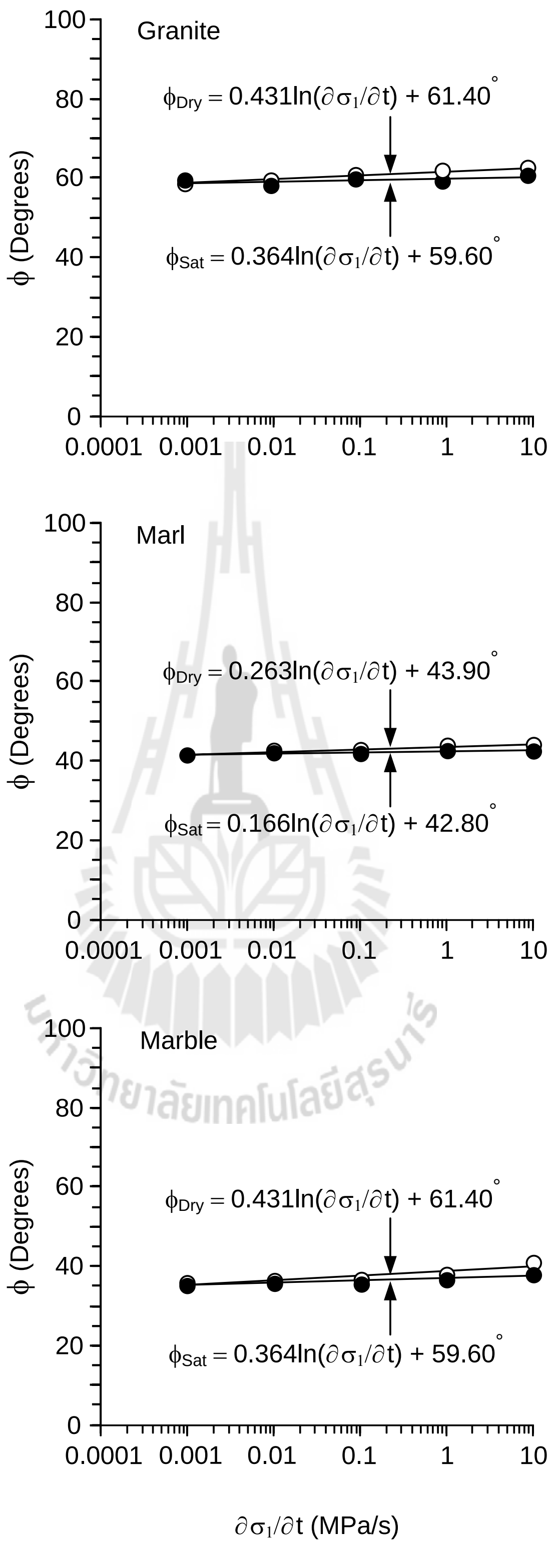

Figure 5.2 Friction angle as a function of applied loading rate for dry (ϕ_{Dry}) and saturated (ϕ_{Sat}) specimens.

The parameters χ, γ, ω, ι are empirical parameters.

Substituting Equations (5.2) and (5.3) into Equation (5.1) the shear strength of rocks can be presented as a function of stress rate:

$$\tau = [\ \chi \cdot \ln(\partial_1/\partial t) + \psi] + \sigma_n \tan [\ \omega \cdot \ln(\partial_1/\partial t) + \iota] \qquad (5.4)$$

5.3 Elastic properties

The elastic parameters are determined from the tangent of the stress-strain curves at about 50% of the failure stress. The elastic modulus of the rock tends to increase with loading rate, and tend to be independent of the confining pressure (Figure 5.3). In contrast to Yang et al. (2012), who have obtained the Young’s modulus increased nonlinearly with increasing confining pressure. The influence of pore pressure on the rock deformability is reflected as the reduction of Young's modulus. The Poisson’s ratios of saturated specimens are slightly higher than those of the dry specimens, and tend to be independent of the loading rate (Figure 5.4). These results generally agree with the experimental observations by Li et al. (2012), Vasarhelyi (2003, 2005) and Yilmaz (2010). Under lower loading rate of 0.001 MPa/s the elastic and Poisson’s ratio under dry and saturated condition are similar. This suggests that the pore pressure has no effect on the rock strengths if there is sufficient time to allow water to flow out of the specimens.

The elastic parameters G and K can be determined for each specimen using the following relations (Figures 5.5 and 5.6):

$$G = \frac{E}{2(1+v)} \qquad (5.5)$$

$$K = \frac{E}{3(1-(2v))} \qquad (5.6)$$

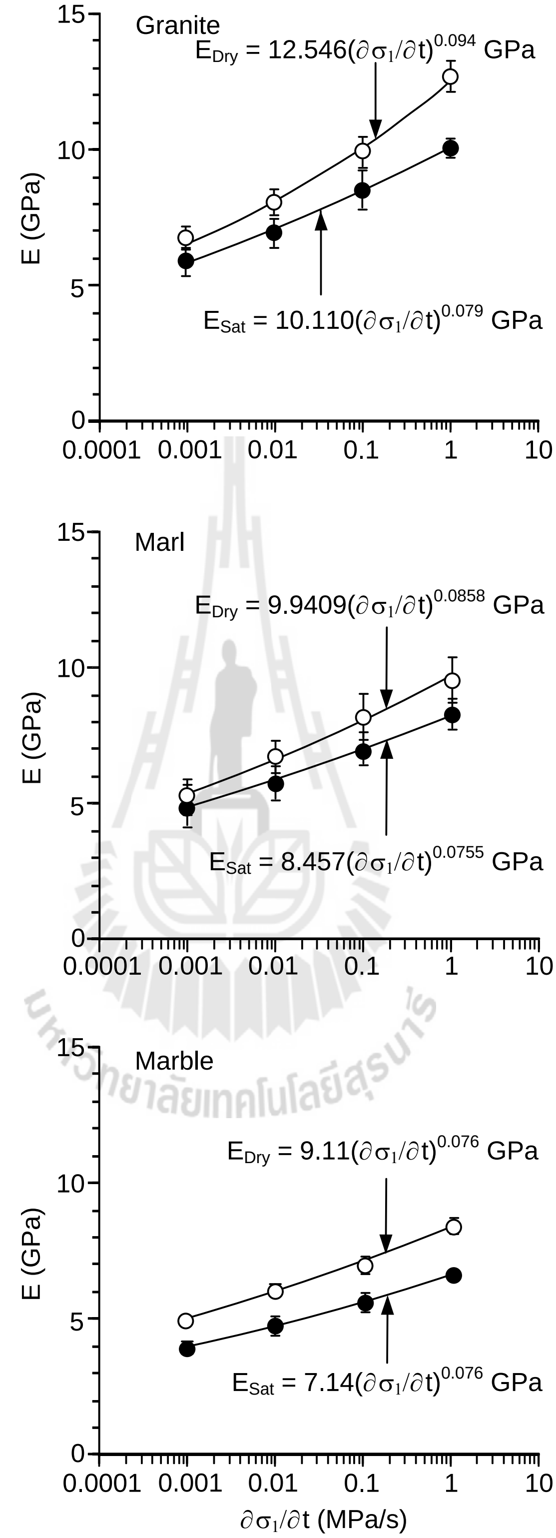

Figure 5.3 Elastic moduli as a function of applied loading rate for dry (E_{Dry}) and saturated (E_{Sat}) specimens.

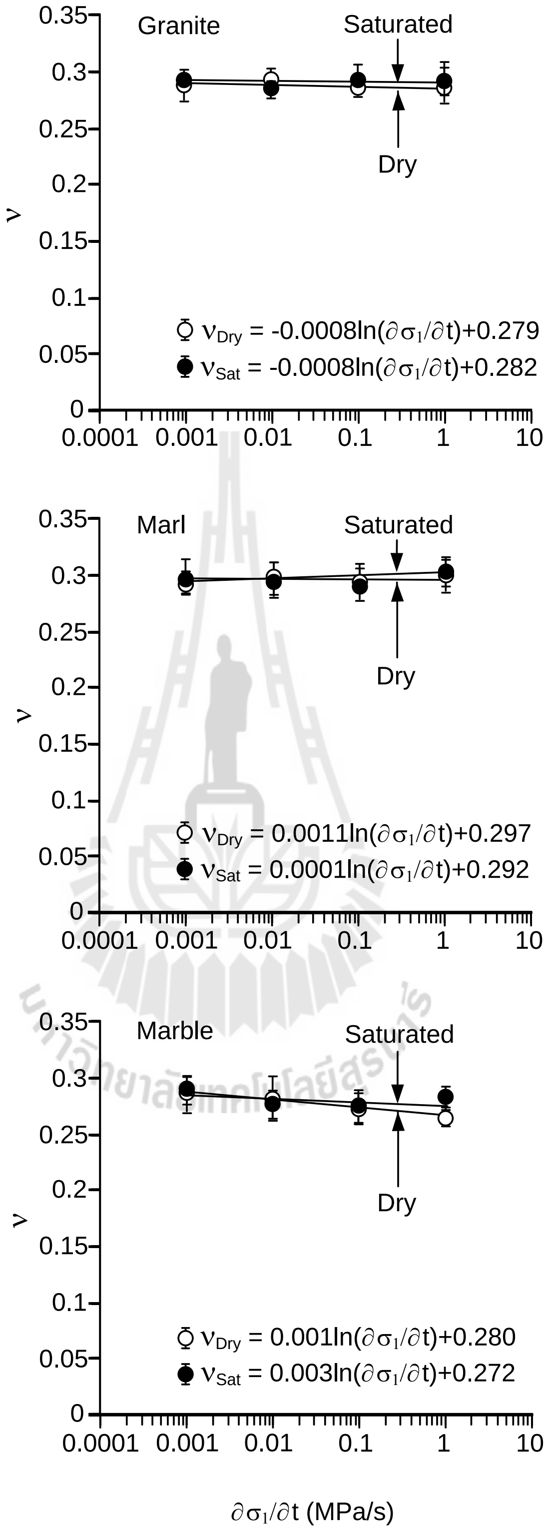

Figure 5.4 Poisson's ratio as a function of applied loading rate for dry (ν_{Dry}) and saturated (ν_{Sat}) specimens.

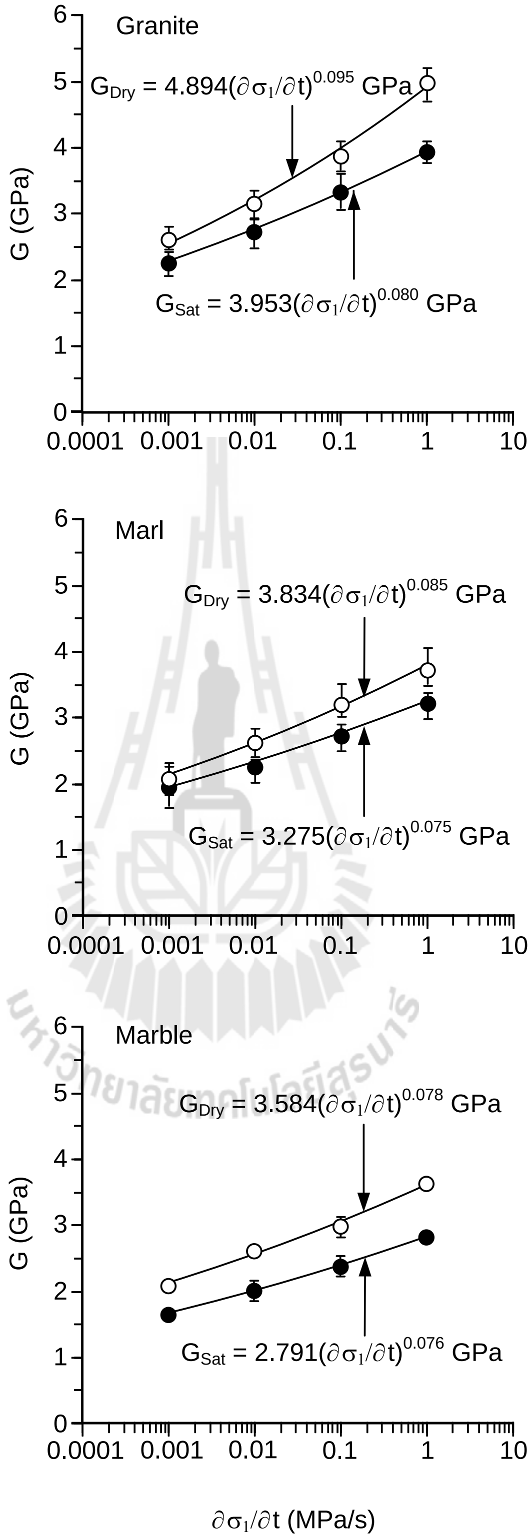

Figure 5.5 Shear modulus as a function of applied loading rate for dry (G_{Dry}) and saturated (G_{Sat}) specimens.

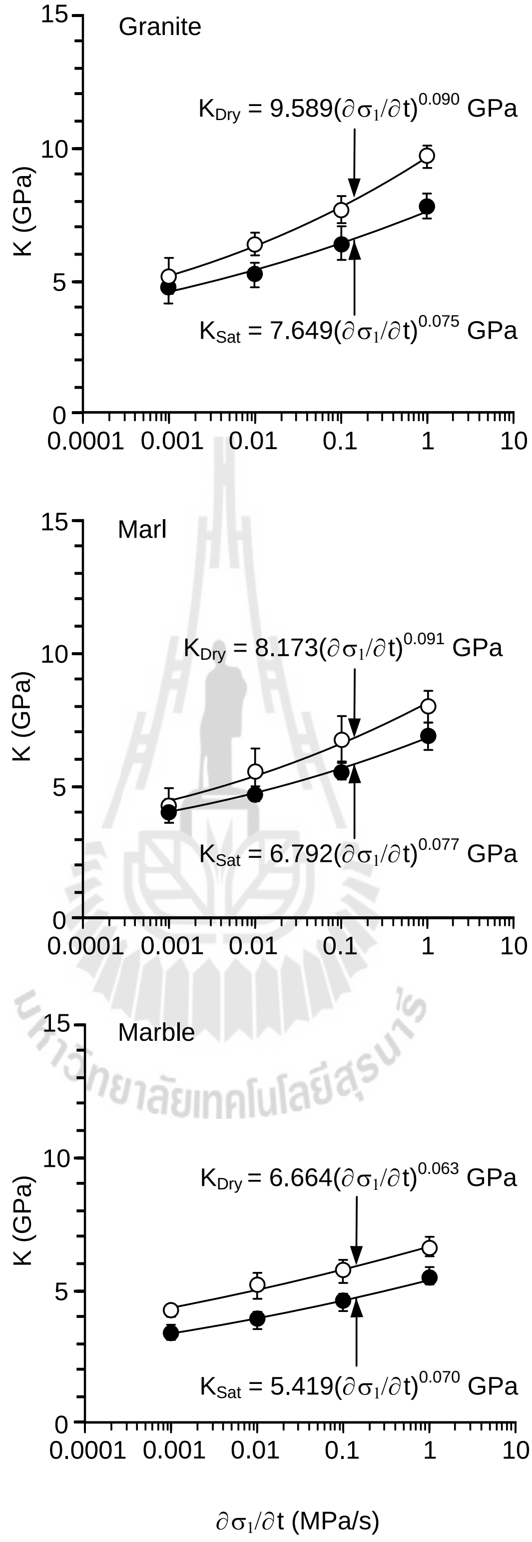

Figure 5.6 Bulk modulus as a function of applied loading rate for dry (K_{Dry}) and saturated (K_{Sat}) specimens.

The best relations between elastic modulus, Poisson's ratio, shear modulus and Bulk modulus with loading rate can be best represented by:

$$E = \kappa\,(\partial\sigma_1/\partial t)^{\xi} \qquad (5.7)$$

$$\nu = \alpha \ln(\partial\sigma_1/\partial t) + \beta \qquad (5.8)$$

$$G = \upsilon\,(\partial\sigma_1/\partial t)^{\eta} \qquad (5.9)$$

$$K = \lambda\,(\partial\sigma_1/\partial t)^{\varphi} \qquad (5.10)$$

The parameters κ, ξ, α, β, υ, η, λ and φ are empirical parameters.

5.4 Strength criterion based on strain energy density

The strain energy density principle is applied here to describe the rock strength and deformation under different loading rates. The distortional strain energy (W_d) at failure can be calculated from the shear modulus and octahedral shear stresses for each rock specimen as follows (Jaeger et al., 2007):

$$W_d = \frac{3}{4}\left(\frac{\tau^2_{oct,f}}{G}\right) \qquad (5.11)$$

The mean strain energy at failure can also be derived as a function of the bulk modulus and mean stress at failure.

$$W_m = \left(\frac{\sigma^2_m}{2K}\right) \qquad (5.12)$$

The elastic parameters G and K can be determined for each specimen using the Equations 5.9 and 5.10

The octahedral shear strength can be determined as (Jaeger et al., 2007):

$$\tau_{oct,f} = [(1/3)[(\sigma_1-\sigma_2)^2+(\sigma_2-\sigma_3)^2+(\sigma_3-\sigma_1)^2]]^{1/2} \quad (5.13)$$

Regression on the test results shows that the distortional strain energy increases linearly with the mean strain energy for dry and saturated conditions (Figures 5.7 and 5.8) which can be best represented by:

$$W_d = aW_m + b \quad (5.14)$$

The parameters a and b are empirical parameters. The strain energy criterion gives an advantage that both stress and strain at failure are incorporated to define the point at which the rock can absorb the maximum energy before failure occurs.

Results for the octahedral shear stresses ($\tau_{oct,f}$), octahedral shear strains ($\gamma_{oct,f}$), mean stress (σ_m), distortional strain energy density (W_d) and mean strain energy (W_m) at failure under dry and saturated are interpreted from these curves and listed in Tables 5.1 and 5.2.

5.5 Correction of loading rate

5.5.1 Strength

The objective of the section is to isolate the effect of loading rate from the rock strength. In this case, $\sigma_{1,f,dry}$ represents the original maximum principal stress of dry condition (data from experimental results) under various loading rates and confining pressures. $\sigma^*_{1,f,dry}$ represents the new (adjusted) maximum principal stress of dry condition corresponding to $\partial\sigma_1/\partial t$ = 0.1 MPa/s. The increase of the strength with loading rate can be represented by a logarithmic equation:

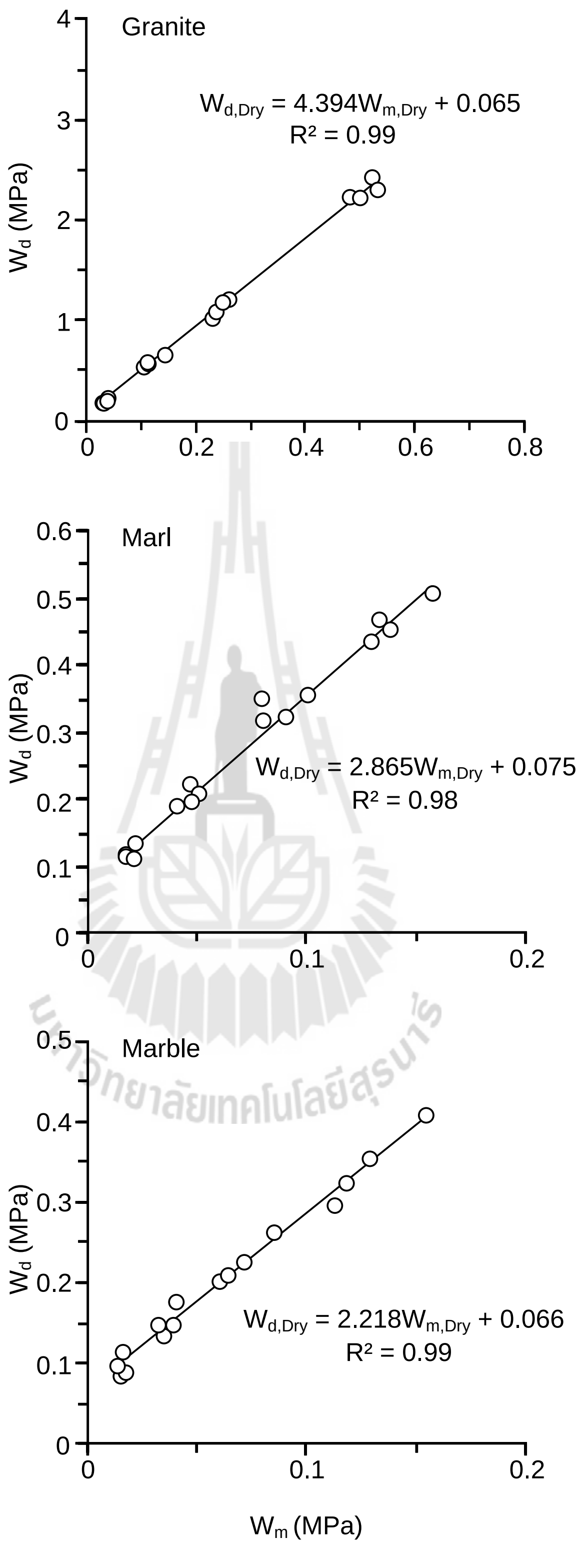

Figure 5.7 Distortional strain energy density ($W_{d,Dry}$) at failure as a function of mean strain energy ($W_{m,Dry}$) for dry specimens.

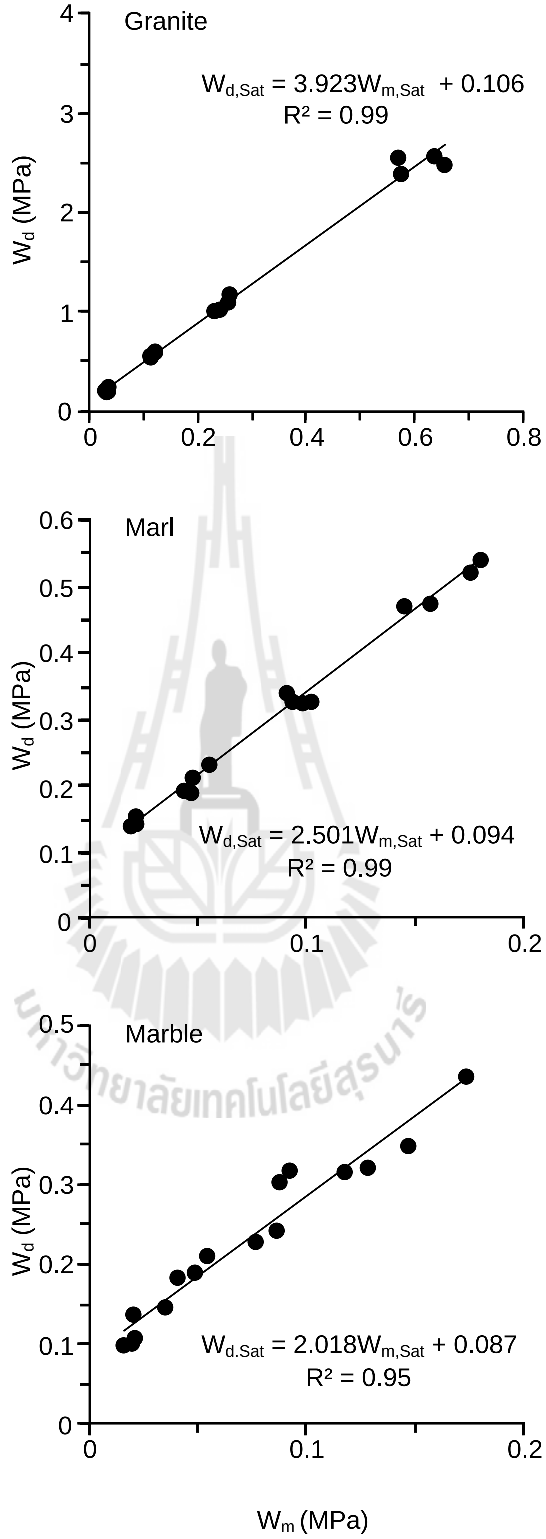

Figure 5.8 Distortional strain energy density ($W_{d,Sat}$) at failure as a function of mean strain energy ($W_{m,Sat}$) for saturated specimens.

Table 5.1 Test results of dry specimens under various loading rates**.**

σ_3 (MPa)	$\partial\sigma_1/\partial t$ (MPa/s)	Granite					Marl					Marble				
		τ_{oct} (MPa)	γ_{oct}	σ_m (MPa)	W_d (MPa)	W_m (MPa)	τ_{oct} (MPa)	γ_{oct}	σ_m (MPa)	W_d (MPa)	W_m (MPa)	τ_{oct} (MPa)	γ_{oct}	σ_m (MPa)	W_d (MPa)	W_m (MPa)
0	10	40.5	N/A	28.7	N/A	N/A	29.2	N/A	20.7	N/A	N/A	21.2	N/A	15.0	N/A	N/A
	1	36.1	4.00	25.6	0.18	0.03	24.8	4.25	17.5	0.12	0.02	20.2	3.63	14.3	0.08	0.02
	0.1	32.9	5.02	23.2	0.19	0.03	22.1	4.12	15.6	0.12	0.02	18.7	3.81	13.2	0.09	0.02
	0.01	30.3	5.49	21.4	0.22	0.04	19.7	5.00	13.9	0.12	0.02	17.9	4.52	12.7	0.10	0.01
	0.001	27.8	6.02	19.6	0.24	0.04	18.1	5.42	12.8	0.14	0.02	17.2	5.09	12.2	0.12	0.02
3	10	65.5	N/A	49.3	N/A	N/A	36.8	N/A	29.0	N/A	N/A	27.8	N/A	22.7	N/A	N/A
	1	58.7	7.48	44.5	0.55	0.11	32.1	4.81	25.7	0.22	0.05	25.0	4.54	20.7	0.13	0.04
	0.1	52.4	7.75	40.0	0.58	0.11	28.1	5.41	22.9	0.20	0.05	23.4	5.43	19.5	0.15	0.03
	0.01	47.6	8.93	36.6	0.60	0.11	25.3	7.05	20.9	0.19	0.04	22.5	6.07	18.9	0.15	0.04
	0.001	45.1	10.09	34.9	0.67	0.14	23.7	8.03	19.8	0.21	0.05	21.5	7.65	18.2	0.18	0.04
7	10	92.4	N/A	72.3	N/A	N/A	45.3	N/A	39.0	N/A	N/A	35.4	N/A	32.0	N/A	N/A
	1	82.6	9.79	65.4	1.03	0.23	40.5	6.21	35.6	0.35	0.08	30.9	4.41	28.8	0.20	0.06
	0.1	76.2	10.06	60.9	1.11	0.24	36.7	7.39	32.9	0.32	0.08	29.3	5.21	27.7	0.21	0.06
	0.01	70.9	11.63	57.2	1.20	0.25	33.7	7.72	30.8	0.33	0.09	28.3	5.91	27.0	0.23	0.07
	0.001	66.5	12.52	54.0	1.21	0.26	31.3	8.84	29.2	0.36	0.10	27.4	8.14	26.4	0.26	0.09
12	10	N/A	N/A	N/A	N/A	N/A	55.6	N/A	51.3	N/A	N/A	42.9	N/A	42.3	N/A	N/A
	1	120.0	13.12	96.9	2.24	0.48	50.9	6.21	48.0	0.45	0.14	38.3	5.25	39.0	0.30	0.11
	0.1	108.8	13.02	89.0	2.31	0.53	46.6	7.30	45.0	0.44	0.13	35.9	5.56	37.4	0.33	0.12
	0.01	100.4	15.90	83.0	2.23	0.50	43.4	8.81	42.7	0.47	0.13	34.4	6.63	36.3	0.36	0.13
	0.001	95.3	18.12	79.4	2.42	0.52	40.8	11.50	40.9	0.51	0.16	33.5	8.42	35.7	0.41	0.15

Table 5.2 Test results of saturated specimens under various loading rates**.**

σ_3 (MPa)	$\partial\sigma_1/\partial t$ (MPa/s)	Granite					Marl					Marble				
		τ_{oct} (MPa)	γ_{oct}	σ_m (MPa)	W_d (MPa)	W_m (MPa)	τ_{oct} (MPa)	γ_{oct}	σ_m (MPa)	W_d (MPa)	W_m (MPa)	τ_{oct} (MPa)	γ_{oct}	σ_m (MPa)	W_d (MPa)	W_m (MPa)
0	10	36.8	N/A	26.0	N/A	N/A	27.3	N/A	19.3	N/A	N/A	20.7	N/A	14.7	N/A	N/A
	1	32.7	5.00	23.1	0.21	0.03	24.0	4.51	17.0	0.14	0.02	19.3	4.43	13.7	0.10	0.02
	0.1	29.8	5.02	21.1	0.21	0.03	21.7	4.91	15.3	0.15	0.02	18.4	5.52	13.0	0.10	0.02
	0.01	27.7	6.64	19.6	0.21	0.04	19.2	5.54	13.6	0.15	0.02	17.4	5.12	12.3	0.11	0.02
	0.001	25.4	7.51	18.0	0.24	0.04	17.9	6.23	12.7	0.15	0.02	16.9	5.48	12.0	0.14	0.02
3	10	58.9	N/A	44.7	N/A	N/A	33.0	N/A	26.3	N/A	N/A	26.4	N/A	20.7	N/A	N/A
	1	54.5	8.31	41.5	0.56	0.11	30.1	5.42	24.3	0.22	0.05	23.5	5.02	19.6	0.15	0.03
	0.1	49.1	9.30	37.7	0.54	0.11	27.1	5.94	22.2	0.19	0.05	22.9	6.32	19.2	0.19	0.04
	0.01	44.8	10.91	34.7	0.62	0.12	25.0	8.12	20.7	0.20	0.04	21.6	7.41	18.3	0.19	0.05
	0.001	42.4	11.96	33.0	0.62	0.12	23.3	9.37	19.5	0.23	0.05	21.0	8.54	17.8	0.21	0.05
7	10	82.0	N/A	65.0	N/A	N/A	40.5	N/A	35.7	N/A	N/A	31.1	N/A	29.0	N/A	N/A
	1	76.2	9.98	60.9	1.05	0.24	38.2	6.08	34.0	0.34	0.09	29.0	4.85	27.5	0.23	0.08
	0.1	71.6	10.78	57.6	1.01	0.23	35.1	7.43	31.8	0.33	0.09	27.8	6.21	26.7	0.25	0.09
	0.01	67.2	14.0	54.5	1.11	0.26	33.0	8.40	30.3	0.33	0.10	27.4	7.43	26.4	0.30	0.09
	0.001	62.3	16.1	51.1	1.16	0.26	30.9	9.59	28.8	0.33	0.10	26.5	8.30	25.7	0.32	0.09
12	10	N/A	N/A	N/A	N/A	N/A	50.0	N/A	47.3	N/A	N/A	37.7	N/A	38.7	N/A	N/A
	1	111.0	13.24	90.5	2.40	0.57	48.1	6.21	46.0	0.47	0.14	35.4	6.06	37.1	0.34	0.12
	0.1	102.0	16.67	84.1	2.56	0.64	44.6	7.82	43.6	0.48	0.16	34.0	6.63	36.1	0.34	0.13
	0.01	95.2	17.53	79.3	2.48	0.65	42.4	10.29	42.0	0.55	0.18	33.0	8.37	35.3	0.38	0.15
	0.001	90.9	21.87	76.3	2.54	0.57	40.1	11.61	40.4	0.52	0.17	32.1	9.39	34.7	0.44	0.17

$$\sigma_{1,f,dry} = d \ln(\partial\sigma_1/\partial t) + e \tag{5.15}$$

The parameters d and e are empirical constants (Table 5.3).

To correlate the strength from samples with identical confining pressure with different loading rates, Equation (5.15) can be rewritten as:

$$\sigma_{1,f,dry} = d \ln(\partial\sigma_1/\partial t)_i + e \tag{5.16}$$

$$\sigma^*_{1,f,dry} = d \ln 0.1 + e \tag{5.17}$$

where $\sigma_{1,f,dry}$ is strength of dry specimen tested at various loading rates, $\sigma^*_{1,f,dry}$ is strength from dry specimen tested at loading rate of 0.1 MPa/s, and $(\partial\sigma_1/\partial t)_i$ is any loading rate. By subtracting Equation (5.17) from Equation (5.16), we obtain:

$$\sigma^*_{1,f,dry} = \sigma_{1,f,dry} + d\,(\ln 0.1 - \ln(\partial\sigma_1/\partial t)_i) \tag{5.18}$$

The new (adjusted) maximum principal stress at failure obtained from the dry testing are used to quantitatively correct the loading rate effect from the saturated rock strengths. The new (adjusted) maximum principal stress of saturated condition can be calculated from:

$$\Delta\sigma^*_{1,f,dry} = \sigma_{1,f,dry} - \sigma^*_{1,f,dry} \tag{5.19}$$

$$\sigma^*_{1,f,sat} = \sigma_{1,f,sat} - \Delta\sigma^*_{1,f,dry} \tag{5.20}$$

Figure 5.9 shows the new (adjusted) maximum principal stress plotted as a function of confining pressure for dry and saturated conditions for loading rate of 0.1 MPa/s. The compressive strengths increase linearly with the increased confining pressure.

Table 5.3 The parameters d and e used in Equations (5.15) through (5.18).

Types of rock	**σ_3 (MPa)**	**$\sigma_{1,dry} = d \ln \partial\sigma_1/\partial t + e$ (MPa)**	
		d	**e**
Granite	0	2.881	77.77
	3	4.801	128.31
	7	5.906	185.40
	12	7.643	263.56
Marl	0	2.547	54.27
	3	3.053	71.97
	7	3.192	93.95
	12	3.431	120.60
Marble	0	0.999	43.10
	3	1.351	57.30
	7	1.737	75.20
	12	2.085	95.20

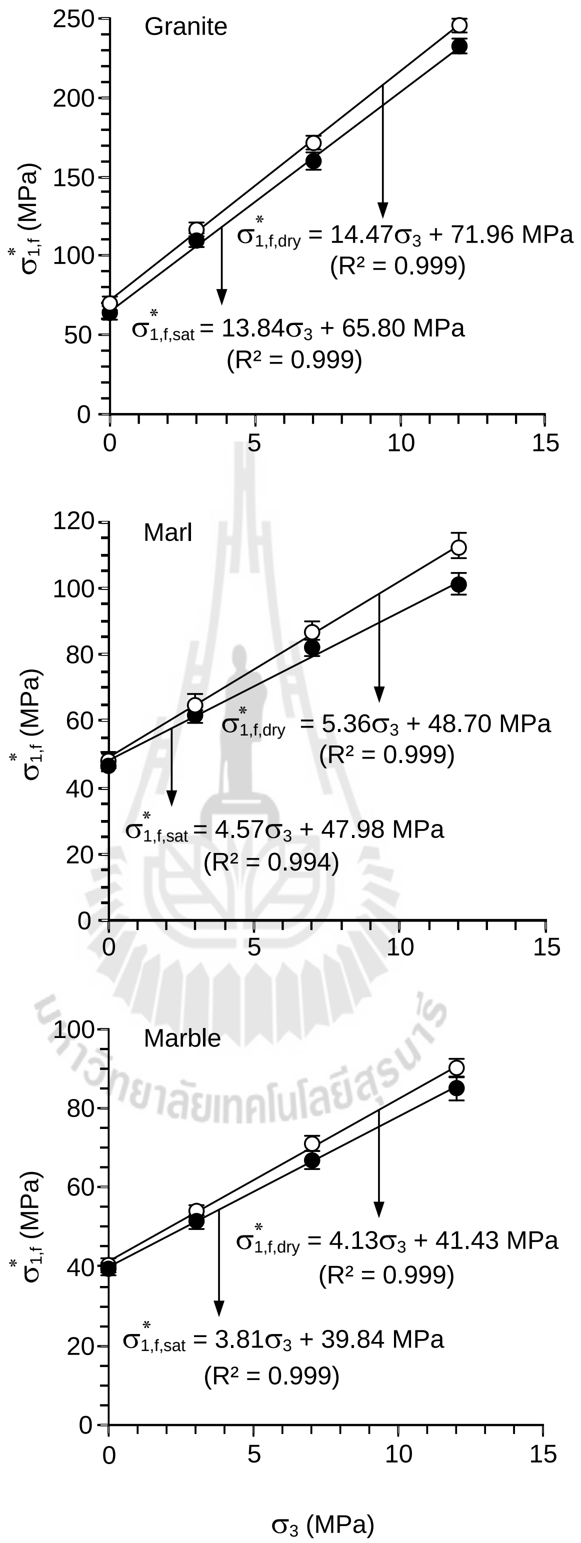

Figure 5.9 New (adjusted) maximum principal stress ($\sigma^*_{1,f}$) as a function of confining pressure (σ_3) for dry and saturated specimens with loading rate is 0.1 MPa/s.

The saturated specimens are lower than those of the dry specimens. Table 5.4 summarizes the average new (adjusted) maximum principal stresses for dry and saturated conditions for each confining pressure.

To calculate the pore pressure, in terms of the principal stresses at peak load conditions, the Mohr-Coulomb criterion can be written as (Goodman, 1989):

$$\sigma_{1,f} = \sigma_{u,f} + \sigma_3 \tan^2 [45 + (\phi/2)] \tag{5.21}$$

where σ_1 is the major principal stress, σ_3 is the confining pressures and σ_u is the uniaxial compressive strength. For a saturated rock, Equation (5.21) in terms of effective stress becomes:

$$\sigma'_{1,f} - \sigma'_3 = \sigma_{u,f} + [\sigma'_3 \tan^2 (45 + \phi/2) - 1] \tag{5.22}$$

The differential stress is unaffected by pore pressure, Equation (5.22) can be rewritten as:

$$\sigma^*_{1,f,sat} - \sigma_3 = \sigma^*_{u,f} + (\sigma_3 - P_w) [\tan^2 (45 + \phi/2) - 1] \tag{5.23}$$

Solving for P_w, Equation (5.23) the following relation can be obtained:

$$P_w = \sigma_3 - [(\sigma^*_{1,f,sat} - \sigma_3) \sigma^*_{u,f}] / [\tan^2 (45 + \phi/2) - 1] \tag{5.24}$$

Table 5.5 and Figure 5.10 show the pore pressure results. Figure 5.11 shows the results using linear regression to obtain the relationship between the new (adjusted) maximum principal stress and pore pressure. The best-fit equation is:

$$\sigma^*_{1,f,sat} = f + (g \cdot \sigma_3) + (h \cdot P_w) \tag{5.25}$$

Table 5.4 Average new (adjust) compressive strengths and elastic parameters under various confining pressure.

Types of rock	**σ_3 (MPa)**	**$\sigma^*_{1,f,dry}$ (MPa)**	**$\sigma^*_{1,f,sat}$ (MPa)**	**E^*_{dry} (GPa)**	**E^*_{sat} (GPa)**	**ν^*_{dry}**	**ν^*_{sat}**
Granite	0	71.14	65.00	10.69	8.06	0.28	0.29
	3	117.26	109.80	9.93	8.51	0.28	0.28
	7	171.80	160.20	10.09	8.96	0.28	0.28
	12	245.97	232.80	10.64	9.92	0.28	0.28
Marl	0	48.41	46.80	8.13	6.85	0.30	0.30
	3	64.94	61.90	8.22	7.04	0.29	0.29
	7	86.60	82.40	8.17	7.23	0.29	0.29
	12	112.70	99.66	8.15	7.81	0.29	0.29
Marble	0	40.80	39.40	7.89	5.86	0.28	0.29
	3	54.19	51.40	7.51	6.02	0.28	0.28
	7	71.20	67.30	7.83	6.32	0.28	0.27
	12	90.40	85.00	7.78	6.69	0.28	0.28

Table 5.5 Pore pressure isolated from loading rate effect for each specimen.

Types of rock	σ_3 (MPa)	P_w (MPa)				
Granite	0	0.632	0.527	0.450	0.424	0.258
	3	0.297	0.237	0.286	0.228	0.173
	7	1.124	0.753	0.409	0.225	0.217
	12	N/A	1.085	0.505	0.249	0.154
Marl	0	0.932	0.466	0.242	0.171	0.076
	3	1.228	0.482	0.327	0.189	0.046
	7	1.497	0.518	0.319	0.084	0.075
	12	2.441	1.275	0.582	0.197	0.365
Marble	0	0.701	0.701	0.350	0.350	0.350
	3	1.113	0.829	0.335	0.124	0.054
	7	1.179	0.933	0.548	0.092	0.197
	12	1.831	1.655	0.779	0.533	0.288

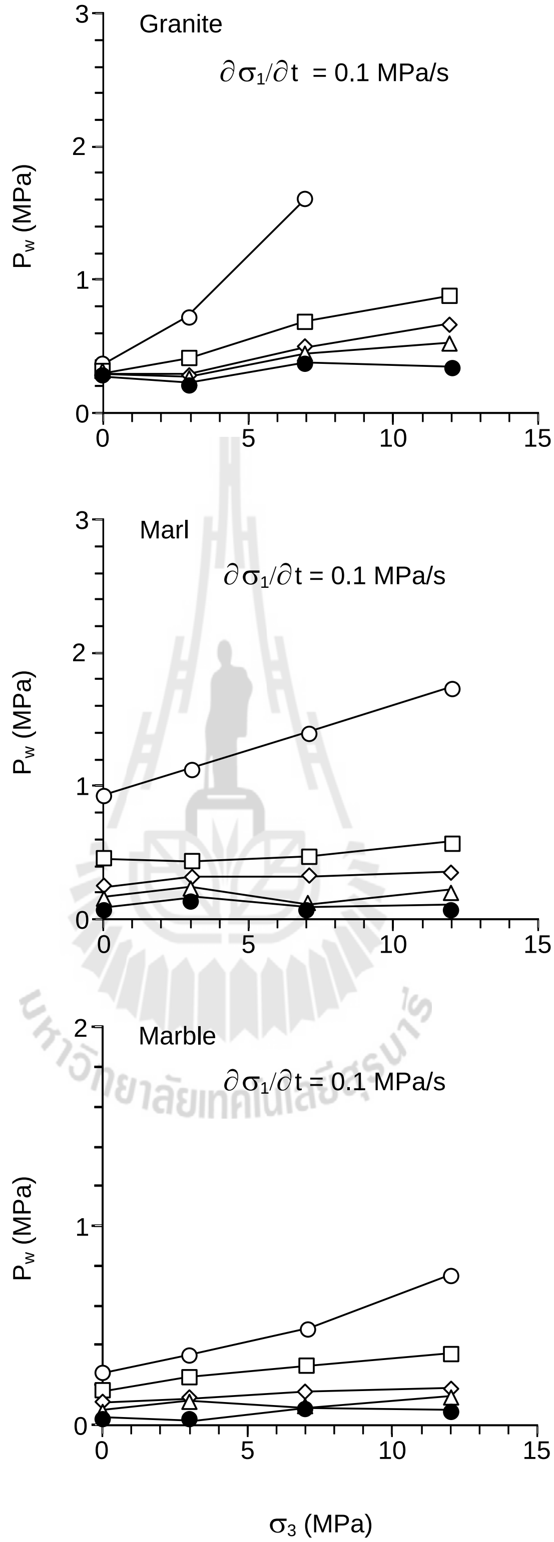

Figure 5.10 Pore pressure (P_w) as a function of confining pressure (σ_3) at loading rate is 0.1 MPa/s.

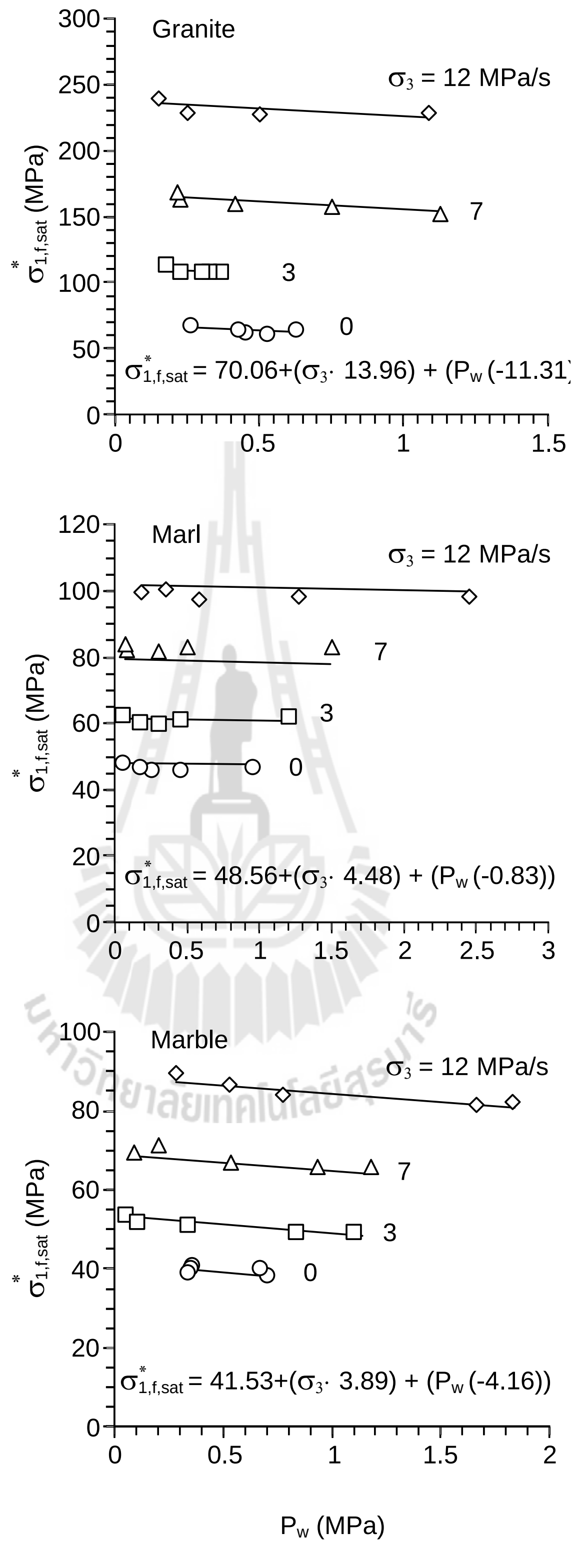

Figure 5.11 New (adjusted) maximum principal stress ($\sigma^*_{1,f}$) as a function of pore pressure (P_w).

The parameters f, g and h are empirical constants. The new (adjusted) maximum principal stress decreases linearly with increasing pore pressure. The new (adjusted) maximum principal stresses as a function of confining pressure with various pore pressures as shown in Figure 5.12.

5.5.2 Elastic parameters

Similar to the strength correlation above, the effect of loading rate can be isolated from the elastic parameter. E_{dry} and ν_{dry} represent the original elastic modulus and Poisson's ratio of dry condition (data from testing results) under various loading rate and confining pressure. E^{*}_{dry} and ν^{*}_{dry} represent the new (adjusted) elastic modulus and Poisson's ratio of dry condition corresponding to $\partial\sigma_1/\partial t$ = 0.1 MPa/s. The increase of the elastic modulus and Poisson's ratio with loading rate can be represented by Equations (5.7) and (5.8). Similar to Equation (5.18) can be rewritten in a correlated form as:

$$E^{*}_{dry} = E_{dry} + \kappa\,(0.1^{\xi} - (\partial\sigma_1/\partial t)_i^{\xi}) \tag{5.26}$$

$$\nu^{*}_{dry} = \nu_{dry} + \alpha\,(\ln 0.1 - \ln(\partial\sigma_1/\partial t)_i) \tag{5.27}$$

The new (adjusted) elastic modulus and Poisson ratio under saturated condition can be determined as:

$$E^{*}_{sat} = E_{sat} - (E_{dry} - E^{*}_{dry}) \tag{5.28}$$

$$\nu^{*}_{sat} = \nu_{sat} - (\nu_{dry} - \nu^{*}_{dry}) \tag{5.29}$$

Figures 5.13 and 5.14 show the new (adjusted) elastic modulus and Poisson's ratio as a function of pore pressure.

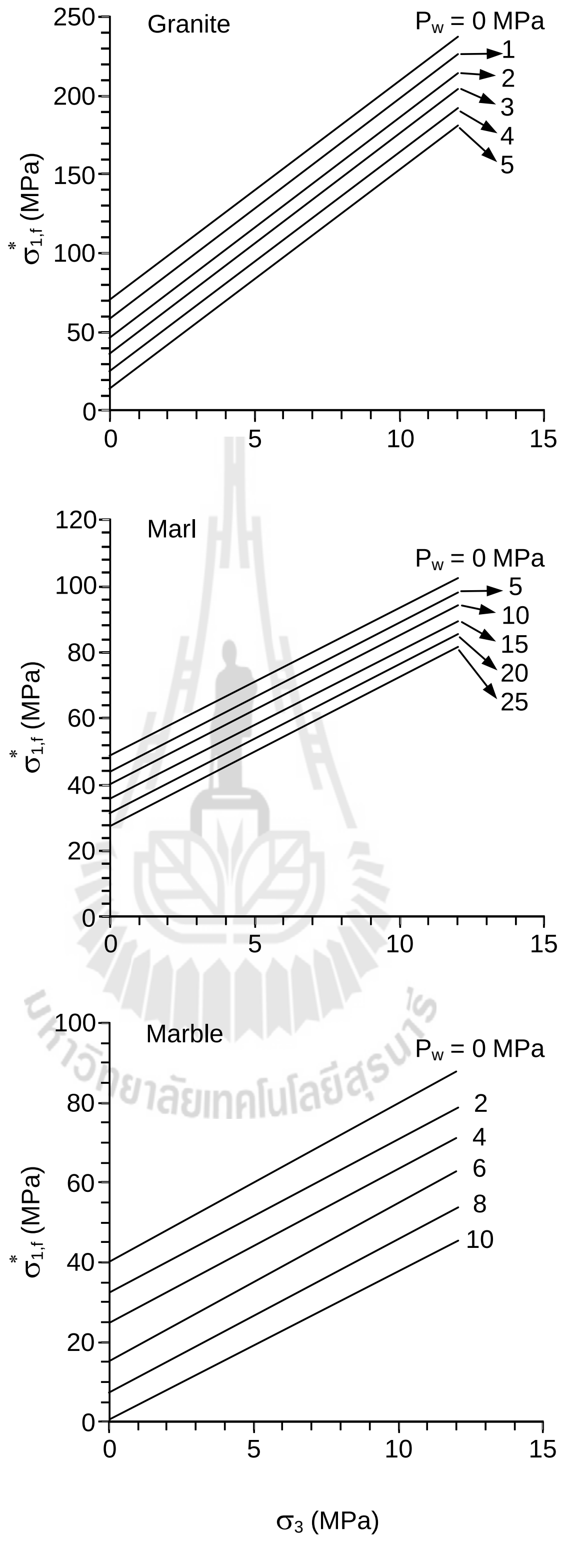

Figure 5.12 New (adjusted) maximum principal stress ($\sigma^*_{1,f}$) as a function of confining pressure (σ_3) under various pore pressure (P_w).

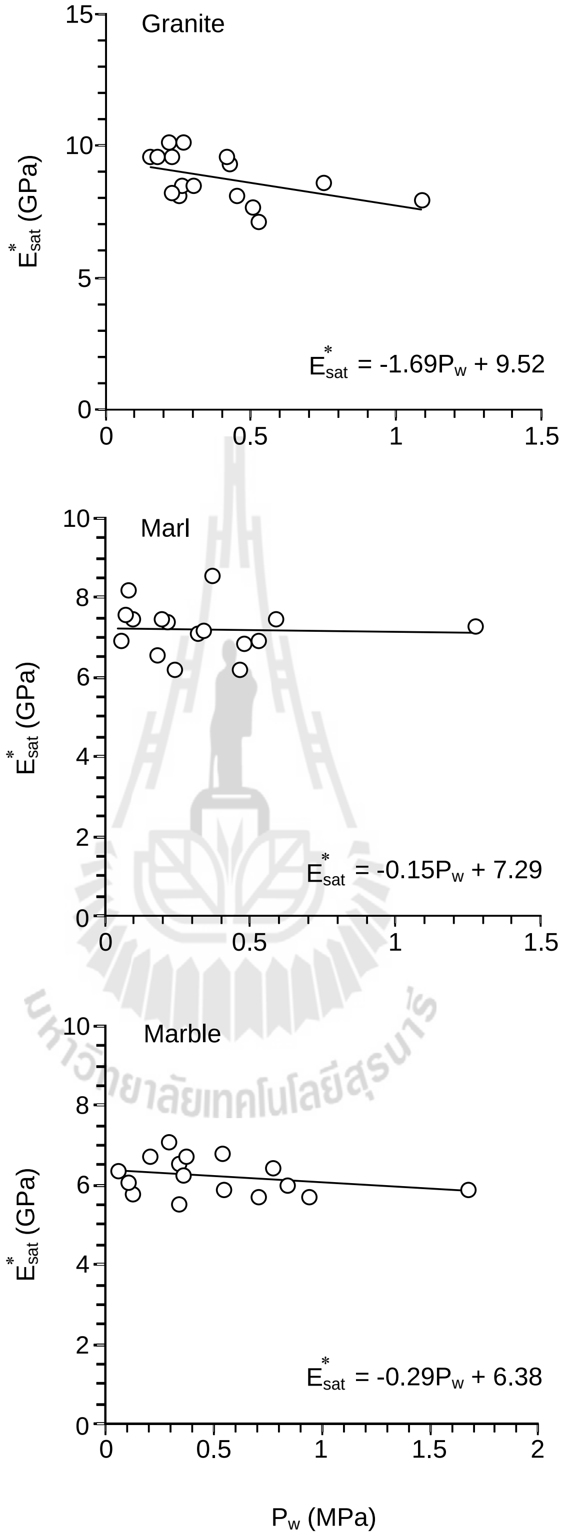

Figure 5.13 New (adjusted) elastic modulus of saturated specimen (E^*_s) as a function of pore pressure (P_w).

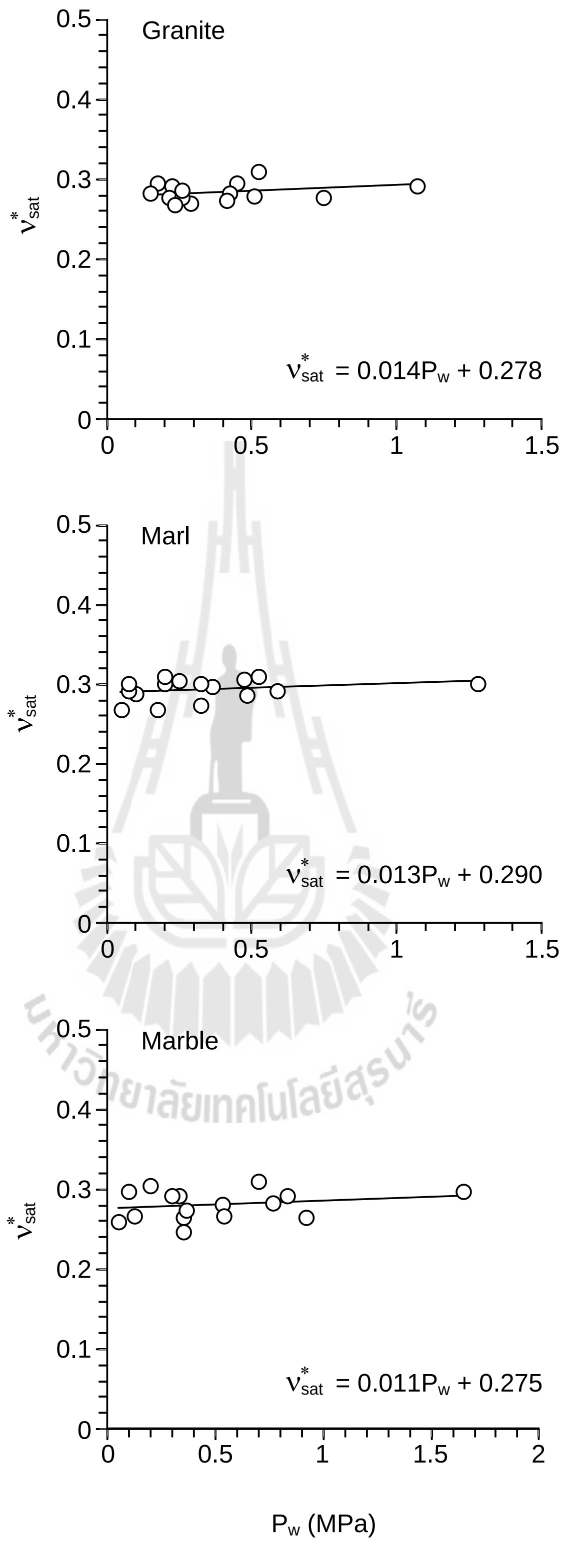

Figure 5.14 New (adjusted) Poisson's ratio of saturated specimen (ν^*_s) as a function of pore pressure (P_w).

The results indicate that, the new (adjusted) elastic modulus to changes in pore pressure is likely to be similar to the new (adjusted) maximum principal stress and the new (adjusted) Poisson's ratios increase as pore pressure increases, which indicates that the saturated rocks will deform more than the dry ones under the same stress condition. The equation of the line of best fit in Figures 5.13 and 5.14 are given by linear equation. The average new (adjusted) elastic modulus and Poisson's ratio as shown in Table 5.4.

An attempt is made to calculate the elastic moduli along the three loading directions. It is assumed here that the Poisson's ratio (ν) of the rock is the same for all principal planes. The new (adjusted) elastic modulus along the major, intermediate and miner principal directions can be calculated by (Jaeger et al., 2007):

$$\varepsilon_1 = \sigma_1/E_1 - \nu\,(\sigma_2/E_2 + \sigma_3/E_3) \tag{5.30}$$

$$\varepsilon_2 = \sigma_2/E_2 - \nu\,(\sigma_1/E_1 + \sigma_3/E_3) \tag{5.31}$$

$$\varepsilon_3 = \sigma_3/E_3 - \nu\,(\sigma_1/E_1 + \sigma_2/E_2) \tag{5.32}$$

where ε_1, ε_2 and ε_3 are the major, intermediate and miner principal strains, and E_1, E_2 and E_3 are the elastic modulus along the major, intermediate and miner directions.

The calculation results are shown in Figure 5.15, Suggesting that the elastic moduli along the principal directions are similar, and that the dry and saturated specimens are isotropic. The elastic modulus values obtained from the saturated specimens tend to be lower than those from dry specimens.

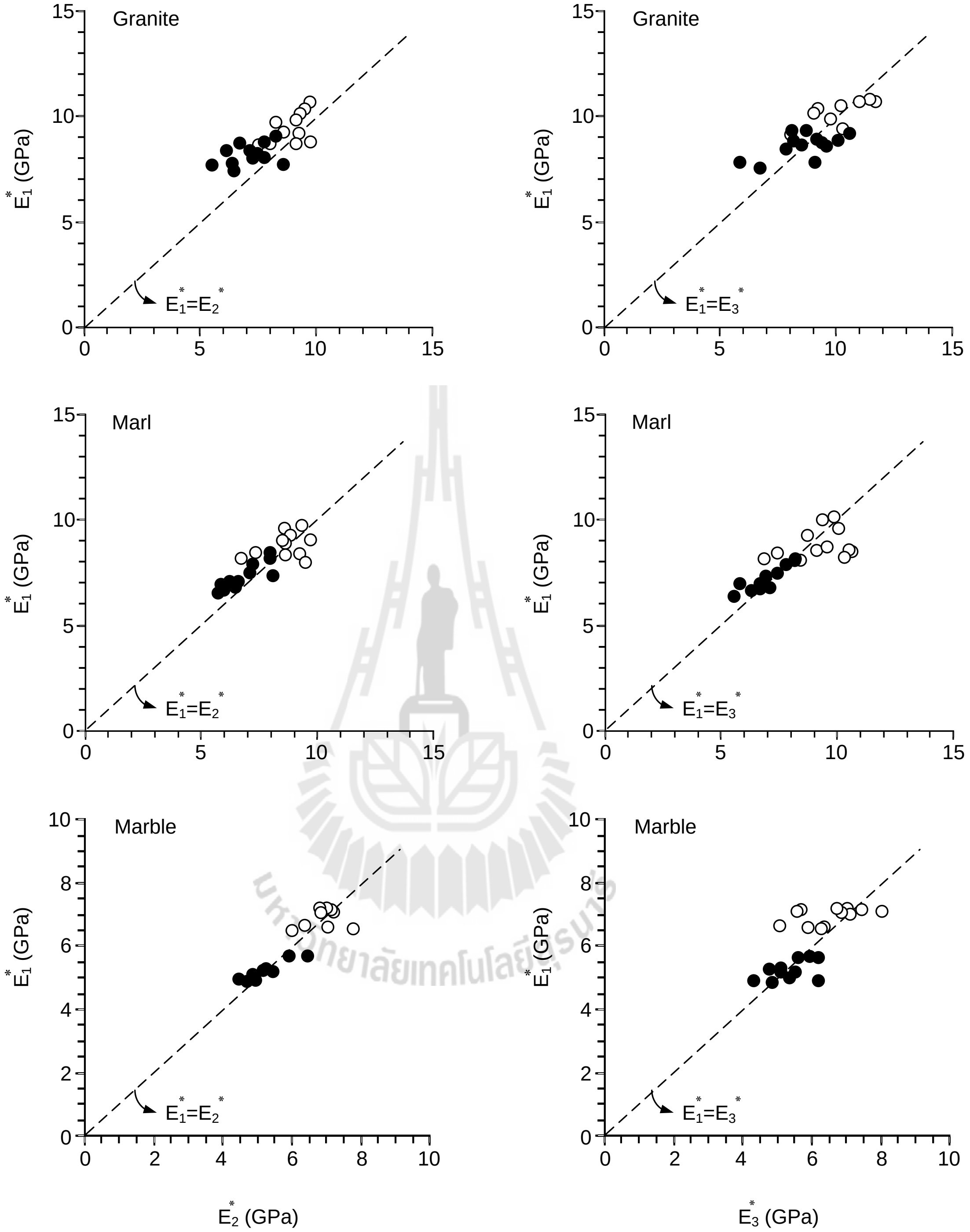

Figure 5.15 New (adjusted) elastic modulus calculated along the major principal axis as a function of the intermediate and minor principal axes.

CHAPTER VI

DISCUSSIONS AND CONCLUSIONS

6.1 Discussions and conclusions

The effect of loading rate on the compressive strength and deformability are determined for rectangular block specimens obtained from the granite, marl and marble. The polyaxial load frame applies constant lateral confining pressures of 0, 3, 7 and 12 MPa while the axial stresses increased at the constant rates of 0.001, 0.01, 0.1, 1.0 and 10 MPa/s until failure occurs.

The results indicate that the granite, marl and marble have average water contents of 0.14%, 2.71% and 0.09%, respectively. The strengths of the saturated specimens are lower than those of the dry specimens, particularly under high confining pressures and high loading rates, which agree well with previous studies obtained elsewhere (Cobanoglu and Celik, 2012; Masuda, 2001; Hawkins and McConnell, 1992; Vasarhelyi, 2003; and Vasarhelyi, 2005). This is because under high loading rates the pore water cannot be drained off, and hence resulting in a built-up of pore pressure. The influences of pore pressure on the rock deformability are reflected as the reduction of Young's modulus and the slight increase of Poisson's ratios. These results generally agree with the experimental observations by Vasarhelyi (2003, 2005), Li et al. (1999, 2012) and Yilmaz (2010). Based on the Coulomb criterion, the cohesions of the dry and saturated specimens are comparable. The dry specimens yield slightly higher friction angles than the saturated specimens. These generally agree with the experimental observations by Li et al. (2012). A multi-axial strength criterion is developed to describe the distortional strain energy density of rock at failure as a function of the mean strain energy. The energy required to fail the low porosity rocks under dry condition is slightly higher than that under saturated condition. The distortional and mean strain energy is calculated from the principal stresses at failure and the rate-dependent elastic modulus. This means that if the total stresses and the loading rate are known, the proposed strength criterion can be used to predict the strength and deformation of in-situ rocks under dry and saturated conditions.

After the effect of loading rate is isolated from the strength results, the maximum principal stress at failure decreases with increasing pore pressure. When pore pressure increases, the elastic modulus decreases and the Poisson's ratios increases. The relations between compressive strength and elastic modulus with pore pressure can be best represented by linear equation. This is opposite to the conclusions drawn by Vasarhelyi and Van (2006), Dyke and Dobereiner (1991), Hawkins and McConnell (1992) and Yilmaz (2010), who found that the uniaxial compressive strength and elastic modulus decreased exponentially with increasing water content.

The results can be used to assess the mechanical stability of these decorating and building stones as applied under various moisture contents and for predicting the strength and deformation of rock embankments and foundations under dry and saturated conditions.

6.2 Recommendations for future studies

The uncertainties of the studied investigation and results discussed above lead to the recommendations for further studies. More testing is required on a variety of rocks with different porosity values. More investigation is also desirable to confirm or verity that the effect of pore pressure acts equally under all confining pressure. This also suggests that test results under higher confining pressure should be obtained.

REFERENCES

ASTM D4543-85. Standard practice for preparing rock core specimens and determining dimensional and shape tolerances. **Annual Book of ASTM Standards** (Vol. 04.08). Philadelphia: American Society for Testing and Materials.

ASTM D7012-07. Compressive strength and elastic moduli of intact rock core specimens under varying states of stress and temperatures. **Annual Book of ASTM Standards** (Vol. 04.08). Philadelphia: American Society for Testing and Materials.

Atherton, M., Brotherton, M. and Mahawat, C. (1992). Integrated chemistry, textures, phase relations and modelling of a composite granodioritic-monzonitic batholith, Tak, Thailand". **Journal of Southeast Asian Earth Sciences** 7(2-3): 89-112.

Bieniawski, Z. T. and Bernede, M. J. (1978). Suggested methods for determining the uniaxial compressive strength and deformability of rock materials. **International Journal of Rock Mechanics and Mining Sciences** 16(2): 138-140.

Bunopas, S. (1992). Regional stratigraphic correlation in Thailand. **National Conference on Geological Resources of Thailand: Potential for Future Development**, Department of mineral Resources, Bangkok, Thailand, 17-24 November.

Cobanoglu, I. and Celik, S. B. (2012). Determination of strength parameters and quality assessment of Denizil travertines (SW Turkey). **Engineering Geology** 129-130: 38-47.

Dyke, C. G. and Dobereiner, L. (1991). Evaluating the strength and deformability of sandstines. **Quarterly Journal of Engineering Geology** 24: 123-134.

Fuenkajorn, K. and Kenkhunthod, N. (2010). Influence of loading rate on deformability and strength of three Thai sandstones. **Geotechnical and Geological Engineering** 28: 707-715.

Fuenkajorn, K., Sriapai, T. and Samsri, P. (2012). Effects of loading rate on strength and deformability of Maha Sarakham salt. **Engineering Geology** 135-136: 10-23.

Goodman, R. E. (1989). **Introduction to rock mechanics**. JohnWiley & Sons, New York.

Hawkins, A. B. and McConnell, B. J. (1992). Sensitivity of sandstone strength and deforability to changes in moisture content. **Quarterly Journal of Engineering Geology** 25: 115-130.

ISRM (1978a). Suggested methods for determining the uniaxial compressive strength and deformability of rock materials – Commission on Standardization of Laboratory and Field Tests. **International Journal of Rock Mechanics and Mining Sciences** 16: 135–140.

ISRM (1978b). Suggested methods for determining tensile strength of rock materials. Commission on Standardization of Laboratory and Field Tests. **International Journal of Rock Mechanics and Mining Sciences** 15: 99–103.

ISRM (1981). In: Brown, E.T. (Ed.), Rock characterization, testing and monitoring. **Pergamon Press** (pp. 211). New York.

Jaeger, J. C., Cook, N. G. W. and Zimmerman, R. W. (2007). **Fundamentals of Rock Mechanics, 4th edition**. Chapman and Hall, London.

Li, D., Wong, L. N. Y., Liu, G. and Zhang, X. (2012). Influence of water content and anisotropy on the strength and deformability of low porosity meta-sedimentary rocks under triaxial compression. **Engineering Geology** 126: 46-66.

Li, H. B., Zhao, J. and Li, T. J. (1999). Triaxial compression tests on a granite at different strain rates and confining pressures. **International Journal of Rock Mechanics and Mining Sciences** 36: 1057-1063.

Li, Z. and Reddish, D. J. (2004). The effect of groundwater recharge on broken rocks. **International Journal of Rock Mechanics and Mining Sciences** 41(3): 409.

Ludovico-Marques, M., Chastre, C. and Vasconcelos, G. (2012). Modelling the compressive mechanical behavior of granite and sandstone historical building stones. **Construction and Building Materials** 28: 372-381.

Masuda, K. (2001). Effects of water on rock strength in a brittle regime. **Journal of Structural Geology** 23(11): 1653-1657.

Palchik, V. and Hatzor, Y. H. (2004). The influence of porosity on tensile and compressive strength of porous chalks. **Rock Mechanics and Rock Engineering** 37(4): 331-341.

Ray, S. K., Srakar, M. and Singh, T. N. (1999). Effect of cyclic loading and strain rate on the mechanical behaviour of sandstone. **International Journal of Rock Mechanics and Mining Sciences** 36: 543-549.

Torok, A. and Vasarhelyi, B. (2010). The influence of fabric and water content on selected rock mechanical parameters of travertine, examples from Hungary. **Engineering Geology** 115: 237-245.

Vasarhelyi, B. (2003). Some observations regarding the strength and deformability of sandstones in case of dry and saturated conditions. **Bulletin of Engineering Geology and the Environment** 62: 245-249.

Vasarhelyi, B. (2005). Technical note statistical analysis of the influence of water content on the strength of the Miocene limestone. **Rock Mechanics and Rock Engineering** 38(1): 69-76.

Vasarhelyi, B. and Van, P. (2006). Influence of water content on the strength of rock. **Engineering Geology** 84: 70-74.

Yang, S. Q., Jing, H. W. and Wang, S. Y. (2012). Experimental investigation on the strength, deformability, failure behavior and acoustic emission locations of red sandstone under triaxial compression. **Rock Mechanics and Rock Engineering** 45: 583-606.

Yilmaz, I. (2010). Influence of water content on the strength and deformability of gypsum. **International Journal of Rock Mechanics and Mining Sciences** 42(2): 342-347.

APPENDIX A

PUBLICATION

List of Publication

Khamrat, S. and Fuenkajorn, K. (2013). Effects of loading rate and pore pressure on compressive strength of rocks. In **Proceedings of the 11th International Conference on Mining, Materials and Petroleum Engineering, the 7th International Conference on Earth Resources Technology, ASEAN Forum on Clean Coal Technology** (pp. 7-12). November 11-13, Centara Duangtawan Hotel, Chiang Mai, Thailand, pp. 7-12.

ASEAN++ 2013 Moving Forward
The 11th International Conference on Mining, Materials and Petroleum Engineering
The 7th International Conference on Earth Resources Technology
ASEAN Forum on Clean Coal Technology
November 11-13, 2013, Chiang Mai, Thailand

Paper ID 99

Effects of Loading Rate and Pore Pressure on Compressive Strength of Rocks.

S. Khamrat[1]*, K. Fuenkajorn[2]
[1]*Graduate Student, Geomechanics Reserarch Unit, Suranaree University of Technology, Thailand*
[2]*Associate Professor, Geomechanics Reserarch Unit, Suranaree University of Technology, Thailand*
**e-mail: B5100477@hotmail.com*

ABSTRACT

The objective of this study is to determine the effects of pore pressures on the compressive strengths of Tak granite, Lopburi marl and Lopburi marble. Failure strengths are determined for various stress rates and confining pressures under dry and saturated conditions. A multi-axial strength criterion is developed to describe the distortional strain energy density of rock at failure as a function of the mean strain energy. The energy required to fail the rocks under dry condition is higher than that under saturated condition. The proposed strength criterion can be useful to predict the strength and deformation of rock embankments and foundations under dry and saturated conditions.

KEYWORDS: *Pore pressure / Strength / Loading rate / Strain energy*

1. INTRODUCTION

The compressive strength and deformability of rocks are important parameters for the design and stability analysis of geologic structures. The effects of stress rate on the compressive strength elastic modulus of rocks have long been recognized. It has been found that rock compressive strength and deformation modulus decrease with the loading rate [1-4]. Pore pressure has also been known as one of the factors lowering the rock strengths [5-8]. The rock compressive strengths decrease significantly as the water content increases. The measurement of pore pressure and its effect on the strength and deformability of low porosity rocks is however very difficult. The influence of water on deformability of rocks is also reflected as a reduction of Young's modulus and increase of Poisson's ratio, which indicates that the saturated rocks will deform more than the dry ones under the same stress condition [9-12].

The objective of this study is to experimentally determine the effects of pore pressures on the compressive strengths of granite, marl and marble. The rock strengths are determined for various stress rates and confining pressures both under dry and saturated conditions. This is primarily to indirectly reveal the effects of pore pressure on the mechanical behavior of low porosity and low permeability rocks. The distortional strain energy density at failure is determined to describe the rock strength as a function of mean strain energy.

2. SAMPLE PREPARATION

The rock samples used in this research are Tak granite, Lopburi marl and Lopburi marble. The specimens have been prepared to obtain rectangular blocks with nominal dimensions of 50×50×100 mm^3 for the uniaxial and triaxial compression tests. A minimum of 40 specimens are prepared for each rock types. The specimens are cut and ground to obtain the perpendicularity and parallelism to comply with the ASTM standard practice [13]. They are prepared to test under dry and fully saturated conditions. Under dry condition the specimen are over dried for 24 hours before testing. Under saturated condition the specimens are submerged under water in pressure vacuum chamber for 24 hours in order to saturate the specimens (Fig. 1.) The granite, marl and marble have average water contents (w) of 0.14%, 2.71% and 0.09%, respectively (Fig. 2).

3. TEST METHOD

The laboratory testing includes uniaxial and triaxial compression tests. Loading rates vary from 0.001, 0.01, 0.1, 1 to 10 MPa/s. A polyaxial load frame [14] is used to apply confining pressures from 0, 3, 7 to 12 MPa (Fig. 3). The sample preparation, test methods and calculation follow relevant ASTM standard practices. The elastic modulus and compressive strength are measured. Neoprene sheets are used to minimize the friction at all interfaces between the loading plate and the rock surface.

The tests are performed by increasing the axial stress to the rock specimen. The axial and lateral strains are measured as a function of time until failure occurs. The polyaxial load frame is used in this study because the cantilever beams with pre- calibrated

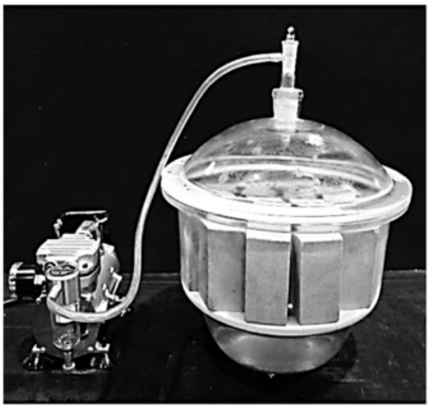

Fig. 1 Sandstone specimens submersed under water in vacuum chamber.

dead weight can apply a truly constant lateral stress to the specimen. The dial gages will be installed to measure the axial and lateral strains. During the test, the axial strain, lateral strain, and time are monitored. The maximum load at the failure and failure modes are recorded.

4. TEST RESULTS

Tab. 1 summarizes the strength results. Fig. 4 shows some post-test marble specimens from the triaxial compression test under confining pressures (σ_3) from 0, 3, 7 to 12 MPa with loading rates ($\partial\sigma_1/\partial$) of 1 and 0.001 MPa/s for both dry and saturated conditions. Post-test observations indicate that under high loading rates, the specimens fail by the extension failure mode. Under the low loading rates shear failure mode is observed.

4.1 Strength properties

The strengths of the saturated specimens are lower than those of the dry specimens, particularly under high confining pressures and high loading rates. Fig. 5 shows the maximum principal stress ($\sigma_{1,f}$) as a function of the applied loading rates. Based on the Coulomb strength criterion the cohesion and internal friction angle of the rocks have been calculated. The cohesions of the dry and saturated specimens are comparable (Fig. 6). The dry specimens yield slightly higher friction angles than the saturated specimens (Fig. 7). According to the Coulomb criterion the shear stress (τ) can be represented by:

$$\tau = c + \sigma_n \tan\phi \qquad (1)$$

where σ_n is the normal stress, c is the cohesion and ϕ is the friction angle. They can be determined as a function of the stress rate as follows (Figs. 6 and 7):

$$c = \chi \cdot \ln(\partial\sigma_1/\partial) + \psi \qquad (2)$$

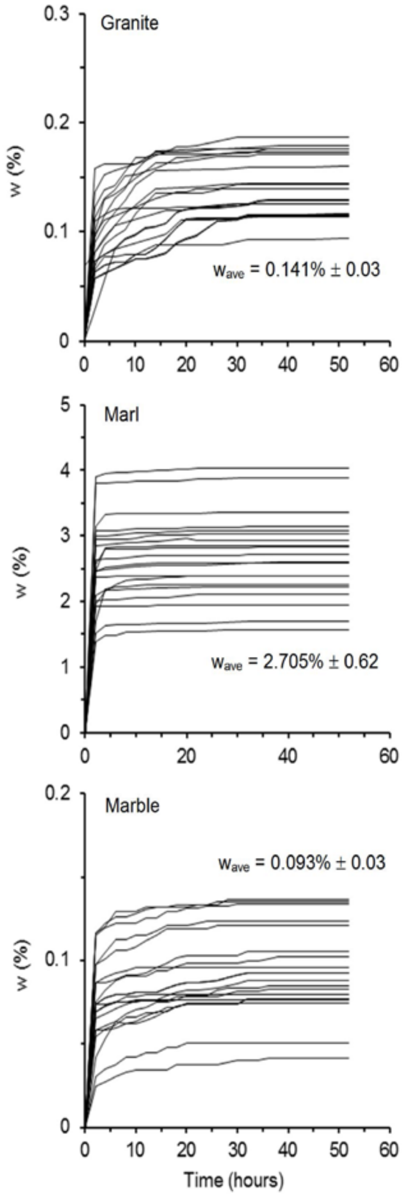

Fig. 2 Water contents as function of time.

$$\phi = \omega \cdot \ln(\partial\sigma_1/\partial) + \iota \qquad (3)$$

The parameters χ, γ, ω, ι are empirical parameters.

Substituting equations (2) and (3) into (1) the shear strength of rocks can be presented as a function of stress rate:

$$\tau = [\,\chi \cdot \ln(\partial_1/\partial) + \psi] + \sigma_n \tan[\,\omega \cdot \ln(\partial_1/\partial) + \iota] \qquad (4)$$

ASEAN++ 2013 Moving Forward
The 11th International Conference on Mining, Materials and Petroleum Engineering
The 7th International Conference on Earth Resources Technology
ASEAN Forum on Clean Coal Technology
November 11-13, 2013, Chiang Mai, Thailand

Tab. 1 Compressive strengths of specimens under various loading rates.

σ_3 MPa	$\partial\sigma_1/\partial t$ MPa/s	Granite Dry σ_1 MPa	Granite Dry E GPa	Granite Dry ν	Granite Saturated σ_1 MPa	Granite Saturated E GPa	Granite Saturated ν	Marl Dry σ_1 MPa	Marl Dry E GPa	Marl Dry ν	Marl Saturated σ_1 MPa	Marl Saturated E GPa	Marl Saturated ν	Marble Dry σ_1 MPa	Marble Dry E GPa	Marble Dry ν	Marble Saturated σ_1 MPa	Marble Saturated E GPa	Marble Saturated ν
0	10	86.0	N/A	N/A	80.0	N/A	N/A	62.0	N/A	N/A	58.1	N/A	N/A	46.3	N/A	N/A	44.2	N/A	N/A
	1	76.7	13.64	0.28	72.2	9.77	0.31	53.0	9.88	0.30	51.4	7.98	0.32	43.0	9.28	0.27	42.5	7.11	0.29
	0.1	69.7	10.75	0.29	66.0	8.16	0.30	47.0	8.08	0.31	45.9	6.31	0.31	39.7	7.22	0.26	40.0	6.22	0.26
	0.01	64.3	8.11	0.27	61.8	6.87	0.29	41.7	6.36	0.27	41.2	4.85	0.31	38.2	6.45	0.32	38.2	5.26	0.26
	0.001	59.0	6.25	0.28	57.4	5.19	0.29	38.3	4.63	0.29	38.0	4.11	0.32	36.8	5.08	0.31	37.0	4.01	0.31
3	10	142.1	N/A	N/A	120.0	N/A	N/A	81.0	N/A	N/A	73.0	N/A	N/A	62.1	N/A	N/A	56.1	N/A	N/A
	1	127.6	12.12	0.29	112.2	10.21	0.28	71.0	8.88	0.29	67.0	8.13	0.29	56.3	8.75	0.26	53.9	7.13	0.29
	0.1	114.0	9.08	0.29	101.6	8.54	0.27	63.2	7.46	0.27	60.8	7.21	0.27	53.4	7.11	0.30	51.5	5.50	0.29
	0.01	104.0	7.31	0.30	97.3	6.23	0.29	56.7	6.44	0.30	56.0	6.18	0.29	50.9	6.48	0.26	48.9	4.68	0.28
	0.001	98.6	5.83	0.27	91.9	5.63	0.29	53.3	5.15	0.27	52.5	4.49	0.28	49.0	5.10	0.29	47.5	3.99	0.27
7	10	203.0	N/A	N/A	174.1	N/A	N/A	103.0	N/A	N/A	93.0	N/A	N/A	82.0	N/A	N/A	73.3	N/A	N/A
	1	182.0	12.64	0.27	165.0	10.56	0.27	93.2	9.11	0.31	88.0	8.21	0.29	73.2	9.10	0.28	69.0	6.98	0.27
	0.1	169.2	10.08	0.28	156.2	9.65	0.27	85.4	8.18	0.30	81.5	7.17	0.28	69.3	7.79	0.28	66.5	5.88	0.27
	0.01	158.5	8.16	0.29	143.8	7.79	0.28	78.5	6.73	0.29	77.3	6.25	0.27	66.8	6.73	0.28	64.0	4.81	0.30
	0.001	147.2	7.06	0.29	139.0	6.45	0.29	73.5	5.32	0.29	72.5	5.61	0.28	64.8	5.49	0.27	62.2	4.30	0.30
12	10	N/A	N/A	N/A	N/A	N/A	N/A	130.0	N/A	N/A	118.0	N/A	N/A	103.0	N/A	N/A	92.0	N/A	N/A
	1	266.7	12.45	0.29	232.3	9.80	0.27	120.4	10.99	0.28	113.8	9.41	0.29	93.0	9.41	0.27	87.7	7.21	0.30
	0.1	243.0	9.83	0.28	221.2	7.72	0.27	111.5	9.67	0.29	107.5	8.00	0.28	88.3	7.94	0.27	85.0	6.49	0.29
	0.01	225.3	8.75	0.29	204.0	6.90	0.26	104.0	7.88	0.31	101.7	6.36	0.28	85.0	6.72	0.28	81.7	5.57	0.28
	0.001	214.2	7.31	0.30	197.8	6.31	0.29	98.5	6.38	0.30	97.0	5.95	0.29	83.2	5.57	0.27	80.0	4.56	0.29

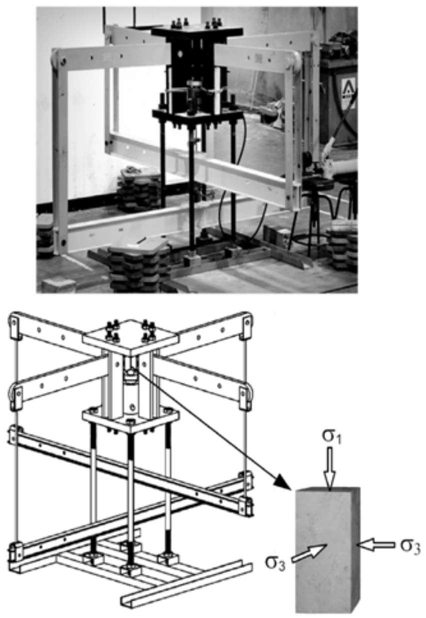

Fig. 3 Polyaxial load frame used in this study.

4.2 Elastic parameters.

The elastic modulus (E) and Poisson's ratio (v) are determined from the tangent of the stress-strain curves at 50% failure. The elastic modulus of the rock appears to increase with loading rate (Fig. 8). The influence of pore pressure on the rock deformability is reflected as the reduction of Young's modulus. The Poisson's ratios of saturated specimens are slightly higher than those of the dry specimens, and tend to be independent of the loading rate (Fig. 9).

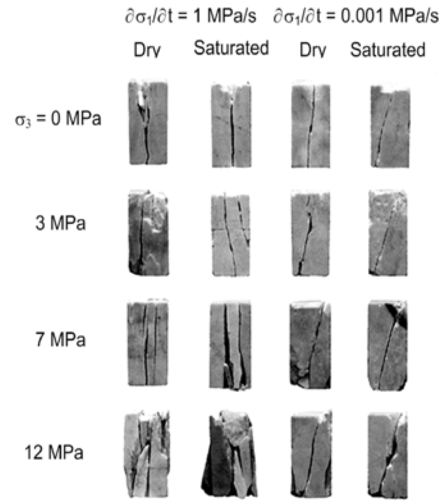

Fig. 4 Some post-test marble specimens from the triaxial compression test.

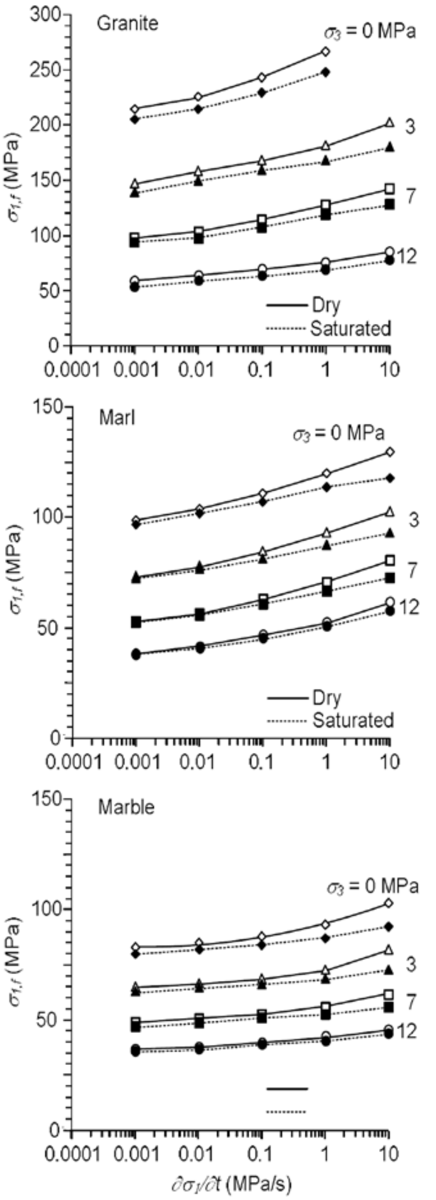

Fig. 5 Maximum principal stress as a function of applied loading rate for dry and saturated specimens.

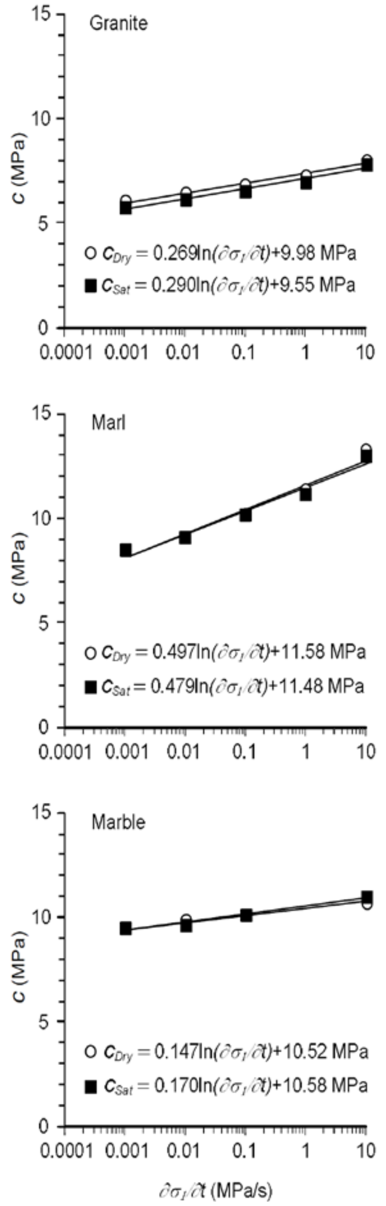

Fig. 6 Cohesion as a function of applied loading rate for dry and saturated specimens.

Under lower loading rate of 0.001 MPa/s the elastic and Poisson's ratio under dry and saturated condition are similar. This suggests that the pore pressure has no effect on the rock strengths if there is sufficient time to allow water to flow out of the specimens. The elastic parameters can be best represented by:

$$E = \kappa\,(\partial\sigma_1/\partial t)^{\xi} \qquad (5)$$

$$\nu = \alpha\, ln\,(\partial\sigma_1/\partial t)+\beta \qquad (6)$$

The parameters κ, ξ, α, β are empirical parameters.

4.3 Strain energy density criterion.

The strain energy density principle is applied here to describe the rock strength and deformation under different loading rates. The distortional strain energy (W_d) at failure can be calculated from the shear modulus

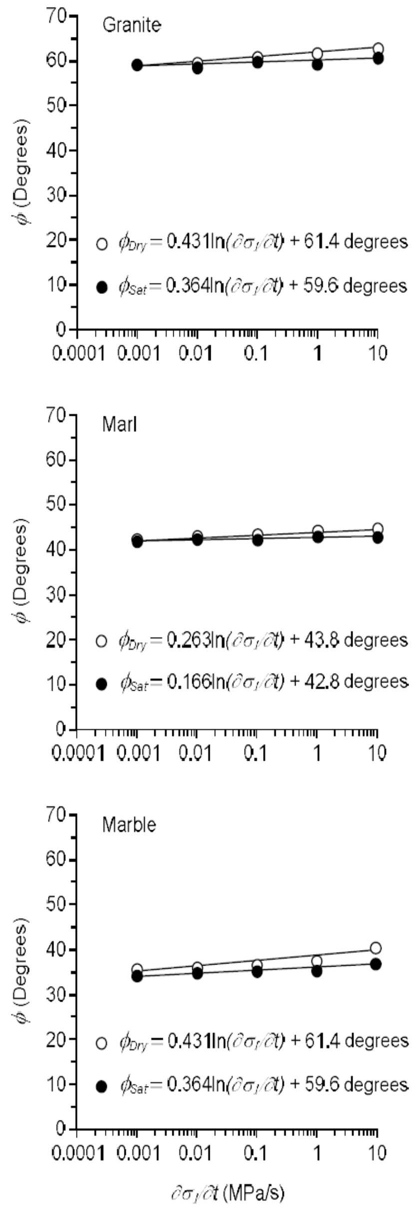

Fig. 7 Friction angle as a function of applied loading rate for dry and saturated specimens.

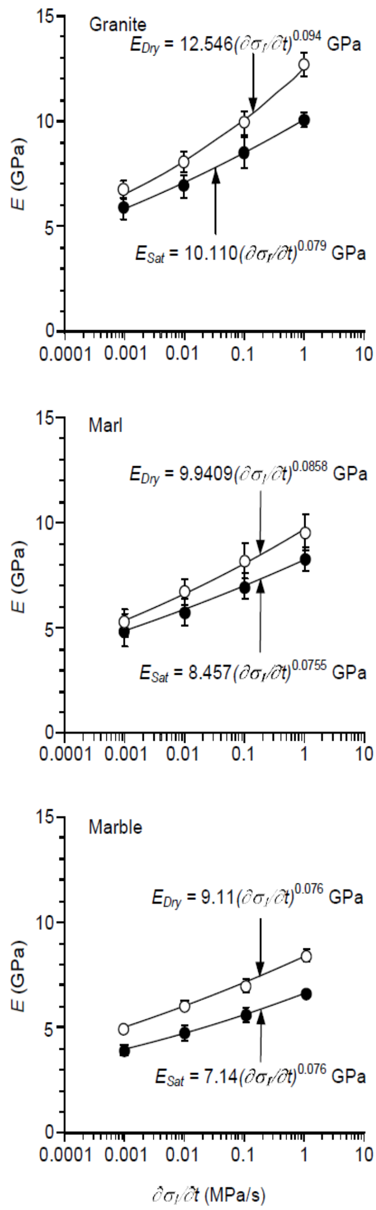

Fig. 8 Elastic modulus as a function of applied loading rate for dry and saturated specimens.

and octahedral shear stresses for each rock specimen as follows [15].

$$W_d = \frac{3}{4}\left(\frac{\tau^2_{oct,f}}{G}\right) \tag{7}$$

The mean strain energy (W_m) at failure can also be derived as a function of the bulk modulus and mean stress at failure.

$$W_m = \left(\frac{\sigma^2_m}{2K}\right) \tag{8}$$

The elastic parameters G and K can be determined for each specimen using the following relations:

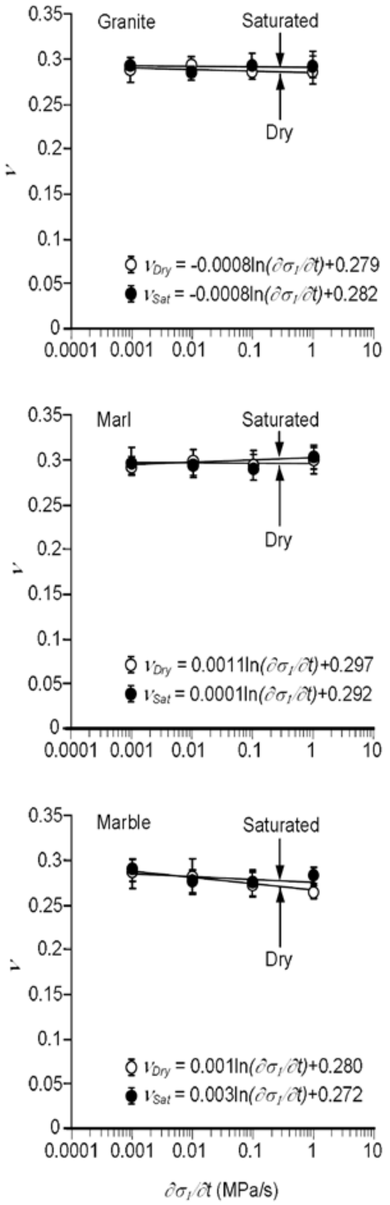

Fig. 9 Poisson's ratio as a function of applied loading rate for dry and saturated specimens.

$$G = \frac{E}{2(1+\nu)} \qquad (9)$$

$$K = \frac{E}{3(1-(2\nu))} \qquad (10)$$

The octahedral shear strength can be determined as [15]:

$$\tau_{oct,f} = [(1/3)[(\sigma_1-\sigma_2)^2+(\sigma_2-\sigma_3)^2+(\sigma_3-\sigma_1)^2]]^{1/2} \qquad (11)$$

Regression on the test results shows that the distortional strain energy increases linearly with the mean strain energy for dry and saturated conditions (Figs. 11 and 12) which can be best represented by:

$$W_d = \lambda W_m + \upsilon \qquad (12)$$

The parameters λ and υ are empirical parameters. The strain energy criterion gives an advantage that both stress and strain at failure are incorporated to define the point at which the rock can absorb the maximum energy before failure occurs.

5. DISCUSSIONS AND CONCLUSIONS

The effect of loading rate on the compressive strength and deformability are determined for rectangular block specimens obtained from the granite, marl and marble. The polyaxial load frame applies constant lateral confining pressures of 0, 3, 7 and 12 MPa while the axial stresses increased at the constant rates of 0.001, 0.01, 0.1, 1.0 and 10 MPa/s until failure occurs.

The results indicate that the granite, marl and marble have average water contents of 0.14%, 2.71% and 0.09%, respectively. The strengths of the saturated specimens are lower than those of the dry specimens, particularly under high confining pressures and high loading rates. This is because under low loading rates the rock specimens are subject to the consolidated drained condition as the pore water has sufficient time to seep out from the specimens. Under high loading rates however the specimens are subject to the consolidated undrained condition where the trapped pore water builds up the pore pressure and reduces the total failure stresses of the rocks. The elastic modulus of dry specimens is higher than that of the saturated specimens. A power equation can be used to describe the increase of the elastic modulus with the loading rate. The Poisson's ratios of saturated specimens are slightly higher than the dry specimens and tend to be independent of the loading rate. Based on the Coulomb criterion, the cohesions of the dry and saturated specimens are comparable. The dry specimens yield slightly higher friction angles than the saturated specimens. A multi-axial strength criterion is developed to describe the distortional strain energy density of rock at failure as a function of the mean strain energy. The energy required to fail the low porosity rocks under dry condition is slightly higher than that under saturated condition. The distortional and mean strain energy is calculated from the principal stresses at failure and the rate-dependent elastic modulus. This means that if the total stresses and the loading rate are known, the proposed strength criterion can be used to predict the strength and deformation of in-situ rocks under dry and saturated conditions.

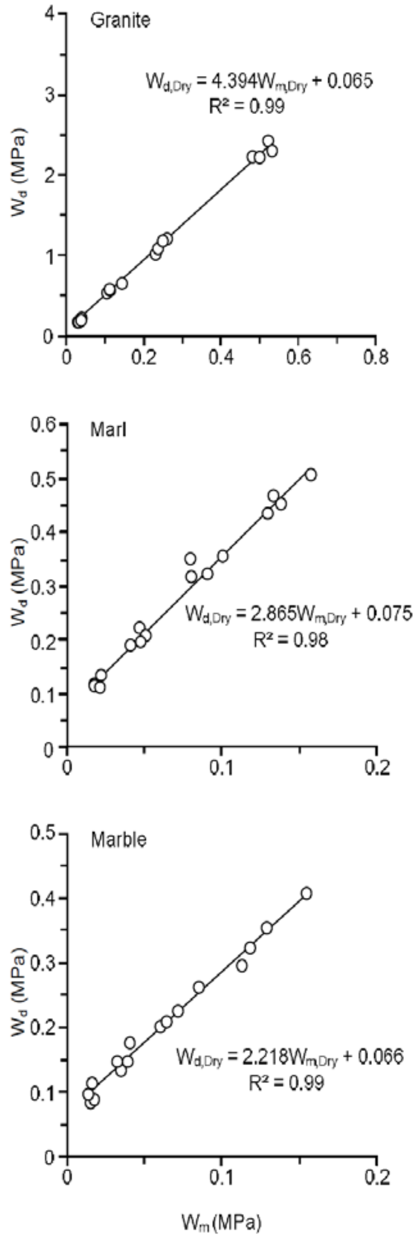

Fig. 11 Distortional strain energy density (W_d) at failure as a function of mean strain energy (W_m) for dry specimens.

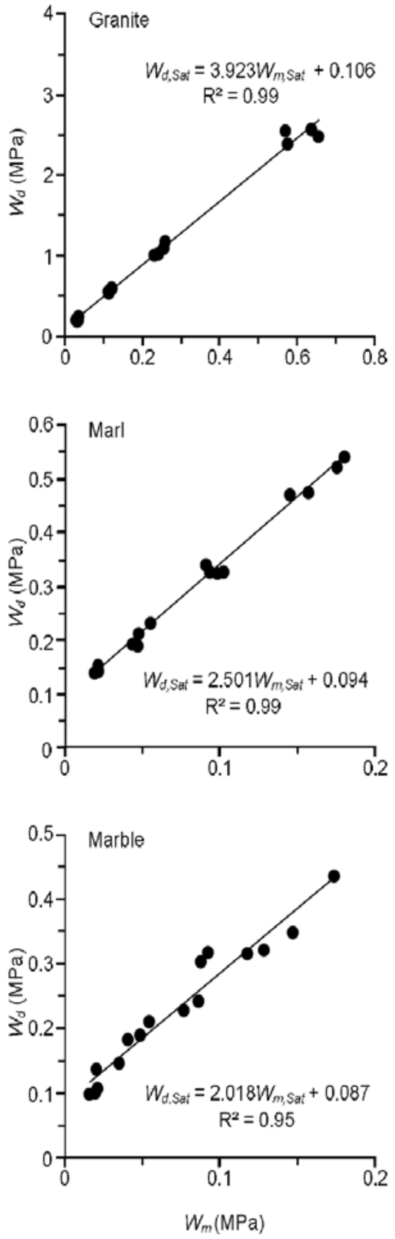

Fig. 12 Distortional strain energy density (W_d) at failure as a function of mean strain energy (W_m) for saturated specimens.

ACKNOWLEDGMENTS

This study is funded by Suranaree University of Technology and by the Higher Education Promotion and National Research University of Thailand. Permission to publish this paper is gratefully acknowledged.

REFERENCES

[1] A.Kumar (1968), The effect of stress rate and temperature on the strength of basalt and granite, *Geophysic.*, 1968, Vol. 33, No. 3, pp. 501-510.

[2] I.W.Farmer (1983), *Engineering Behavior of Rock*, 2nd Edn., Chapman and Hall, London.

[3] J.C.Jaeger, and N.G.W.Cook (1979), *Fundamentals of Rock Mechanics*, 3rd Edn., Chapman and Hall, London.

[4] N.D.Cristescu, and U.Hunsche (1998), *Time Effects in Rock mechanics*, John Wiley and Sons, New York.

[5] K.Masuda (2001), Effects of water on rock strength in a brittle regime, *J. Struct. Geol.*, 2001, Vol. 23, No. 11, pp. 1653-1657.

[6] B.Vasarhelyi (2003), Some observations regarding the strength and deformability of sandstones in case of dry and saturated conditions, *Bull Eng Geol Env*, 2003, Vol. 62, pp. 245-249.

[7] A.Torok, and B.Vasarhelyi (2010), The influence of fabric and water content on selected rock mechanical parameters of travertine, examples from Hungary, *Eng Geol*, Vol. 115, pp. 237-245.

[8] J.Sun, and Y.Y.Hu (1997), Time-dependent effects on the tensile strength of saturated granite at three gorges project in China, *Int. J. Rock Mech. Min. Sci.*, 1997, Vol. 34, No. 3-4, pp. 306.e1-306.e13.

[9] I.Yilmaz (2010), Influence of water content on the strength and deformability of gypsum, *Int. J. Rock Mech. Min. Sci.*, 2010, Vol. 42, No. 2, pp. 342-347.

[10] R.Yoshinaka, T.V.Tran, and M.Osada (1997), Pore pressure changes and strength mobilization of soft rocks in consolidated-undrained cyclic loading triaxial tests, *Int. J. Rock Mech. Min. Sci.*, 1997, Vol. 34, No. 5, pp. 715-726.

[11] M.S.A.Perera, P.G.Ranjith, and M.Peter (2011), Effect of saturation medium and pressure on strength parameters of Latrobe Valley brown coal: Carbon dioxide, water and nitrogen saturations, *Energy*, 2011, Vol. 36, No. 12, pp. 6941-6947.

[12] D.Li, L.N.Y.Wong, G.Liu, and X.Zhang (2012), Influence of water content and anisotropy on the strength and deformability of low porosity meta-sedimentary rocks under triaxial compression, *Eng Geol*, 2012, Vol. 126, pp. 46-66.

[13] ASTM D4543-85. Standard practice for preparing rock core specimens and determining dimensional and shape tolerances, In Annual Book of ASTM Standards, 04.08, American Society for Testing and Materials, Philadelphia.

[14] K.Fuenkajorn, and N.Kenkhunthod (2010), Influence of loading rate on deformability and strength of three Thai sandstones, *Geotech. Geol. Eng.*, 2010, Vol. 28, pp. 707-715.

[15] J.C.Jaeger, N.G.W.Cook, and R.W.Zimmerman (2007), *Fundamentals of Rock Mechanics*, 4th Edn., Chapman and Hall, London.

BIOGRAPHY

Miss Supattra Khamrat was born on December 21, 1989 in Chaiyaphum Province, Thailand. She received her Bachelor's Degree in Engineering (Geotechnology) from Suranaree University of Technology in 2011. For her post-graduate, she continued to study with a Master's degree in the Geological Engineering Program, Institute of Engineering, Suranaree university of Technology. During graduation, 2012-2013, she was a part time worker in position of research assistant at the Geomechanics Research Unit, Institute of Engineering, Suranaree University of Technology.